Shimul Chandra Saha

RF MEMS Switches and Switch Circuits

Modeling of RF MEMS switches and development of RF MEMS capacitive switches and MEMS tunable filters

Thesis for the degree of Dr. Ing

Trondheim, August 2008

Norwegian University of Science and Technology
Faculty of Information Technology, Mathematics and Electrical Engineering
Department of Electronics and Telecommunications

NTNU
Norwegian University of Science and Technology

NTNU
Norwegian University of Science and Technology

Thesis for the degree of Dr. Ing.

Faculty of Information Technology, Mathematics and Electrical Engineering
Department of Electronics and Telecommunications

ISBN 978-82-471-1150-5 (printed ver.)
ISBN 978-82-471-1151-2 (electronic ver.)
ISSN 1503-8181

Doctoral theses at NTNU, 2008:230

Printed by NTNU-trykk

Preface

The research work presented in the thesis was carried out as a partial fulfillment of the requirements to obtain the degree of "Doctor Ingeniør" (PhD/Dr. Ing.) at the department of Department of Electronics and Telecommunications (IET), Faculty of Information Technology, Mathematics and Electrical Engineering (IME), Norwegian University of Science and Technology (NTNU), Trondheim, Norway. I was employed as a research fellow at the department within the project Smart Microsystem for Diagnostic Imaging in Medicine (SMiDA). The funding for the project was provided by Norwegian research council. I would like to thank Norwegian Research Council for their financial support to my work.

I would like to express my sincere thanks to my principle supervisor Prof. Trond Sæther, to give me the opportunity to work on RF MEMS, an exciting and new area of RF and Microwave technology. I also like to thank him for his continuous support, guidance and encouragement during my last 3 and half years study and work. I would also like to express my gratitude to my supervisor Prof. Tor Fjeldly for his encouragement during my work and his help in articles preparation and course work completion. I am also grateful to my both supervisors for helping me in proof reading and their advice on my thesis writing.

I would like to thank Prof. Trond Ytterdal, SMiDA project leader to introduce me to Prof. Trond Sæther initially and his continuous friendly and encouraging attitude during my stay at the department. I would like to thank all SMiDA family members, circuit and system group members and colleagues at the IET department for their friendly and helping minded behavior during my stay at the department. Special thanks to Sigrid Berg for her help in proof reading of the thesis.

I would like to express my deepest gratitude to Dr. Geir Uri Jensen from SINTEF MiNa lab, to introduce me to the MiNa lab at Oslo for the fabrication of the switches and filters and his help during my work in the lab. I would also like to thank Dr. Håkon Sagberg for his continuous help during process work inside clean room and his valuable

advice on various issues regarding process development. He was very encouraging and friendly all the time to me. I like to thank Dr. Erik Poppe for his help in the various process developments, especially metallization, nitride deposition and various dry etching. I would also like to express my gratitude to all the process engineers and scientists at MiNa lab for their help in various process developments and their friendly behavior.

Special thanks to Assoc. Prof. Ulrik Hanke, HIVE (previously at SINTEF ICT, Trondheim), for his valuable help in my thesis work. He was always very patience and encouraging to me when I went to him for any kind of discussion. He provided guidance in modeling and simulation work, also in preparing articles for submission to various conferences and journals. I would also like to thanks Dr. Anton M. Bøifot, Dr. Kirsten Husby and Dr. Bengt Holter for their help in characterization of the switches and other issues.

I like to express my deepest thank to my family members, especially my parents, brother, sister and uncle for their ever lasting support as well as their encouragement to my work. They were very kind and responsive to me always. Warm regards from my heart to my wife Sharmistha Saha for her lovely, supportive and encouraging attitude to my work. Also special thanks to my parents in law. I would also like to thank my friends from school, college and universities and all my relatives for their support during all these years.

Trondheim, August 2008

Shimul Chandra Saha.

Abstract

This thesis presents the design and fabrication of Radio Frequency Microelectromechanical Systems (RF MEMS) switches and switch circuits. The work primarily concerns novel MEMS tunable low pass and band pass filters. A novel model of spring constant and pull-down voltage for non-uniform bridge and cantilever is also reported in this work. It also presents RF MEMS capacitive switches, first ever to be produced in Norway. The reliability of the switch is very good compared to the present state of art works presented elsewhere. Modeling and design of high speed switches and high capacitance ratio switches are performed. Design and simulation of tunable low-pass and band-pass filters are also presented. A model for pull down voltage of a non-uniform bridge and cantilever is developed. Fabrication of the capacitive switches and MEMS tunable filters is conducted in the SINTEF MiNa lab. Measurements of pull down voltage and characterization of RF performance for the switches and filters are also performed.

A high speed switch (short switching time) is required to switch the capacitive micromachined ultrasonic transducer (CMUT) array for medical diagnostic application. A switching time of less than 5 μs is required to switch the same CMUT from the transmitter to the receiver electronics. A study is performed on different beam structures, like bridges and cantilevers, different beam materials and damping coefficients. The simulations are performed in CoventorWare to verify and compare the results. A high capacitance ratio shunt switch is designed and simulated for RF front end technology. The switch has to work from 10-32 GHz, with a certain specified insertion and return loss in upstate and isolation in downstate. A capacitance ratio of 180 is specified for these requirements. A switch is designed and simulated, with a reasonably low pull-down voltage. The switch performances are verified using simulation in MathCad, ADS (Advance design system) and HFSS (High Frequency Structure Simulator).

Tunable low-pass and band-pass filters at C to X band are designed for transmitter and receiver blocks and RF front end circuits. The filters are designed using both

transmission line and MEMS variable capacitors (a novel approach). Stepped impedance transmission line low-pass filters are used as basic building blocks. The low impedance is replaced by shunt capacitors. The band-pass filter is obtained using the basic low-pass filter and series capacitors. The cut-off frequency for the low-pass filter and the center frequency for the band pass filter can be tuned by shunt capacitors. The bandwidth of the band-pass filter can be tuned by the series capacitors. The design and simulation of the filters are performed in ADS with verification in HFSS.

A novel model for spring constant and pull-down voltage of non-uniform bridges and cantilevers is developed through basic force deflection calculation. The non-uniform beam, which is wider at the electrode area and narrower at the anchor area, can be used to reduce the pull-down voltage. To our knowledge, very few reports exist on accurate modeling of non-uniform beams to date. We have developed a model for the spring constant and the pull-down voltage of non-uniform beams, considering the distributed force, using basic force-moment calculation. The model includes residual stress (bridge) and stress gradient (cantilever). The model pull-down voltage is verified by CoventorWare simulations, and the results agree well with simulation results.

The fabrication of RF MEMS shunt capacitive switches and MEMS tunable filters is performed at SINTEF, Micro and Nano Lab (MiNa) Lab, Oslo, Norway. Several experiments were performed to develop the various process steps. An experiment on the hard-baking parameters was conducted to tune the sacrificial resist layer angle at the anchor position. An elaborate experiment was performed on DC sputtering to develop a recipe for low tensile stress gold for the suspended bridge. Also an experiment was performed on release methods to release the RF MEMS switch successfully without any residue left.

A range of capacitive shunt switches are fabricated with various widths and lengths. The fabricated switches have slightly different dimensions than the simulated high capacitive ratio switches. This is done in order to facilitate the fabrication and to obtain a successful prototype in the first round. A reduced initial gap of 2.5 μm is used for the first prototype. A thicker dielectric layer of ~200 nm is also used instead of the 100 nm

used in the simulations. The switch RF performance is measured using a vector network analyzer at Norwegian University of Science and Technology (NTNU). The switch has reasonably low insertion loss and low return loss in the upstate. A higher upstate capacitance is found than the simulated value due to a reduced initial gap and a wider bridge. A comparatively lower isolation is measured in the downstate due to reduced capacitance. A reduction in the downstate capacitance occurred, due to a thicker dielectric. A lower downstate capacitance can also occur, due to surface roughness and non-planarity of the bridge at the downstate.

Low-pass and band-pass filters are also fabricated, using traditional parallel plate capacitances. The filter performance is also measured using a vector network analyzer. Tuning of both center and cut-off frequency and also bandwidth is obtained by actuating different combination of shunt and series capacitors. The measured results agree very well with the simulations results.

Contents:

1. Introduction to RF MEMS

1.1: A brief history of the MEMS switch

Radio Frequency Microelectromechanical Systems (RF MEMS) are becoming a popular technology for many RF applications. Although MEMS have been developed since the 1970s for sensors, accelerometers, gas chromatographs, and other sensor devices, it did not get much attention from the RF and Microwave frequency community for a long time. MEMS switches use the same principle as the simple mechanical moving switch, like basic single pole single through (SPST). The beam moves mechanically either to make an open or short circuit. The difference is that it is miniaturized and works at RF and Microwave frequencies. Figure 1.1 shows a basic MEMS cantilever switch with a separate actuation electrode. When a DC voltage is applied between the actuation electrode and the suspended beam, an electrostatic force will develop and pull the beam down. This will create a contact between the signal in and signal out electrodes. Depending on the configuration the contact can be two types: DC contact and capacitive contact.

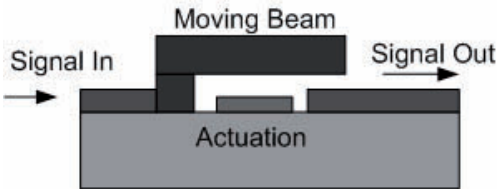

Figure 1.1: A basic MEMS switch

Under the support of DARPA (Defense Advanced Research Projects Agency), Dr. Lary Larson at the Hughs research labs in Malibu, California, developed the first MEMS switch (a varactor) in 1990-91 [1.1]. The switch was specifically designed for microwave applications. Although the switch was not mature and reliable, it demonstrated excellent RF performance up to 50 GHz. The initial results of this research were very outstanding and stirred the interest of several groups in the U.S.

government. By 1995, Rockwell Science Center and Texas Instruments both had developed outstanding RF MEMS switches [1.1]. The Rockwell switch was a DC (metal-to-metal) contact type, suitable for DC-60 GHz applications [1.1]. Texas Instrument developed a capacitive contact switch suitable for 10-120 GHz applications. From that time on many universities, laboratories and companies have been actively pursuing the research on RF MEMS devices. Nowadays there are also many companies working in this area, such as Motorola, Analog Devices, Samsung, Omron, NEC, and ST-Microelectronics [1.1]. The potential of RF MEMS in high frequency applications is also presented in a paper by Linda P. B. Katehi et al. [1.2].

Today there is a great interest and activity in research and development of RF MEMS due to their huge potential in both commercial and defense application. At the same time, significant advancements are taking place in the semiconductor industry, in areas such as HEMTs (high electron mobility transistors), MOSFETs (metal oxide semiconductor field effect transistors), etc. The gate lengths are becoming smaller and the power consumption is reduced for CMOS (complementary metal oxide semiconductor). But the advancement in the semiconductor switching technology, for example, on p-i-n diodes has not advanced in the same rate. The cut-off frequency of p-i-n diode switches is not advancing as the same rate as other technologies. The cut-off frequency of a device is the frequency, at which the on and off impedance becomes equal. For satellite and short-range communication applications, the operating frequency is increasing and they are approaching to the THz range. So a new switching technology is required to meet the demands for higher cut-off frequencies. RF MEMS device can fulfill these demands at a lower loss. The cut-off frequency of a typical RF MEMS switch can go up to 40 THz, which is truly outstanding. RF MEMS are nowadays becoming very popular due to their very low insertion loss, high isolation and high operating frequency. The bias circuitry is very simple compared with that of p-i-n diodes and FET switches. The power consumption of the RF MEMS switch is in the micro watt range which is very low. This will make them very suitable for portable device applications, like mobile handsets and satellite communication.

1.2: RF MEMS technology

There are several RF MEMS technology areas where the research is going on nowadays. They are briefly mentioned below [1.1].

1) RF MEMS switches, varactors and inductors are nowadays mature enough for use in practical application. They can operate from DC to several tens of GHz with very good RF performances. In the RF MEMS switch, the suspended beam can move up to several micrometers during actuation without any problem.

2) Acoustic vibrations can be used in FBAR (thin film bulk acoustic resonator) and filters. They have very excellent performance with very high quality factor (Q) up to several GHz. They are widely used for wireless applications, particularly in cellular telephones. The interdigital surface acoustic wave (SAW) filters are usually large at low frequencies but they can be miniaturized at higher frequency.

3) Lots of research is taking place in the field of mechanical resonators. The mechanical movement of the beam is very small, in the range of nanometers. The structure can be a bridge, a cantilever and a radial disk. The mechanical resonance frequency of the bridge or cantilever depends on the dimensions and material of the beam. These resonant elements can be used in filters, oscillators (for reference clock), etc. Usually they have very high Q. Both bulk and surface micromachining technique can be used for the processing of such devices. The resonance frequency is not very high at present. As the process technology is advancing, smaller devices can be fabricated with better control in resolution and higher resonance frequency.

1.3: RF MEMS Applications areas

RF MEMS have very good RF performance in the RF and Microwave region. DC contact switches provide very good insertion loss and isolation at low frequency from DC to several tens of GHz. Capacitive contact switches provide very good insertion loss and isolation at higher frequency from 3-4 GHz to 100 GHz. The power consumption of RF MEMS switches is very low or close to zero, so it can be used in portable systems where the battery life time is very important. The cut-off frequency of RF MEMS

switches is 30 to 50 times better than their counterparts. They can be used in phase shifters and tunable circuits (matching networks, filters, etc.).

The prominent applications for RF MEMS lie in the following systems such as wireless handsets, base stations, space applications, test and instrumentation, RF instrumentation, aerospace and defense, etc [1.3, 1.4, 1.5, 1.6, 1.7]. For RF radio convergence toward a single multi band radio, two clear conditions should be met, reduced size and power consumption. RF MEMS ohmic contact switches and variable capacitors can be very efficient in meeting these requirements [1.5]. Reconfigurability is a key issue in base stations in terms of various air interface standards, like Global System for Mobile communications (GSM), Universal Mobile Communications System (UMTS), and Code Division Multiple Access (CDMA). Also each system has various frequency bands where the system can operate. RF MEMS technology can perform this reconfigurability with great flexibility [1.5].

Satellites need to manage the home, ground, mobile and space information with limited available power generation and storage capabilities. Thus RF MEMS are a very suitable candidate as they consume very little power during transmission and also in the standby period [1.5]. They are also very lightweight, which is an advantage in space applications.

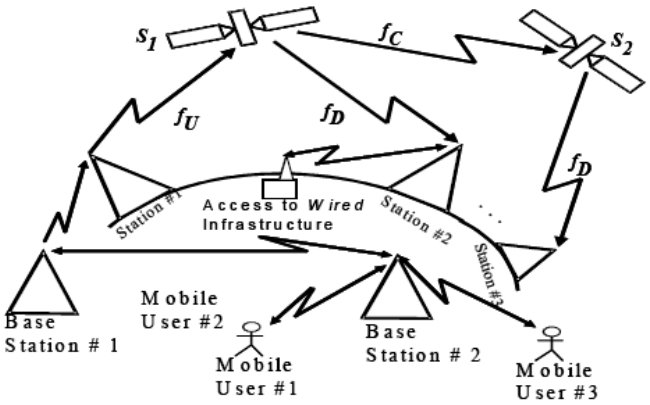

*Figure 1.2: Potential RF MEMS based system applications [1.6, *].*

A typical wireless connectivity for a satellite application is shown in Figure 1.2. The prospects of a RF MEMS mass market are promising according to [1.3, 1.6, and 1.7]. The application areas and the lifetime of RF MEMS devices and number of cycles required for a typical system are shown in Table 1.1 [1.1, p7]. The subsystems and circuits that can be benefited from RF MEMS technology are also mentioned in the Table 1.2 [1.1, p7].

Table 1.1: Application areas of MEMS switches, varactors, and High-Q Inductors [1.1]

Area	System		Number of cycles (Billions)		Years
Phased arrays	Communications systems		Ground	1-10	2-10
			Space	10-100	2-10
			Airborne	10-100	2-10
Phased arrays	Radar systems		Ground	10-100	5-10
			Space	10-100	5-10
			missile	0.1-10	1-5
			Airborne	1-100	5-10
			Automotive	1-10	5-10
Switching and reconfigurable networks	Wireless Communications	portable	0.01-4		2-3
		Base station	0.1-100		5-10
	Satellite (communications and radar)		0.1-1		2-10
	Airborne (communication and radar)		0.1-10		2-10
	Instrumentation		10-100		10
Low-power oscillators and	Wireless communications (portable)		0.1		2-3

amplifiers (varactors, inductors)	Satellite (communication and radar)	0.1-1	2-10
	Airborne (communication and radar)	0.1-10	2-10

Table 1.2: Subsystems and circuits that can benefit from RF MEMS elements [1.1]

RF MEMS Elements	Switch, Varactor, Inductor
	Switching networks
	Transmit/receive switches
	Very high isolation switches (instrumentation)
	Programmable attenuators
	Phase shifters (digital and analog)
	Reconfigurable antennas
	Reconfigurable matching (or impedance) networks
	Reconfigurable Butler matrices for multi-beam systems
	Tunable filters
	Switched filter banks
	Miniature
	Switched diversity antennas, oscillators, amplifiers
	Low phase-noise oscillators (fixed and tunable)
	High-efficiency networks (low-power systems)

1.4: ***Performance of RF MEMS switches***:

RF MEMS switches have extremely low insertion loss during the on-state and very high isolation during the-off state. They are very suitable for operation at RF and Microwave frequency region. They are extremely linear and have very low intermodulation products. They consume very little power during actuation and can provide a very high capacitance ratio compared to their counterparts. The performance of RF MEMS

switches compared to their counter parts, PIN diode and FET switches, is shown in table 1.3 [1.1, p5]:

Table 1.3: Performance comparison of FETs, PIN Diodes, and RF MEMS [1.1]

Parameter	RF MEMS	PIN	FET
Voltage (V)	10-80	±3-5	3-5
Current (mA)	0	3-20	0
Power consumption (mW)	0.05-0.1	5-100	0.05-0.1
Switching time	1-300 μs	1-100 ns	1-100 ns
C_{up} (series) fF	1-6	40-80	70-140
R_s (series) Ω	0.5-2	2-4	4-6
Capacitance ratio	40-500	10	n/a
Cutoff frequency (THz)	20-80	1-4	0.5-2
Isolation (1-10 GHz)	Very high	High	Medium
Isolation (10-40 GHz)	Very high	Medium	Low
Isolation (60-100 GHz)	High	Medium	None
Loss (1-100 GHz) (dB)	0.05-0.2	0.3-1.2	0.4-2.5
Power handling (W)	<1	<10	<10
Third-order intercept point (dBm)	+66-80	+27-45	+27-45

1.5: *Limitation of RF MEMS switches*

Although RF MEMS switches have very good RF performance they have some limitations also. Firstly they require comparatively high actuation voltage. The switching time is in the range of micro seconds, slower than their counterparts. Reliability is one of the major issues in commercialization of RF MEMS switches. The lifetime of a switch can be affected by factors like environment, contact degradation, dielectric stiction, and mechanical failures [1.1, 1.8].

RF MEMS switches are very sensitive to moisture or out-gassing. A slight amount of moisture may cause stiction in the switches and make them useless. Contact degradation occurs mainly in ohmic or DC contact switches. The contact resistance may change or micro welding may happen after a certain time or a certain numbers of cycles. Dielectric stiction occurs in the capacitive switch. This happens due to electric charge storage in the dielectric layer. The charge can lead the switch to stay at upstate or stick to downstate; also it may cause a drift in the actuation voltage. Usually the mechanical failure is minimal compared with the other failure mechanisms. A ductile and less wearable metal is required for the suspended beam to have a better mechanical performance.

In order to reduce the stiction due to environment, RF MEMS switches need hermetic packaging. This will increase the cost of the switch. Cost is still a major issue for commercialization of RF MEMS switches. In order to penetrate the mass mobile market, RF MEMS have to be in a price range, which is lower than or similar to their counterparts. The RF power handling capability of MEMS switches is still lower than in their counterparts. There is a lot of research going on to address these limitations.

1.6: *RF MEMS devices*

Various kinds of basic RF MEMS switches are shown in Figures 1.3 -1.6. From an electrical contact point of view the MEMS switches can be two types: a) Capacitive contact, and b) DC contact. A dielectric is deposited on top of the bottom electrode of the capacitive contact switch as shown in Figure 1.3 and 1.5. When the suspended beam is in the upstate the capacitance is in the range of fF. When a DC actuation voltage is applied between the actuation electrode and the suspended beam, the suspended beam will move downward and collapse on the bottom electrode. This will increase the capacitance in the range of pF, 20-100 times higher than the upstate capacitance. The upstate capacitance depends mainly on the initial gap. The downstate capacitance depends on the dielectric thickness, dielectric constant etc. SiO_2, Si_3N_4, TiO_2 can be used as dielectric for RF MEMS switches. The capacitive contact switch is suitable for

high frequency application. At low frequency (DC), the impedance always will be very high for a capacitive switch, whatever the capacitance value is.

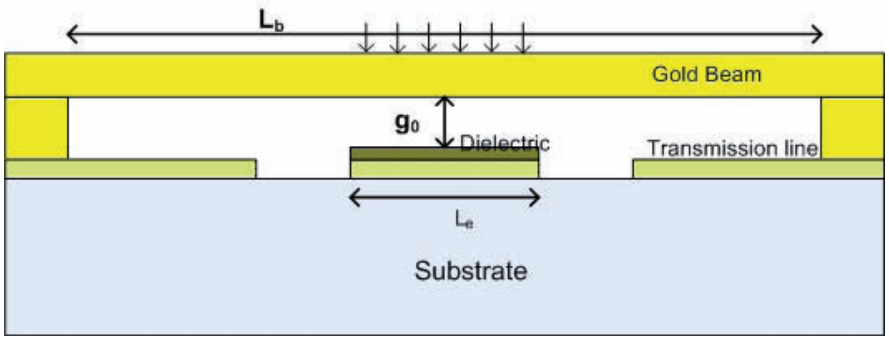

Figure 1.3: A capacitive contact shunt bridge

For DC contact switches, a metal to metal contact is created between the suspended beam and the bottom electrode or transmission line, as shown in Figures 1.4 and 1.6. When the beam is in the upstate the resistance is very high, in the range of Mega Ohm. When the beam is actuated and in the downstate, a metal to metal contact is formed and the resistance becomes very small, in the range of 0.1-1 Ohm. The DC contact switch is suitable for low frequency application (from DC to several tens of GHz). For a DC contact switch a separate actuation electrode is always required. For capacitive contact switches, the same electrode can be used for the electrostatic actuation and the capacitive contact, as shown on Figure 1.3. A separate actuation mechanism can also be used for capacitive contact switches, as shown in Figure 1.5.

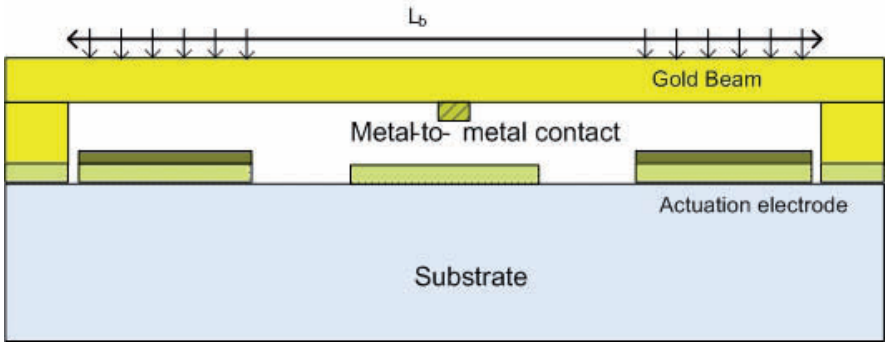

Figure 1.4: A DC contact shunt bridge.

Depending on the electrical configuration, RF MEMS switches can be two types: a) shunt, b) series. For a shunt switch, as shown in Figures 1.3 and 1.4, the switch will stay on electrically, when the beam in upstate, and off when the beam is in downstate. For a series switch as shown in Figures 1.5 and 1.6, the switch will stay on when the beam is in downstate and off when the beam is in upstate.

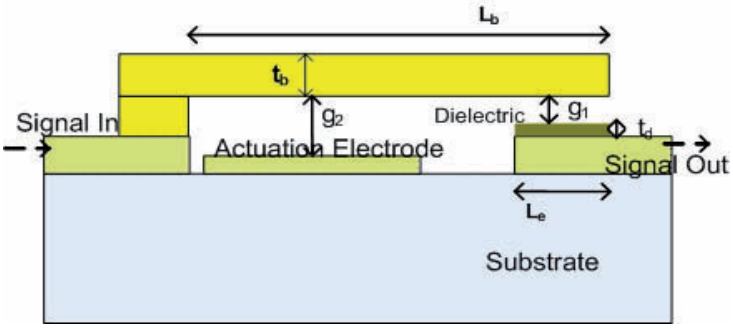

Figure 1.5: A capacitive contact series cantilever

In terms of the mechanical structure the switches fall in two types: a) fixed-fixed bridge, b) free end cantilever. Figures 1.3 and 1.4 shows the fixed-fixed bridges and Figures 1.5 and 1.6 shows the free end cantilever beams. For fixed-fixed bridge the beam is rigidly anchored at both ends. This makes the beam very stiff and the spring constant very high. For free end cantilever the beam is rigidly anchored at one end and the other end is freely suspended. The cantilever is much less stiffer than the bridge [1.1]. For similar dimensions of the bridge and the cantilever, the pull down voltage is higher for the bridge than the cantilever.

Residual stress in the bridge and stress gradient in the cantilever may develop during the fabrication process. The pull down voltage for a bridge will increase due to tensile stress. The positive stress gradient in the cantilever will buckle the beam upwards and increase the pull down voltage. A compressive stress in the bridge will buckle the bridge upward or downward. A higher value of compressive stress may make the beam useless. A negative stress gradient in the cantilever will bend the beam downward. A

higher value of stress gradient may bend the beam enough to touch bottom electrode and lead to a useless switch.

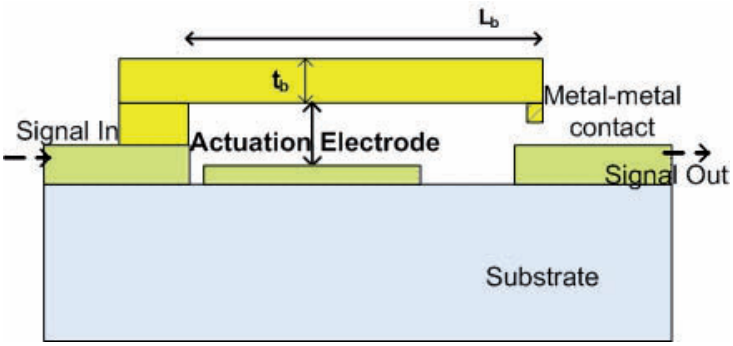

Figure 1.6: A DC contact series cantilever.

For most of the MEMS switches, the beam movement is vertical as shown in Figures 1.3-1.6. A lateral movement can also be used, but they are not very common to date. The actuation mechanism is predominantly electrostatic as discussed already. The other actuation mechanisms are thermal, magneto-static, and piezoelectric. The sizes of these kinds of switches are larger than for electrostatic actuation switches. For miniaturization and low power consumption, electrostatic switches are mostly used for RF and microwave applications.

1.7: Present status of the RF MEMS

Although RF MEMS started with great promises, they had suffered some disappointment. This is due to reliability issues, packaging, price and inability to deliver to mass market in time as promised. The RF MEMS hype curve is shown in Figure 1.7, according to Jeremie Bouchaud and Bernardo Knoblich, [1.3, 1.7].

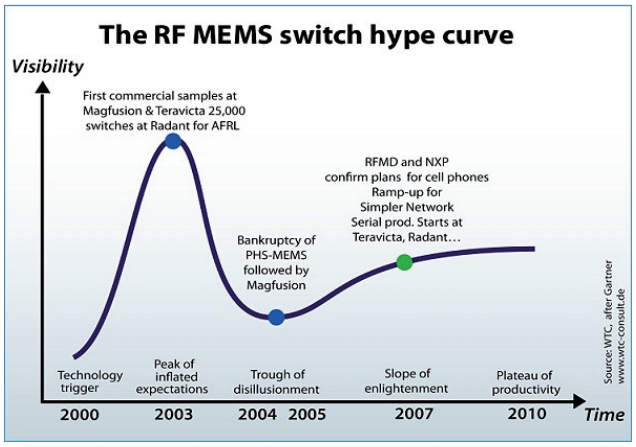

*Figure 1.7: The hype curve of RF MEMS Switch [1.3, *]*

From the Figure 1.7, it can be seen that the RF MEMS switches started with a great expectation and had a sudden rise until 2003, when Teravicta and Magfusion had announced their first sample. The expectation curve suffered a major blow after 2003. This happened as they could not provide samples to all prospective customers in time and the performance was not as good as specified. After that many companies and research groups were discouraged and stopped their work on RF MEMS. Luckily some patient and enthusiastic researchers and companies still continued their work on RF MEMS. Now RF MEMS have left the 'trough of disillusionment phase' and emerged shining into the 'slope of enlightenment'. The present RF MEMS trend and their future are also described in an interview [1.4].

At present there are a number of companies who have started to commercialize RF MEMS switches. Among them Teravicta, Radant, Advantest and Matsushita are prominent. They are only available in USA market yet. The price of a commercial RF MEMS switch is still high compared with their counterparts, like FET and PIN diode switches. Radant has the cheapest switch with a price range of $ 25 for a SPST and $ 40 for a SPDT switch [3]. Until 2006 the Market for RF MEMS switches was only $ 6 million. The forecast says that the market can be up to $ 210 million by 2011. The

market forecast for RF MEMS switch is shown in Figure 1.8. A commercial RF MEMS SPST switch from Radant is shown in Figure 1.9.

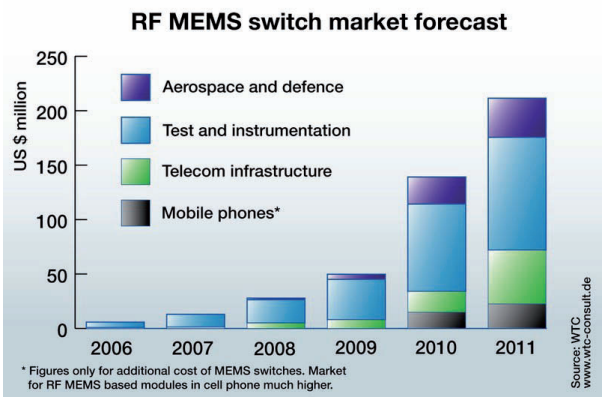

Figure 1.8: The market forecast for RF MEMS switches [1.3,].*

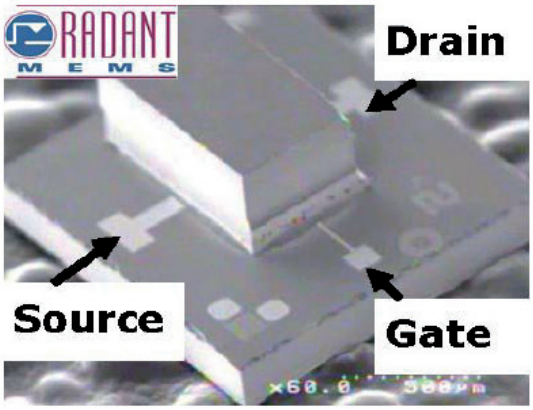

Figure 1.9: A SPST hermetically-sealed MEM switch [1.6,].*

Figure 1.8 shows the market potential only for RF MEMS switches. There are many other RF MEMS components presently in the market at component and system level. They are tunable capacitors, BAW resonators, micro-mechanical resonator, MEMS inductors, and cavity resonators. The expected implementation scheme for RF MEMS

components is shown in Figure 1.10. The total market for RF MEMS component in 2004 was US $ 126 million. The forecast for RF MEMS turnover by 2009 is shown in figure 1.11.

Applications	RF MEMS products: MEMS Switches	Tunable Capacitors	BAW Resonators	Micro-mechanical Resonators	MEMS Inductors	Cavity Resonators
Mobile phones	x	x	x	x		
Consumer electronics & IT	x		x	x	x	
WLAN and WPAN			x	x		
Base Stations	x	x	o			
Microwave communications	o					o
RF Test and ATE	x					
Automotive Radar and Roof Antennas	o					
Satellites	x	x	o	o		x
Military Tactical Radio	x	x	o	o	o	
Military Phased Arrays	x	o				

X: implementation expected
O: implementation uncertain

Figure 1.10: Implementation of RF MEMS by applications, 2009 [1.7,]*

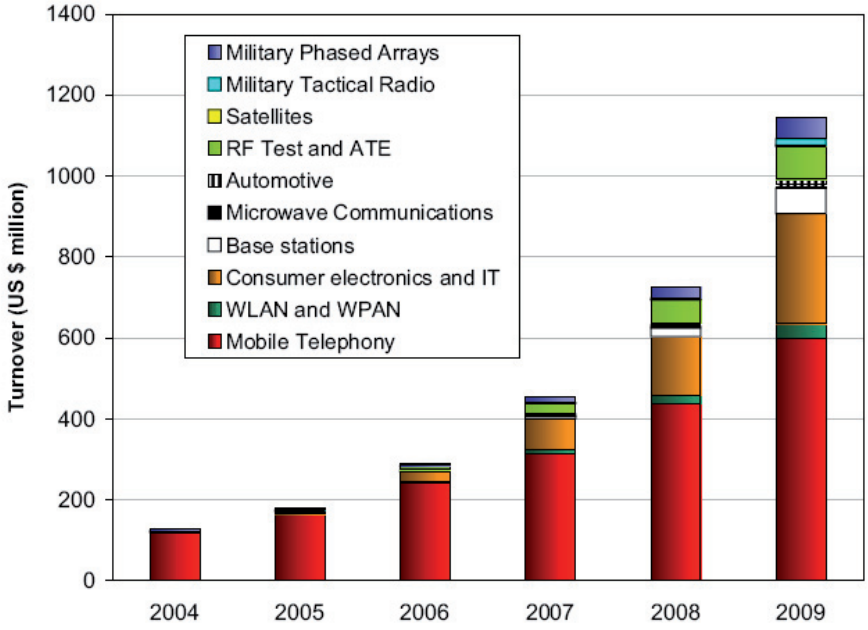

Figure 1.11: Total turnover forecasts for the RF MEMS market by applications, 2004-2009 [1.7,].*

References:

[1.1] G. M. Rebeiz, *RF MEMS Theory, Design and Technology*, John Willey and Sons, 2003.

[1.2] Linda P. B. Katehi, F. Harvey, Elliott Brown, MEMS and Si Micromachined Circuits for High-Frequency Applications, IEEE Transactions on Microwave Theory and Techniques, Vol. 50, No 3, March 2002.

[1.3] J. Bouchaud and B. Knoblich, RF MEMS switches deliver early promises, MEMS, Microfluidics, Microsystem Executive review, MEMS Investor Journal, October 11, 2007.

[1.4] RF MEMS: A brief history and future trends, MEMS, Microfluidics, Microsystem Executive review, MEMS Investor Journal, October 05, 2006.

[1.5] Hector J. De Los Santos, Georg Fischer, Harrie A. C. Tilmans, and Joost T. M. Van Beek, RF MEMS for Ubiquitous Wireless Connectivity, Part 2-Application, IEEE Microwave Magazine, pp 50- 65, December 2004.
[1.6] Hector J. De Los Santos, Scott Rassoulian, and John Maciel, MEMS for future microwave systems, 2005 IEEE MTT-S, 905-908.
[1.7] Jeremie Bouchaud, Bernardo Knoblich, Henning Witch, Will RF MEMS live up their promise?, 36th European Micorwave Conference, Sept 2006, pp 1076-1079.
[1.8] Brandon Pillans, Gabriel Rebeiz, Jeong-Bong Lee, Advances in RF MEMS Technology, GaAs IC Symposium, 2003, pages 17-20.

* Permission obtained from the respective authors through e-mail communications

2. Motivation of the work

MEMS technology is on the verge of revolutionizing high frequency applications. Present and future RF systems require lower weight, volume, cost and power consumption, especially in portable devices and satellite communications. The system also demands increased functionality and frequency of operation. Reconfiguration is another important issue for present RF system, as they work in different operating standards and frequency bands. As discussed in introduction chapter 1, RF MEMS can address these requirements very efficiently. RF MEMS consume very little power (μW). They have very high cut-off frequency compared with their counter part PiN diode and FET switches, and can operate up to 40 THz. They have very low insertion loss and high isolation over a wide frequency range 0 to 100 GHz. The bias circuitry is also very simple compared with the FET and PIN diode switches. RF MEMS switches are still not commercially mature enough. At present very few commercial RF MEMS switches are present at market. There are not many commercial foundries available to date, to fabricate RF MEMS component. So research and development on design and fabrication of RF MEMS switches and switch circuits are very prospective and essential for the advancement of RF MEMS products.

This thesis is based on the work performed on two projects named: Smart Microsystem for Diagnostic Imaging in Medicine (SMiDA) at the Department of Electronics and Telecommunications (IET), Norwegian University of Science and Technology (NTNU) [2.1] and Integrated Reconfigurable Radio Front-end Technology (IRRFT) at the Department of Information and Communication Technology (ICT), SINTEF [2.2]. A brief introduction of theses projects and the motivation to use RF MEMS components are presented below.

2.1: Smart Microsystem for Diagnostic Imaging in Medicine (SMiDA)

It is believed that more than 80% of sudden heart attacks are caused by rupture of vulnerable plaques, which lead to blood clots in the coronary arteries. The rupture occurs in the unstable plaque. Figure 2.1 shows a coronary artery with possible plaque.

A smart and convenient way is required to detect the plaque in the coronary arteries and also to characterize them as stable or unstable. The project aim is to develop the smart microsystem for detection of plaque with characterization. Capacitive Micromachined Ultrasonic transducer (CMUT) is proposed as a device to image the plaque in the coronary artery. An array of CMUT will be placed on a catheter shown in Figure 2.2 with interface electronics inside the catheter. A brief discussion of CMUT and RF MEMS involvement in the imaging system is mentioned in the following paragraphs.

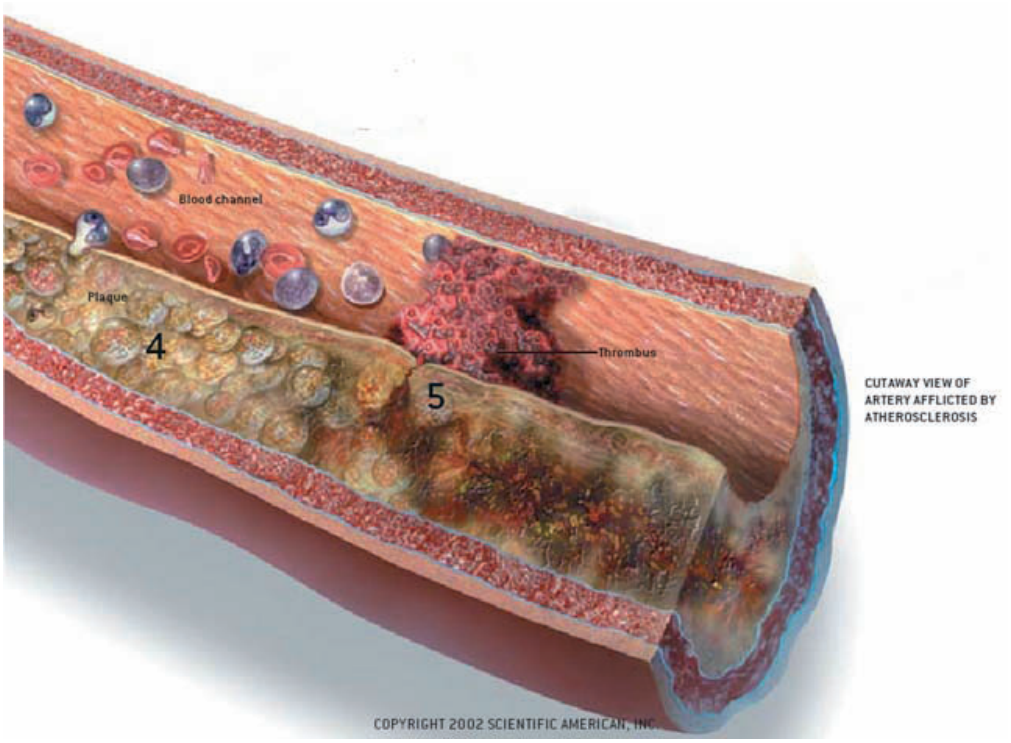

Figure 2.1: A coronary with possible plaque [2.3]

CMUTs are an upcoming technology in the field of medical imaging which promises to offer advanced automation possibilities. They will also offer, unlike the conventional piezoelectric transducer probes, compatibility with the CMOS process and integration

of the signal processing circuitry on the probe itself. This will drastically reduce the hard-wiring of the probe to the signal processing console. The possibility of signal processing near the transducers opens new prospects of 'Smart probes' capable of handling large amounts of data, required for example, for 3D ultrasound imaging. Another imaging application of the CMUTs is in the detection of plaque inside the coronary arteries for an early heart disease diagnosis.

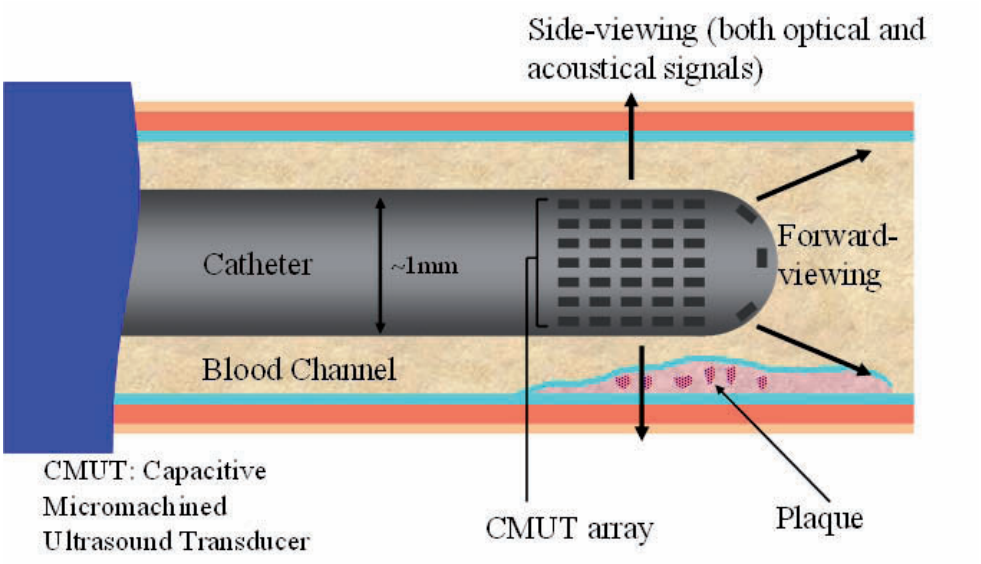

Figure 2.2: A catheter with CMUT element in the blood vessel [2.4]

The active part of a the CMUT is usually a metal coated Si_3N_4 membrane. A highly doped silicon substrate constitutes the bottom electrode. When a DC bias voltage is applied between the top and bottom electrodes, the membrane is pulled towards the substrate (electrostatic actuation). If an AC voltage is applied along the bias point, a harmonic motion is obtained; thus the membrane will generate an ultrasonic wave into the medium outside the transducer. As in piezoelectric ultrasound probes, there are two modes of operation namely, transmit, and receive. CMUT elements require to be switched ON and OFF at different times either to send the actuation signal, or to receive the reflected signal. Hence it is necessary to have a switching matrix to switch the

elements from transmit mode to receive mode as shown in Figure 2.3. Also the elementary mechanism for CMUT switching between transmitter and receiver, with bridge and cantilever are shown in Figures 2.4 and 2.5. As the actuation signal is low, it is necessary to have a low insertion-loss and very good isolation of the switching matrix, for which RF MEMS switches are a good candidate. However as the vein radius is small, the time of flight of the signal to travel to the vein wall and back to the catheter surface is very short. Thus it is necessary to design the switch with very short switching time. The release time is less important considering the switching configuration. For the CMUT application a DC contact switch will be necessary as the operating frequency is in the range of 30 MHz. A switch with a switching time (from upstate to downstate) of less than 5 μs is desired for the above application. Some works on reasonably fast switch are published in [2.5, 2.6]. They are not fast enough to meet our requirement.

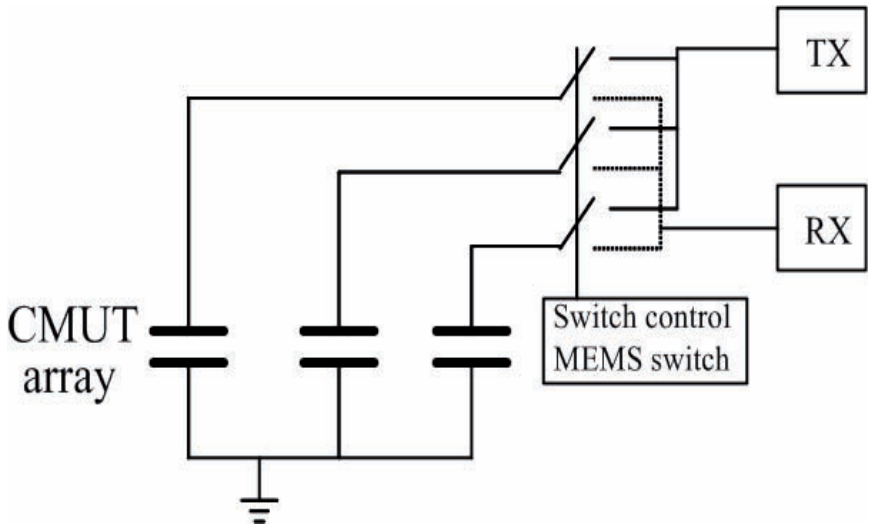

Figure 2.3: A CMUT array with transmit and receive block including switching control.

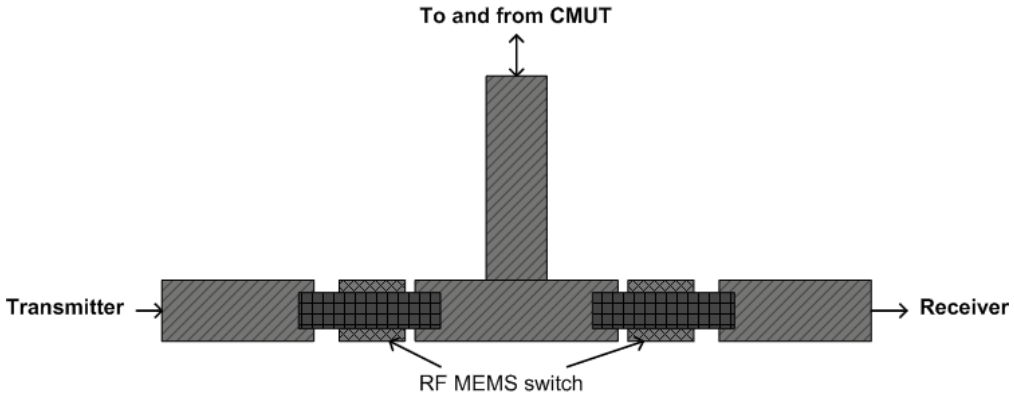

Figure 2.4: The possible switching mechanism for CMUT with MEMS cantilever

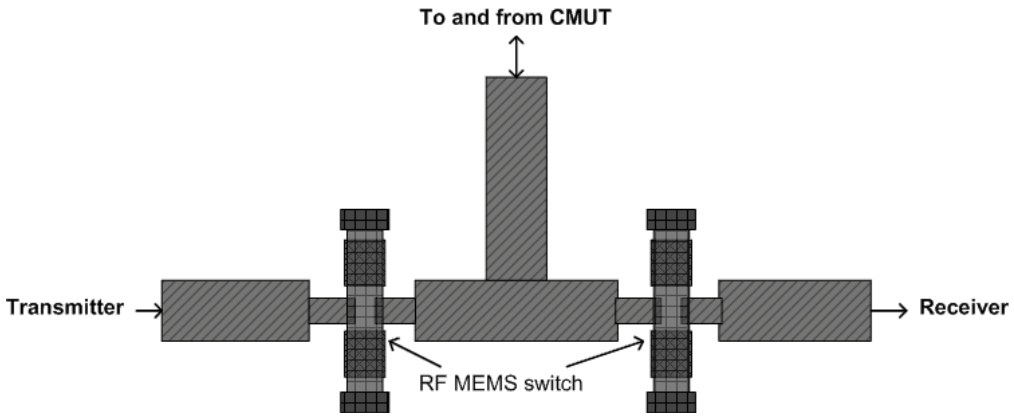

Figure 2.5: The possible switching mechanism for CMUT with MEMS bridge

RF front end circuits for the transmitter and receiver blocks, as shown in Figure 2.3 is also required for the medical application. Power consumption is the key issues in such

kind of application. In terms of power saving, RF MEMS are a prominent technology, as they consume very little power. So RF circuits, specially filter with MEMS varactor, inductor are of prime importance for RF front end circuits. Also MEMS technology will better facilitate integration. MEMS capacitances will also be very useful for RF architectures and signal processing units, such as oscillators, LNAs, etc. Traditionally the half wavelength length filters are larger in dimensions and also their tuning range is not that high. In our work we proposed a stepped impedance transmission line filter, which is compact. Some works on stepped impedance filters are published in [2.7, 2.8 and 2.9]. In our work, we considered a continuous of tuning frequency using a MEMS varactor at relatively lower frequency.

2.2: Integrated reconfigurable Radio Front-end Technology (IRRFT)

This project involves design and implementation of different RF circuits for front end technology. They includes antenna, efficient power amplifier, low noise amplifier, low noise high frequency synthesizer etc. The antenna can be reconfigured using RF MEMS switches and capacitances. The frequency synthesizer can be tuned using RF MEMS capacitances. This will reduce the power consumption of the device. The possible use of MEMS components in a typical transceiver application is shown in Figure 2.6.

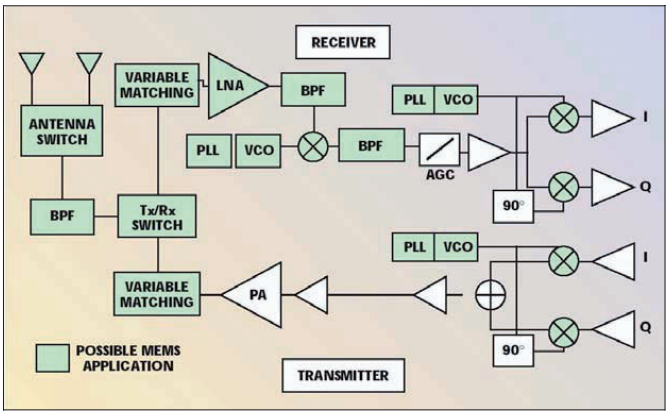

Figure 2.6: Bottom-up approach: The green (grey on black-white copy)-colored sub-systems in the conventional transceiver are replaced by MEMS based components [2.2].

An array of identical antenna elements is used in the antenna architectures. The elements are separated by a half-wavelength of the resonant frequency of each individual element. MEMS switch capacitors can be used to connect these antennas. By tuning the MEMS capacitances the antenna resonant frequency and polarization can be changed. The frequency synthesizer can be consisting of a phase lock loop (PLL) and a voltage controlled oscillator (VCO). The capacitance tuning can be done using MEMS varactors instead of PIN diodes. The capacitances can be changed using an actuation voltage. An initial case study is performed on different kinds of RF MEMS switches, in term of performances like isolation, insertion loss, frequency of operation and process overview. According to SINTEF personnel, a capacitive shunt switch with high capacitance ratio (~180) is preferable for their RF front end application [2.10].

2.3: Combined work for the above mentioned projects

This thesis is based on the work performed on the SMiDA and the IRRFT projects. In order to reduce the pull-down voltage, for both the high-speed switch and high capacitance ratio switch, a non-uniform beam is preferable. Although some works are present [2.11, 2.12] on this kind of modeling, they are not accurate enough. So a comprehensive model for spring constant and pull-down voltage of the non-uniform bridge and the cantilever is developed. A fabrication foundry is required to fabricate RF MEMS switches and switch circuits for the SMiDA projects. The IRRFT project from SINTEF has a similar goal, to fabricate the RF MEMS capacitive switches. They planned to fabricate their switch in SINTEF Micro and Nano Lab (MiNa Lab), Oslo, Norway. So we collaborated with SINTEF to fabricate our switch together at MiNa lab. Instead of using technology by others, our goal was to develop our own technology. In terms of fabrication, we have chosen a capacitive switch for the first prototype. Capacitive switches require less process steps than DC contact switches. Our preference was to develop a working device rather than making a device with precise specifications. For the first prototype, our goal was to fabricate capacitive shunt switches and MEMS tunable filters, with similar process parameters.

References:

[2.1] Trond Ytterdal et al, Project description: Smart Microsystem for Diagnostic Imaging in Medicine, May 2003.

[2.2] Ulrik Hanke et al, Project Description: Integrated Reconfigurable Radio Front-end Technology, SINTEF memo.

[2.3] Scientific America, May 2002.

[2.4] Trond Ytterdal, A presentation on the project: Smart Microsystem for Diagnostic Imaging in Medicine

[2.5] D. Peroulis, S. Pacheco , K. Sarabandi and L. P. B. Katehi, Electromechanical considerations in developing low-voltage RF MEMS switches, IEEE Transactions on MTT, Vol.51, No. 1 January 2003.

[2.6] N. Nishijima, J. Hung, G. M. Rebeiz, A Low-voltage high contacts force RF-MEMS switch, IEEE MTT-S Digest, 2004.

[2.7] D. Peroulis, S. Pacheco , K. Sarabandi and L. P. B. Katehi, Tunable Lymped Components with Applicatins to Reconfigurable MEMS Filters, Microwave Symposium Digest, 2001 IEEE MTT-S, Volume 1, 20-25 May 2001 Page(s):341 - 344 vol.1

[2.8] S. Lee, J. Kim , J . Kim, Y. Kim. and Y. Kwon, Millimeter-Wave MEMS tunable low pass filter with reconfigurable series inductor and capacitive shunt switches, IEEE Microwave and Wireless Components letters, vol 15, No 10, October 2005. pp 691-693.

[2.9] J. Park, S. Lee, J. Kim., H. Kim, Y. Kim. and Y. Kwon, Reconfigurable millimeter-wave filters using CPW-based periodic structures with novel multiple-contact MEMS switches, IEEE Journal of Microelectromechanical Systems, Vol 14, Issue 3, June 2005, pp 456-463.

[2.10] Ulrik Hanke, Anton M. Bøifot and Geir U. Jensen, SINTEF Memo on Integrated Reconfigurable Radio Front-end Technology, Assessment and performance for various capacitive switches. Version 1.3, July 2005.

[2.11] S. Afrang and G. Rezazadeh, Design and Simulation of Simple and Varying Section Cantilever and Fixed-Fixed End Types MEMS Switches, Proceeding of ICSE 2004. pp. 593-596.

[2.12] L. Lv, Z. Deng, F. Zhao, Y. Liu, K. Han, Analysis and Simulation of RF MEMS for Wireless Communication, Proceedings of ISCIT 2005, pp 1095-1098.

3. Thesis Overview

This thesis is based on the work performed on the SMiDA project from NTNU and the IRRFT project from SINTEF. Modeling and simulation of various switches and filters were performed initially. The fabrication of the switches is done in the SINTEF Micro and Nano Lab (MiNa). We had to develop all the process steps by ourselves, as the fabrication of RF MEMS switches had not been performed earlier at MiNa lab. The thesis work is divided into three parts.

3.1 : Modeling and simulation of various RF MEMS switches and switch circuits
3.2: Development of various process steps for fabrication of the RF MEMS switches and the switch circuits
3.3: Measurement of the fabricated RF MEMS switches and switch circuits

3.1: Modeling and simulation of various RF MEMS switches and switch circuits

At first the modeling and simulation of various types of switches, beam structures, and MEMS tunable filters are presented. Design and simulation is performed on a high speed switch and a high capacitance ratio switch. Novel electromechanical models of spring constant and pull down voltage for non-uniform beam bridges and cantilevers are developed. Design and simulation of MEMS tunable filters with a transmission line and MEMS variable capacitors are also performed. The modeling and simulation work of this thesis is based on the following papers. A brief description of the paper is also added with the paper titles.

Paper 1: Shimul Chandra Saha, Tajeshwar Singh, Trond Sæther, "*Design and Simulation of RF MEMS Switches for High Switching Speed and Moderate Voltage Operation*", In proceedings of IEEE PRIME 2005, pp 207-210, July 2005, EPFL, Lausanne, Switzerland.

This paper describes the modeling and simulation of high switching speed RF MEMS switch for CMUT switching application. In the simulation, a capacitive contact bridge

with comparatively large dimensions is considered for initial design. The targeted switching time (from upstate to downstate) is less than 5 μs. The switching time for different metals, like gold and aluminum is simulated and compared. The switching time for various damping coefficient is also considered. The damping coefficient can be controlled by pressure of the media and introducing holes in the suspended beam. The switching time can also be reduced by increasing the actuation voltage above pull-down voltage.

Paper 2: Shimul Chandra Saha, Tajeshwar Singh, Trond Sæther, "*Design and simulation of RF MEMS cantilever and bridge switches for high switching speed and low voltage operation and their comparison*", In proceedings of IEEE ISSCS 2005, pp 131-134, July 2005, Iasi, Romania.

This paper also describes the modeling and simulation of high speed RF MEMS switch for CMUT switching application. The targeted switching time (from upstate to down state) is less than 5 μs. A comparison between the bridge and the cantilevers as beam structures is performed. Different metals like Gold, Aluminum, and Nickel is considered as beam material. The damping factor in term of pressure in the media and perforation in the suspended beam is also considered. The switching speed can be increased by increasing the actuation voltage, above pull down voltage. The simulations are performed in CoventorWare and a suitable switch is proposed for the CMUT application. In the simulation, capacitive switches with relatively larger dimensions are considered for the initial design, considering fabrication issues. The smaller dimension of DC contact switches can be rescaled and designed easily afterwards.

Paper 3: Shimul C. Saha[1], Ulrik Hanke[2], Geir U. Jensen[3], Anton M. Bøifot[4], Tor A. Fjeldly[1], Trond Sæther[1], "*Modeling and Simulation of High Capacitance Ratio RF MEMS Capacitive Shunt Switch*", In proceedings of third IASTED international conference on Circuits, Signals and Systems CSS 2005, pp 186-193, October 2005, Marina Del Rey, CA, USA.

This paper describes the design, modeling and simulation of the RF MEMS switch for IRRFT project. The switch will be used for RF front end applications, such as antennas,

frequency synthesizers, etc. The switch is simulated in term of RF performance like insertion loss, isolation, and return loss at the frequency range 10-32 GHz. The simulations also consider the pull-down voltage, switching time. A high capacitance ratio (~180) switch is proposed, which meets the RF performance with reasonable pull-down voltage.

Paper 4: Shimul Chandra Saha, Trond Sæther, "*Modeling and Simulation of Low Pass Filter using RF MEMS Capacitance and Transmission line*", Proceedings of IMAPS Nordic conference 2005, pp 155-159, September 2005, Tønsberg, Norway.

This paper describes modeling, design and simulation of the MEMS tunable low-pass filter at C band. The filter is based on the theory of stepped impedance transmission line filters. The high impedance transmission line is equivalent to a series inductance. The low impedance transmission line is equivalent to a shunt capacitor, where we propose to use a MEMS shunt capacitor. The MEMS capacitors are combined in shunt with a high impedance transmission line to obtain the low-pass filter. The MEMS shunt capacitor can be used to tune the cut-off frequency.

Paper 5: Shimul C. Saha, Ulrik Hanke, Trond Sæther, "*Modeling, Design and Simulation of Tunable Band Pass Filter using RF MEMS Capacitance and Transmission line*", In Proceedings of Microelectronics: Design, Technology, and Packaging II, Vol. 6035, pp 60350-C1-C11 part of SPIE Symposium on Microelectronics, MEMS, and Nanotechnology, December 2005, Brisbane, Australia.

This paper describes the work on modeling, design and simulation of the MEMS tunable band-pass filter at C band. The filter uses a stepped impedance transmission line low pass filter as discussed in paper 4, with series capacitances to obtain band-pass filter characteristic. The filter has capability of tuning both the center frequency and the bandwidth. High capacitance ratio MEMS shunt and series capacitances are proposed for continuous tuning of the center frequency and the bandwidth. The filter is much more compact than traditional half wavelength filters. The design is done in ADS and a comparison is performed with high frequency structure simulator (HFSS) simulation.

Paper 6: Shimul Chandra Saha, Ulrik Hanke, Geir Uri Jensen and Trond Sæther, *"Modeling of Spring Constant and Pull-down Voltage of Non uniform RF MEMS Cantilever"*, In proceedings of 2006 IEEE International Behavioral Modeling and Simulation Conference, pp 56-60, September 2006, San Jose, California, USA.

This paper presents a novel model for the spring constant and the pull-down voltage of non-uniform cantilevers. The suspended beam is narrower close to the anchor and wider at the actuation area. This will reduce the spring constant and the pull-down voltage compared to a uniform beam. A comprehensive model for the spring constant is developed using the basic force-deflection calculation. The modeled pull-down voltage is compared with CoventorWare architect simulations and matches very well.

Articles submitted to journal:

Paper 7: Shimul Chandra Saha, Ulrik Hanke, Geir Uri Jensen and Trond Sæther, "*Modeling of Spring Constant and Pull-down Voltage of Non uniform RF MEMS Cantilever Incorporating Stress Gradient*", has been submitted to Sensors and Transducers Journal.

This paper is an extension of paper 6, and includes the effect of the stress gradient. The presence of a stress gradient in cantilever beams is very common. For a positive stress gradient the cantilever will buckle up and will have a gradual increase in the initial gap from the actuation electrode. This will increase the pull-down voltage, as it strongly depends on the initial gap. The model for the pull-down voltage including the stress gradient is presented and verified with CoventorWare analyzer Finite Element Method (FEM) simulation.

Paper 8: Shimul Chandra Saha, Ulrik Hanke, Geir Uri Jensen and Trond Sæther, "*Modelling of Spring Constant of a Non uniform RF MEMS Bridge*" has been submitted to International Journal of Modelling and Simulation (ACTA press/IASTED).

This paper presents a novel model for the spring constant and the pull-down voltage of non-uniform bridge. The suspended beam is narrower at the two ends, close to the anchor and wider at the actuation area. The model includes the residual stress and can be used for more general cases. A tensile stress will increase the pull-down voltage and its effect is dominant in the longer and thinner beams. A comprehensive model is developed using basic force-deflection calculation. The model is verified and agrees well with CoventorWare analyzer FEM simulations.

3.2: Development of various process steps for fabrication of the RF MEMS switches and switch circuits

The fabrication of the RF MEMS switches and switch circuits is done in SINTEF MiNa lab in Oslo, Norway. We had to develop all the process steps by ourselves, as RF MEMS had not been fabricated at MiNa lab earlier. From the fabrication point of view, a capacitive switch is easier to fabricate than a DC contact switch since it requires fewer process steps. Our main goal was to fabricate a workable device and the SINTEF IRRFT project also recommended capacitive shunt switches. So we planned to fabricate the capacitive switches, as a first prototype. There are some deviations in the dimension of the fabricated switches from the initially simulated switches, such as a reduced initial gap, a shorter beam length and a wider bridge. This is done in order to facilitate a successful fabrication of the switches and reduce the process complexity. A brief overview of the fabrication is described below.

A 280 μm thick 4" silicon wafer with 4-8 kΩ-cm resistivity was used as process wafer. A 0.5 μm thick oxide (SiO_2) was grown on the wafer using wet oxidation. Tungsten was used for the transmission line. Gold could also have been used, but due to possible contamination problems we had to use tungsten. A significant amount of stress was present in the sputtered tungsten (~1 GPa and compressive). This caused the tungsten to peel off from some of the wafers after sputtering and in some cases during nitride deposition. We therefore used a titanium adhesive layer to protect the tungsten from peeling off. To increase the probability of success, some wafers were sputtered with

aluminum as transmission lines. Also some wafers were processed without the oxide layer, as tungsten shows better adhesion to silicon than to the oxide. Plasma enhanced chemical vapor deposition (PECVD) Si_3N_4, a thickness of approximately 200 nm was used as the dielectric layer for the bridge capacitors. The measured thickness was slightly higher, 220 nm. HiPR 6517 was used as a sacrificial layer for the switch. The initial gap was 2.5 μm. A special baking method was used to tune the resist angle at the edge of the rising anchor. Gold DC sputtering was used for the suspended bridge with a thickness of approximately 1.1 μm. A thickness of 1.2 μm was also used for the second round of the fabrication. An elaborate experiment was conducted to develop a recipe for low tensile stress gold. A compressive stress will make the device useless and a high tensile stress will increase the pull-down voltage significantly. So a low tensile stress is preferable for low pull-down voltage and a reliable operation of the switch. After gold patterning, the switch was released by dissolving the sacrificial layer in Microposit 1165 using a method developed as part of the project. Finally the switches were dried in critical point dryer. A 3-D view of the capacitive switch and an illustration of the process flow are shown in Figures 3.1 and 3.2.

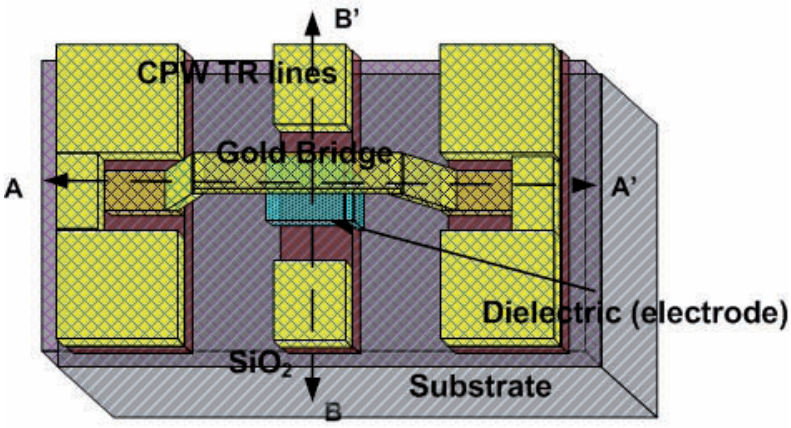

Figure 3.1 : A 3D view of the proposed fabricated switch

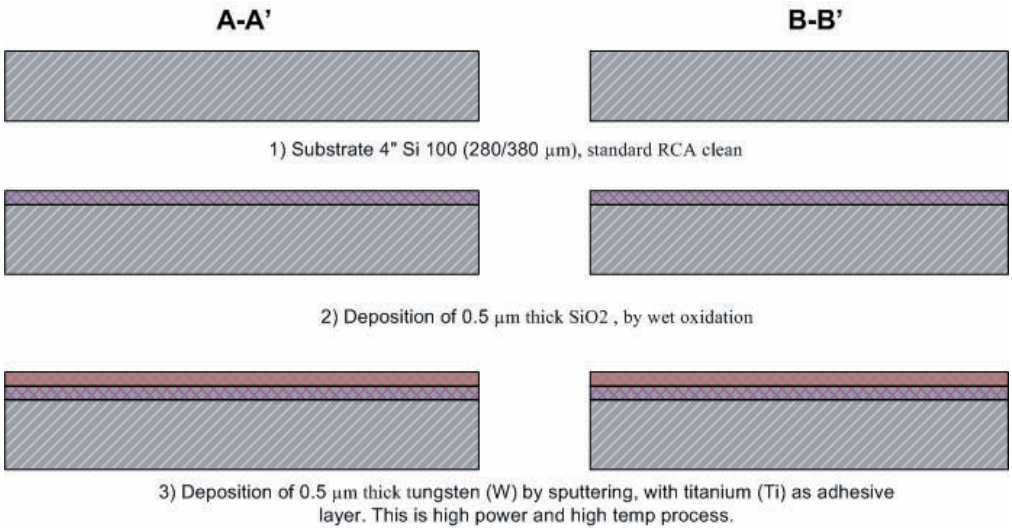
A-A'
B-B'
1) Substrate 4" Si 100 (280/380 μm), standard RCA clean
2) Deposition of 0.5 μm thick SiO2 , by wet oxidation
3) Deposition of 0.5 μm thick tungsten (W) by sputtering, with titanium (Ti) as adhesive layer. This is high power and high temp process.

4) Standard priming and coating of resist for patterning transmission line, in manual coater. HIPR 6517 is used to a thickness of 2.5 um.

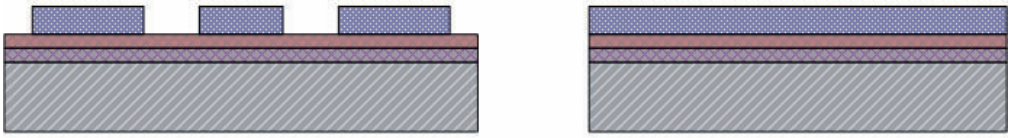

5) Expose the resist in automatic aligner and develop the resist in standard developer. Hardbake the resist in the oven to make the resist tougher for dry etching.

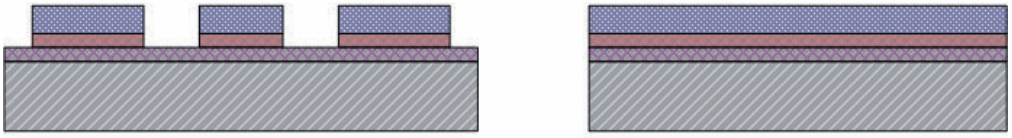

6) Dry etching the tungsten with standard recipe, to patteren CPW transmission line and actuation electrode

7) Remove the resist by acetone dip and plasma strip

8) Deposit the PECVD Si_3N_4 dielectric for actuation electrode. The deposited thickness is ~200 nm.

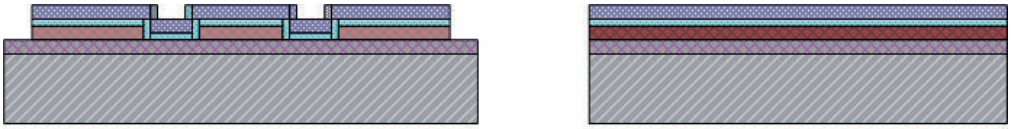

9) Priming and HIPR 6512 resist coating in automatic coater. The thickness is 1.5 um.

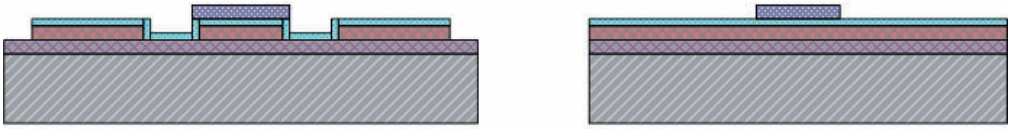

10) Expose the resist in automatic aligner and develop in standard developer. Hardbake the resist in oven.

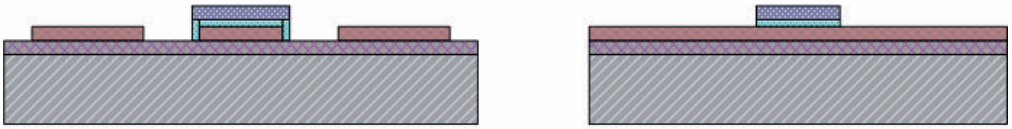

11) Dry etch the dielectric using standard recipe for nitride, to pattern the electrode

12) Remove the resist by acetone dip and plasma strip

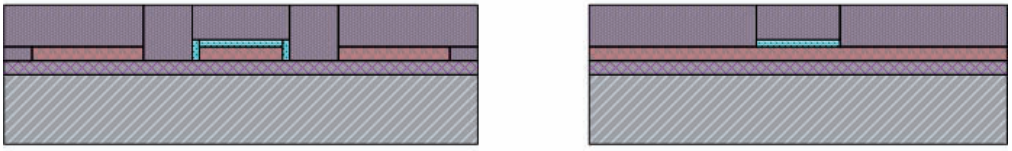

13) Spin and coat the sacrificial layer (2.5 um think, HiPR 6517 at 2000 rpm or Diluted AZ 4562 at 3250 rpm), The exact resist profile can be bit different due to differnt height

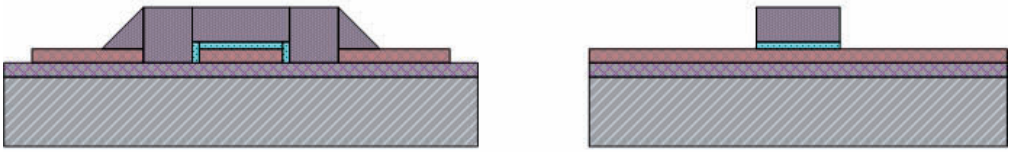

14) Expose the resist in automatic aligner and develop in standard developer (MF 312), to define anchor and keep the sacrificial layer. Special hardbaking is done on hotplate to tune the angle.

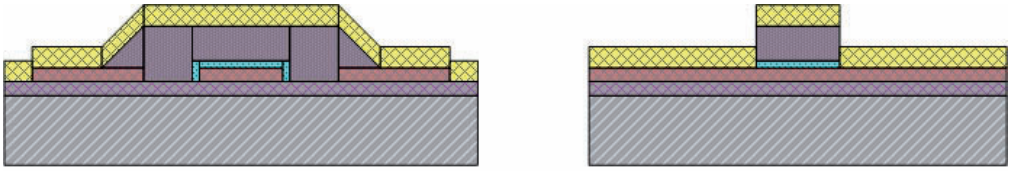

15) Deposit 1 μm thick Gold by DC sputtering. Very low power is used for sputtering to protect the sacrificial resist.

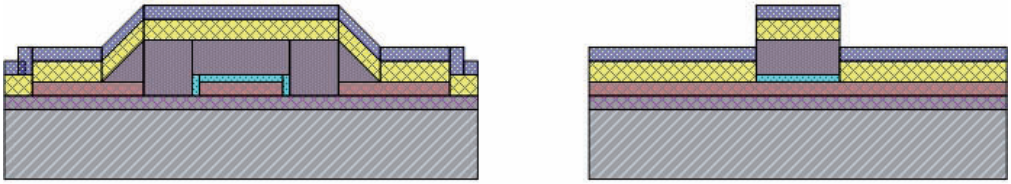

16) Prime and spin HIPR 6512 resist in manual coater in gold line.

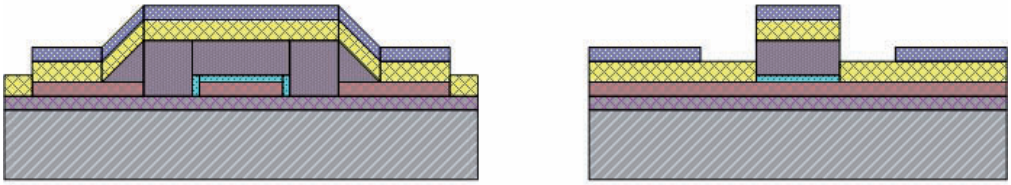

17) Expose the resist in manual aligner and develop the resist to define bridge and additional TL. The resist is hardbaked in oven.

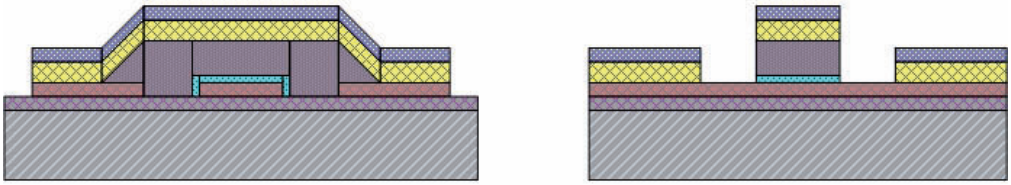

18) Etch away the gold except the beam and additional TL region, by potassium iodide wet etch

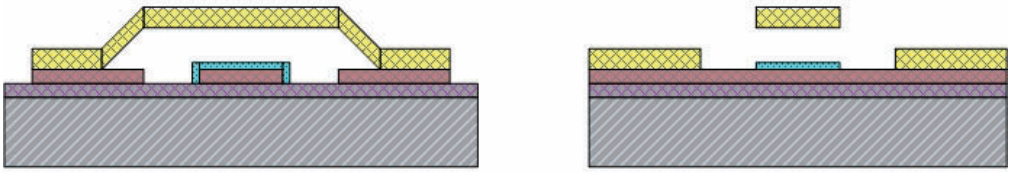

19) Strip the resist, by plasma strip and microposit 1165 solution. Dry the sample in CO_2 critical point dryer.

Figure 3.2: The cross section side view of the process flow.

The fabrication work of the thesis is based on the following published articles.

Paper 9: Shimul Chandra Saha, Håkon Sagberg, Geir Uri Jensen, and Trond Sæther, "*Tuning of Resist slope for RF MEMS with hard baking parameters"*, In proceedings of 19th international Microprocess and Nanotechnology Conference (MNC 2006), pp 314-315, October 2006, Kanagawa, Japan.

This paper presents the works on tuning of the resist slope by hardbaking parameters. A photoresist is used as a sacrificial layer in the fabrication of the RF MEMS switches. In order to reduce the number of process steps, a climbing anchor is chosen over a vertical anchor. In order to obtain a thick enough gold layer at the anchor positions during the sputtering, the resist angle should be close to 45°. Hardbaking parameters like the hotplate temperature and the baking time can be used to tune the resist angle. We have shown that the baking temperature and time can be chosen in an optimum way to tune the resist angle.

Paper 10: Shimul Chandra Saha, Håkon Sagberg, Erik Poppe, Geir Uri Jensen, Tor A Fjeldly and Trond Sæther, *Tuning of resist slope with hardbaking parameters and release methods of extra hard photoresist for RF MEMS switches*, *Journal of Sensor and Actuators A*: Phys. Vol. 142 (2), pp 452-461, 2008.

This paper describes the work on tuning of the resist slope and the release methods for RF MEMS switch. For a climbing anchor, a slope close to 45° in the sacrificial resist is preferred. The resist angle can be tuned by the baking parameters. In order to release the MEMS switches, the sacrificial resist needs to be dissolved completely. It is not easy to dissolve the sacrificial resist by anordinary acetone dip. We have also used Microposit 1165, which is specially suited for dissolving the hard resist. It is found that some residue is still left after the Micorposit 1165 dissolution and drying. We have developed a special method to release the RF MEMS switches successfully without any residue left. The resist can be dissolved by an initial short plasma strip and then Microposit 1165 with heating.

Paper 11: Shimul Chandra Saha, Håkon Sagberg, Erik Poppe, Geir Uri Jensen, and Trond Sæther, *Metallization scheme and release methods for fabrication of RF MEMS switches*, In proceedings of 33rd Micro- and Nano- Engineering conference (MNE 2007), September 2007, pp 773-774, Copenhagen, Denmark.

This paper presents the metallization scheme and release methods for the RF MEMS switch. Residual stress in the suspended bridge plays a significant role in the reliability and the pull-down voltage. If a reasonably high compressive stress occurs, the bridge will be useless. A high tensile stress will significantly increase the pull-down voltage. We have performed several sputtering experiments in terms of sputtering parameters to develop a recipe for low tensile stress gold for the suspended beam.

3.3: Measurement of the fabricated RF MEMS switches and switch circuits

We have successfully fabricated the shunt capacitive switches and MEMS tunable filters. The filters measurement results are submitted and in process of submission to journal. The measurement work of this thesis is described in the following, submitted and published papers and memo.

Paper 12: Shimul Chandra Saha, Ulrik Hanke, Håkon Sagberg, Tor A. Fjeldly, Trond Sæther, *Tuneable Low-Pass Filter from C to X band with RF MEMS Capacitance and Transmission line*, has been submitted to *Microelectronics Journal*.

The paper presents a tuneable low pass-filter. The filter is based on the stepped impedance transmission line theory as presented in papers 4 and 5. A filter with high capacitance ratio switch is proposed. For verification a filter with simple parallel plate capacitors is fabricated. The tuning of the cut-off frequency can be obtained by actuating different combinations of parallel shunt bridges. A comparison between the simulations and measurement results is also performed.

Paper 13: Shimul Chandra Saha, Ulrik Hanke, Håkon Sagberg, Tor A. Fjeldly, Trond Sæther, *Tunable Band-Pass Filter at C band with RF MEMS Capacitance and Transmission line*, has been submitted to Journal of European Microwave Association (EuMA).

The paper presents a tuneable band-pass filter. The filter is based on the stepped impedance transmission line theory as presented in paper 5. The filter has the possibility of both tuning the centre frequency and the band width. The tuning of the centre frequency can be obtained by tuning the shunt capacitors. The tuning of bandwidth can be obtained by tuning the series capacitors. For verification, a filter with simple parallel plate capacitors is fabricated. The tuning of the centre frequency and bandwidth can be obtained by actuating different combinations of parallel shunt bridges and series cantilever. A comparison between simulations and measurement results is also performed.

M 14: Memo: Measurement results for the capacitive shunt switches from fist round of fabrication are presented. The pull-down voltage is measured for a range of switches with different widths and lengths. Some SEM and optical images are included in the memo. A brief description of reliability, like the number of successful operating cycles, and the charge stiction, is also presented. An article describing the switch fabricated in the 2nd round is accepted in MEMSWAVE 2008.

Paper 15: Bengt Holter, Karsten Husby, Håkon Sagberg, Geir Uri Jensen, Ulrik Hanke, Shimul Chandra Saha, *A capacitive shunt RF MEMS switch for coplanar waveguide transmission lines*, ***In press,*** MEMSWAVE 2008, 30th June -3rd July 2008, Crete, Greece.

This paper describes measurement results of the capacitive shunt switch fabricated in second round, for SINTEF IRRFT project. The process parameters are almost identical to the first round except the thickness of the substrate and the suspended bridge. The thickness of the substrate is 380 µm instead of 280 µm used in first round. The

thickness of the gold bridge is 1.2 μm. The paper presents the reliability test and life cycles of the switch. RF performance of the switch like insertions loss and return loss in upstate and isolation in downstate is also presented.

4. Discussion

This thesis presents design and fabrication works on RF MEMS switches and switch circuits (MEMS tunable filters) for RF front end applications and CMUT switching. Modeling, design and simulation of various kinds of RF MEMS switches and MEMS tunable filters are performed. A high speed switch (switching time from upstate to downstate), is considered for CMUT switching between the transmitter and receiver block. For CMUT applications, a switch with dimensions 50 µm × 20 µm will be convenient considering miniaturization and integration. A DC contact switch will be appropriate for this kind of switching as the operating frequency for CMUT is in the range of several tens of MHz (30 MHz). For the initial design, switches with larger dimensions are simulated. The capacitive contact switch is simulated instead of a DC contact switch. In the simulations, the switching time is considered primarily in terms of beam material, packaging pressure and environment and beam structures like bridges or cantilevers. The actuation voltage is also considered, which obviously reduce the switching time with increasing value. The capacitive contact switch can be converted to a DC contact switch, by introducing a separate contact point other than the actuation electrode. This can be done both for bridges and cantilevers. Possible ways of designing a DC contact switch from a capacitive contact switch are shown in Figures 4.1, 4.2 and 4.3.

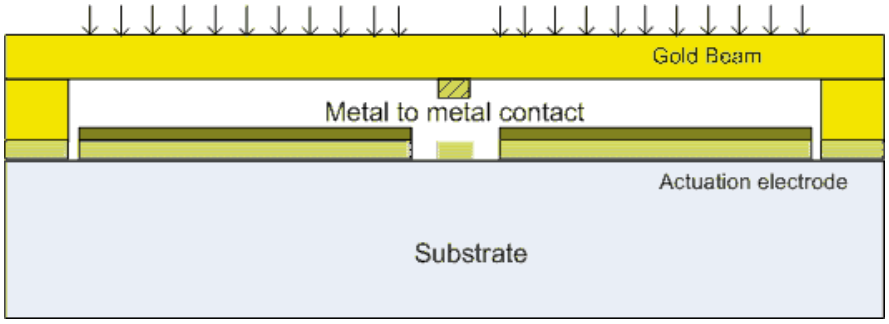

Figure 4.1: A side view of a bridge DC contact bridge. A metal to metal contact point is formed by introducing a gap in the electrical actuation electrodes.

From the figures it can be seen that the switch can be converted easily by modifying the actuation mechanism slightly and introducing a DC contact point. The contact point can

be formed at the middle (bridge) or at the end (cantilever) of the beam. The switching time will change slightly with actuation voltage due to the rearrangement in the actuation electrode. The fabrication process for the DC contact switches will be more complex and will require some more process steps than capacitive contact switches. In order to design a miniaturized switch with a similar actuation voltage and switching time, it is possible to use a reduced initial gap, a thinner beam and a non-uniform or folded spring type suspended beam.

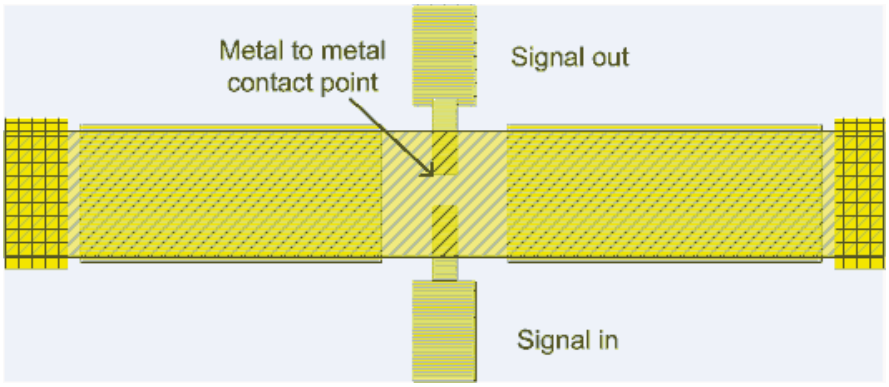

Figure 4.2: The top view of a bridge DC contact switch. The DC contact is formed between the signal in and the signal out electrodes when the beam moves down.

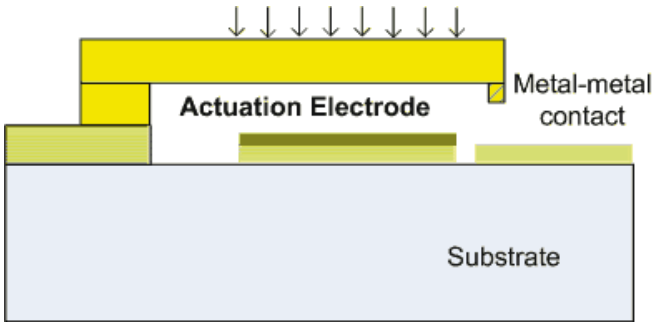

Figure 4.3: The side view of a cantilever DC contact switch. The DC contact can be formed by extending the suspended beam beyond the actuation electrode.

The spring constant 'k' for a typical bridge is mentioned in equation 4.1. In this equation 't' is the thickness of the beam and 'L' is the length of the beam. 'E' is the Young's modules and 'w' is width of the beam. It can be seen that the spring constant significantly depends on beam length and thickness. The spring constant of the uniform and shorter beam will increase significantly as it is inversely proportional to the 3rd power of the length (L^3). The pull-down voltage for a typical bridge or cantilever is given by equation 4.2 and y=1 for uniform beam case. Here 'g_0' is the initial gap and 'L_e' is the length of the electrode. The spring constant and the pull-down voltage can be reduced significantly by reducing the thickness of the beam. Also a reduced initial gap will reduce the pull-down voltage. A non-uniform beam (narrower at the anchor and wider at the actuation area) or a folded spring type beam will also reduce the pull-down voltage.

$$K = 32Ew(t/L)^3 \frac{1}{8(x/L)^3 - 20(x/L)^2 + 14(x/L) - 1} \qquad 4.1$$

$$V_p = \sqrt{\frac{8kg_0^3}{27\varepsilon_0 L_e wy}} \qquad 4.2$$

The folded part of the beam can be simplified to a longer beam, which is narrower than the actuation electrode. This beam can be modeled as a non-uniform beam. So the model of the spring constant and the pull down-voltage of the non-uniform beam will be a very useful tool for predicting the pull-down voltage. The model is verified with well known commercial tools like CoventorWare and shows that the model is very accurate. It would be better if we could have verified the model with experimental results. However, no such data were available.

For the SINTEF IRRFT project front end circuits, a capacitive shunt switch with a high capacitance ratio is desired. The operating frequency for these circuits is 10 GHz to 32 GHz. A shunt switch with an initial gap of 3.75 μm is designed. Si_3N_4 is used as a dielectric with a thickness 100 nm. The beam length for a reasonable pull-down voltage

(15-30 V) is 600 μm with a thickness of 1 μm. From the simulation it is found that this switch can provide a capacitance ratio of 180 which is desirable. A bridge with smaller length and reduced initial gap is fabricated to increase the probability of success. The reduced gap is used, to have a reliable anchor at the rising part of the beam. Also a thicker dielectric is used to reduce the probability of breakdown during electrostatic actuation.

Tunable low-pass and band-pass filters are designed at C to X band for RF front end applications. Stepped impedance transmission line theory is used to design the filter. High capacitance ratio MEMS shunt capacitors are proposed to tune the cut-off and center frequency. This will facilitate a continuous tuning instead of stepwise tuning. For fabrication, ordinary parallel plate capacitors are used as tuning element. This is done in order to reduce the process complexity for the initial prototype and for verification of the RF characteristic of the filters. Stepped impedance filters are more compact than traditional half-wavelength band-pass filters.

A significant amount of the time was spent on process development and fabrication of RF MEMS switches and switch circuits. As SINTEF IRRFT project required a capacitive contact switch, our initial plan was to fabricate a capacitive contact switch. From the process point of view, capacitive contact switches require fewer process steps than DC contact switches. As the process for RF MEMS switches is new in the MiNa lab, we had to develop all the process steps ourselves. It was not straightforward and all the process steps had some peculiarity and difficulty to make them work properly.

We had to use tungsten as a transmission line. We could not use gold in the main clean room because of a potential contamination problem. Although it looks very straight forward to deposit tungsten on Si or SiO_2, it was not that easy. The tungsten has a very high melting point, requiring a relatively high power to eject atoms from the target. The residual stress in the deposited tungsten is very high, in the range of 1.0 GPa and compressive in nature. This high stress makes the wafer buckle significantly. This leads to peeling of the tungsten from some of the wafers. Also it is found that the peeling is

higher in the wafer with oxide than in the bare silicon wafer. In order to avoid the peeling, we had to use titanium (Ti) as an adhesive layer.

It is also found that even if the tungsten survives after sputtering, it may peel off during the dry etching. In some wafers, when we deposited liquid phase chemical vapor deposition (LPCVD) nitride on top of tungsten, most of the tungsten peeled off due to high temperature. So we had to deposit plasma enhanced chemical vapor deposition (PECVD) nitride, instead of LPCVD nitride as dielectric. The nitride deposition was somehow less complicated, except the peeling off the tungsten. The etching of nitride was rather complicated. The standard recipe for nitride etch contains SF_6, which also etches the tungsten. It is found that the underlying tungsten etches much faster than the Si_3N_4. So we had to use a different recipe, with a gas mixture without SF_6. In order to increase the probability of successful fabrication, we also used aluminum in a few wafers as transmission line. Aluminum is a soft metal and it has the problem of forming bumps during subsequent high-temperature processes, like nitride deposition. This will reduce the downstate capacitance significantly.

The tuning of the resist slope for the climbing anchor was an important part of this fabrication work. Although it was somewhat time consuming, the experiment was quite straightforward. First we had to choose a suitable exposure power and exposure gap. Exposure parameters, especially the exposure gap has a significant effect on the resist slope. It was not very convenient to change the lamp power and exposure gap, so we chose the standard exposure parameters used by the MiNa lab. We used the hotplate instead of an oven to tune the resist angle. The hotplate has much faster heating capability and better controllability. To tune the resist angle we varied the baking temperature and the baking time. After some experiments and inspection in SEM, it was found that the resist angle can be tuned in an optimum way using baking temperature and time.

After the sacrificial layer patterning, gold was sputtered to form the suspended beam. A significant amount of experiments was performed on gold sputtering, to develop a

reliable recipe. A compressive stress will buckle the bridge upward or downward. For a relatively high amount of compressive stress, the bridge will be useless. A small amount of tensile stress is preferable for a reliable operation. The higher amount of tensile stress will significantly increase the pull down voltage.

Initially we used a power of 1500 watts for the DC sputtering of gold. A significant amount of heat was produced in the chamber which was enough to burn all the sacrificial resist. So a high power was not possible to use, for our application. We used a very low DC power (500 watts) for gold sputtering and it was not possible to vary the power to tune the stress. We had to vary only the sputtering pressure to control the residual stress in the sputtered gold. We have developed different test structures for stress characterization. Bridges were used for characterizing the compressive stress, Guckel rings were used for the tensile stress and cantilevers were used for the stress gradient. A negative stress gradient was present in all cases. There were slight uncertainties in the stress characterization due to the stress gradient. Using CoventorWare and Guckel rings we characterized the stress. The experiment showed, a tensile stress was present for all the cases and for higher pressure a lower tensile stress were found. Later a strain gauge was also designed and fabricated, and showed the presence of tensile stress in the sputtered gold.

After that the gold was patterned in the gold line of MiNa lab. Although all the tools are old and manual they worked satisfactorily for the process. Gold was etched in potassium iodide solution. The process was very convenient although we had to check the etching rate. The release was somewhat more complicated. We used acetone in the beginning to dissolve the resist. After drying we found that some threads and residue are left on the substrate. Later we used Microposit 1165, which is specially used to dissolve hard resist. We kept the samples in the solution for a longer time including overnight with stirring. After drying we still found some resist residue left. So we had to develop our own method. We used plasma strips to ash the initial skin, or tough parts of the resist. Then we used Microposit 1165 with heating and stirring. After drying we found that the switches were fully clean and no residues were left. For drying, we used a CO_2 critical point dryer. This is a very standard procedure to release RF MEMS switches without

stiction. Also I had some experience from my Master's thesis on RF MEMS release using critical point dryer, hence this method was very convenient to use for us.

As mentioned earlier, our initial goal was to fabricate a capacitive shunt switch. It was a priority also, to realize a workable switch rather than to have a switch with precise specifications. So there were some deviations in the fabricated switches from the switch proposed in paper 3. The initial gap of the fabricated switch was 2.5 μm, instead of 3.75 μm used in the simulation. It is slightly complicated to obtain a thicker sacrificial layer. Also a thicker sacrificial may cause a thinner bridge at the rising part of the anchor and will reduce the reliability of the switch. The length of the bridge is also reduced compared to the simulated bridge, although a range of different lengths are used for fabrication. Although a shorter bridge will increase the pull-down voltage significantly, the reduced initial gap will also reduce the pull-down voltage to some extent. A thicker dielectric ~220 nm is deposited instead of 100 nm used in simulation. This was done in order to reduce the probability of breakdown due to the higher actuation voltage. The tensile stress was reasonably low (~ 30-40 MPa), so the pull-down voltage was not very high. In fact the pull-down voltage was in the range of 15-20 volts for most of the switches, even lower than the expected value.

The S parameters for the switches are measured in a vector network analyzer at NTNU. The insertion loss and reflection coefficient were very good until 32 GHz. The isolation was somewhat lower than expected. The main reason is the thicker nitride, which will reduce the downstate capacitance. Also due to planarity and roughness issues, the capacitance will be somewhat lower than expected. It is also found that the switch has a stiction problem. A test is conducted with bipolar actuation, and it is found that the switches operate until 300000-400000 cycles successfully before they stick to the bottom electrode. For a thicker gold bridge (second round, 1.2 μm) the number of successful operating cycles was more than 1.000.000 cycles, although a higher pull down voltage (30 volt) was required for actuation. It is also found that if the pulse width is reduced, the number of operation cycles increases. This gives us an indication of charge stiction, which is very common in capacitive contact switches. The test is conducted in an ordinary clean room, which may increase the probability of stiction due

to contamination and vapor. SINTEF is now conducting some more tests to identify and solve the major issues responsible for the stiction. A test setup in a nitrogen chamber is planned to make sure that vapor or other contamination may not cause the stiction. Also an additional anchor on top of the gold bridge is planned for later fabrication, to reduce the probability of stiction during actuation.

The tunable filters were fabricated with the same process parameters as the capacitive shunt switches. A number of parallel bridges are used for shunt capacitors. Also a number of parallel cantilevers were used for series capacitors. The change in the shunt capacitance was obtained by actuation different numbers of bridges. As a negative stress gradient was present in the cantilever, different sets of cantilevers were used for different designs. If the cantilever is already downstate due to the stress gradient, it will be not possible to change the capacitance by actuating different cantilevers. The first round of measurements was very interesting and gave a proper validation of the simulation results. The measured filters were with an aluminum transmission line. Although the downstate capacitance is somewhat smaller due to bumps in the metal, still very good results were obtained. We also got some measurement result with tungsten transmission lines. The wafers with the tungsten transmission lines suffered significant over-etch in the suspended beam and the capacitance value was reduced drastically. The cut-off and center frequency shifted to some extent (2-3 times than expected). The measurement results of the filter with aluminum transmission lines showed very good match with simulation results considering the fabrication issues.

5. Conclusions

In this work, novel RF MEMS tunable low pass and band pass filters are designed and fabricated. A new model for non uniform bridge and cantilever is also presented. We have developed the first RF MEMS switch ever to be produced in Norway, making it pioneering work in Norway. The switch reliability and RF performances are very promising compared to the present state of art work published recently else where. Some other research groups at different universities and research organization already started working on RF MEMS in Norway. This work will give a valuable input for the RF MEMS research community in Norway including NTNU and SINTEF and international community.

This thesis presents design and fabrication of RF MEMS switches and MEMS tunable filters. Modeling and simulation of high-speed switching and comparison between bridge and cantilevers is performed. A high capacitance ratio shunt capacitive switch is also designed and simulated. A switch is proposed for the desired specifications with reasonable pull-down voltage. Design and simulation of tunable low-pass and band-pass filters are also performed. The tuning of cut-off and center frequency and also bandwidth can be obtained by actuation of different combinations of shunt and series capacitances. A significant amount of work is performed on the process development. As the process for RF MEMS switch is new in the MiNa lab, we had to develop all the process steps by ourselves. The metallization of the transmission line and the suspended beam required special efforts. After several experiments and evaluations, we developed a successful method for tungsten sputtering for the transmission line. We also proposed a recipe for low-stress planar gold for the suspended beam. A special method to release the RF MEMS switches is also developed. The fabricated shunt switch has slightly different dimension, specially reduced gap and thicker dielectric, than the simulated switch. The S parameters of the switches are measured at NTNU using a vector network analyzer. The measured results of the first prototype look very promising. The pull-down voltage is also within a reasonable limit around 15-20 volts for most of the switches. The pull down voltage for second version of the switch (1.2 μm thick suspended beam) is around 30 volts. The filters are also measured in the vector network

analyzer. Although the cut-off and center frequency shifted slightly toward higher frequencies, the measured result shows very good agreement with theory. The comparison of measurements results with simulations, considering the process constraints, agrees quite well.

Correction lists

1) Considering the scope and editorial board advice Paper no 7 is submitted to Sensors and Transducers Journal
2) Considering the scope and editorial board advice Paper no 8 is submitted to International journal of modeling and simulation (ACTA press).
3) The Final version of Paper no 15 (4 pages) is modified and updated according to conference review committee.

DESIGN AND SIMULATION OF RF MEMS SWITCHES FOR HIGH SWITCHING SPEED AND MODERATE VOLTAGE OPERATION

Shimul Chandra Saha, Tajeshwar Singh, Trond Sæther

Department of Electronics and Telecommunications, Norwegian University of Science and Technology (NTNU), 7491 Trondheim, Norway
E-mail: shimul.saha@iet.ntnu.no

In proceedings of IEEE PRIME 2005, pp 207-210, July 2005, EPFL, Lausanne, Switzerland.

DESIGN AND SIMULATION OF RF MEMS SWITCHES FOR HIGH SWITCHING SPEED AND MODERATE VOLTAGE OPERATION

Shimul Chandra Saha, Tajeshwar Singh, Trond Sæther

Department of Electronics and Telecommunications, Norwegian University of Science and Technology (NTNU), 7491 Trondheim, Norway
E-mail: shimul.saha@iet.ntnu.no

ABSTRACT

In this paper we present the design and simulations of an RF MEMS switch with regard to its switching speed and pull-down voltage. The switch is required to fulfill the requirements of high speed and a moderate pull down voltage for the switching of CMUT (Capacitive Micromachined Ultrasonic Transducer) elements used for ultrasound imaging

1. INTRODUCTION

The objective of this paper is to present the design of a high speed RF MEMS switch. MEMS are nowadays becoming increasingly popular in RF applications due to their attractive advantages such as high isolation and low insertion loss. Depending on the switch type (DC contact or capacitive), the MEMS switches can show very good RF performance from DC to several tens of GHz. However, there are two sides for this coin too; there are also some disadvantages of the RF MEMS switches, as compared to their solid-state counterparts, which include high pull-down voltage and slow switching speed. In this paper it is shown that by a careful design, a compact switch with a moderate applied voltage can be optimized for the switching speed (<5μs).

2. MOTIVATION

CMUTs are an upcoming technology in the field of Medical Imaging which promises to offer advanced automation possibilities. It will also offer, unlike the conventional piezoelectric transducer probes, compatibility with the CMOS process and integration of the signal processing circuitry on the probe itself, thus drastically reducing the hard-wiring of the probe to the signal processing console. The possibility of signal processing near the transducers opens new prospects of 'Smart probes' capable of handling large amount of data, required for example, for 3D ultrasound imaging. Another imaging application of the CMUTs is in the detection of plaque inside the coronary for an early heart disease diagnosis.

The active part of a CMUT is usually a metal coated Si_3N_4 which forms the top membrane/electrode. A highly doped silicon substrate constitutes the bottom electrode. When a DC bias voltage is applied between the top and bottom electrodes, the membrane is pulled towards the substrate (electrostatic actuation). If an AC voltage is applied along the bias point, a harmonic motion is obtained; thus the membrane will generate AC detection currents. As in piezoelectric ultrasound probes, there are two modes of operation namely, transmit, and receive. CMUT elements require to be switched ON and OFF at different times either to send the actuation signal, or to receive the reflected signal. Hence it is necessary to have a switching matrix to switch the elements from transmit mode to receive mode. As the actuation signal is low, it is necessary to have a low insertion-loss and very good isolation of the switching matrix, for which an RF MEMS switch is a good candidate. However as the vein radius is small, the time of flight of the signal to travel to the vein wall and back to the catheter surface is very short. Thus it is necessary to design the switch with very short switching time. For our design we target for a switching time, (to switch from the up-state to down-state) <5μs which is 3-6 times lower compared to 15-30μs shown by the present designs, for example [2][3] operating at similar actuation voltages (15-25V) .

3. DESIGN AND SIMULATION

We consider a very simple RF MEMS capacitive switch for our design. The structure is a Fixed-Fixed beam using electrostatic actuation. The beam material is chosen to be Aluminum because it has a moderate Young's modulus which favors lower actuation voltage at a smaller switch size. Selecting a metal membrane also means simple fabrication

process. Preliminary simulations for switching time & pull-down voltage were done with Mathematica®. The pull-down voltage V_p and switching time t_s of the bridge are given by [1][3]:

$$V_p = \sqrt{\frac{8 \cdot k \cdot g^3}{27 \cdot \varepsilon_0 \cdot W \cdot w}} \quad (1)$$

$$t_s = \frac{V_p}{\omega_0 \cdot v_S} \sqrt{\frac{27}{2}} \quad (2)$$

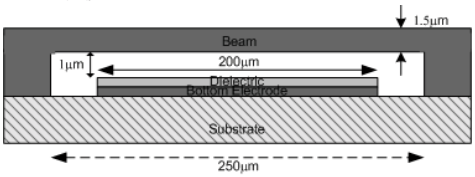

Figure 1: The capacitive bridge

The actuation voltage V_s is selected slightly higher than the pull-down voltage calculated in (1), to increase the switching speed. The proposed switch is shown in Fig. 1.

The dimensions of the beam are $250\mu m \times 40\mu m \times 1.5\mu m$, the bottom electrode is $200\mu m \times 40\mu m$, and initial gap $g_0 = 1\mu m$. From the simulations in Mathematica®, a pull-down voltage of 12V is obtained. Hence, with an actuation voltage of 15V, which is of the order of the present state-of-the-art (10-15V), pull down time of $t_s \approx 2.9\mu s$ is obtained, which is around 10 times lower than reported results [2]. Final device simulations were done in Coventorware®. The switching time and actuation voltage is shown on the Table 1. For comparison, the Gold beam is also simulated and as we can clearly see that the switching time is more than 2.5 orders better for *Al* than for *Au* for the same actuation voltage. The switching time (transient) and pull down voltage simulations are shown in Figure 2 and Figure 3 respectively.

Table 1: The switching time for the switch with Q≈1

Material	Pull down voltage (V)	Actuation voltage(V)	Switching time (μs)
Aluminum	11	12	4.90
Aluminum	11	15	2.95
Aluminum	11	20	1.85
Aluminum	11	25	1.40
Gold	12	15	7.55

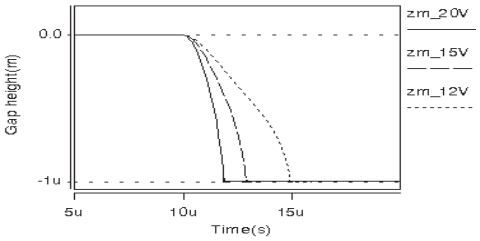

Figure 2: Switching time simulations for *Al* beam with 10μs pulse delay and Q≈1

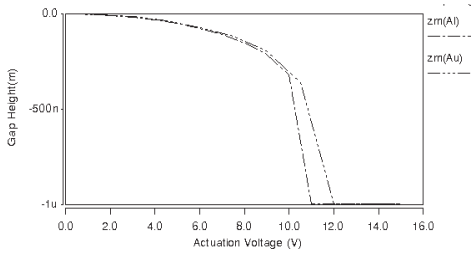

Figure 3: Pull down voltages for *Al* and *Au* beams.

3.1 The damping and the Quality factor

The damping (dominantly squeeze film damping) plays an important role in the switching time of MEMS switches (Equation 3). Within small gap heights, as in MEMS devices, the gaseous medium acts like a viscous liquid. During switch actuation when the beam moves down, the gaseous medium present within the gap must be pushed out and the molecules undergo several collisions between the beam and electrode [3]. The viscosity of the medium and in turn the quality factor can be controlled by reducing the pressure of the switch medium through packaging. The equations (4-7) for effective viscosity are shown below [3].

$$m \frac{d^2 z}{dt^2} + b \frac{dz}{dt} + kz = F_{total} \quad (3)$$

$$\lambda_a = \frac{p_0}{p_a} \lambda_0 \quad (4)$$

$$K_n = \frac{\lambda}{g} \quad (5)$$

$$\mu_e = \frac{\mu}{1 + 9.638 \; K_n^{1.159}} \quad (6)$$

Where λ_a is the mean free path at pressure p_a. g is the gap height and K_n is the Knudsen number. K_n is a measure of viscosity of the gas under MEMS

beam. μ_e is the effective viscosity, a function of the Knudsen number. A high Knudsen number means low effective viscosity and the gas experiences few collisions and the flow is not viscous anymore. So by reducing the pressure of the medium (vacuum) the viscosity can be reduced and the switching speed increased.

The effective damping coefficient can also be reduced by having perforations in the moving plate. The equations for damping without, and with perforations on the beam are given in Equation (7) and Equation (8) respectively [3, 4].

$$b = \frac{3}{2\pi}\frac{\mu A^2}{g_0^3} \quad (7)$$

$$b_h = \frac{12}{N\pi}\frac{\mu A^2}{g_0^3}\left(\frac{p}{2} - \frac{p^2}{8} - \frac{\ln(p)}{4} - \frac{3}{8}\right) \quad (8)$$

Here, N is the number of holes; p is the fraction of open area in the plate. From Equation (8) it can be seen that by having perforations in the membrane, the damping coefficient can be reduced significantly. This option widely used because even by having the perforations, the upstate capacitance is not affected because the fringing fields 'fill' the empty space.

The beam was simulated with different values of Quality Factor 'Q' (Equation 9) which depends on damping i.e. mainly gas damping and modal damping 'D' ($D=a\cdot M+b\cdot K$, where 'M' is the mass of the beam and 'K' is the beam spring constant, 'a' and 'b' depend on the damping medium and the beam structure). Q was varied from 0.05 to 10 and for different actuation voltage.

$$Q = \frac{k}{\omega_0 b} \quad (9)$$

Thus, Q can be easily controlled by adjusting the damping coefficient which in turn decides the switching speed. As the gap height is low, the obtained Q is very low ≈0.05 under normal condition (atmospheric pressure, no perforations).

Figure 9 shows the 3-D view of a beam with 80 holes (4×4 μm^2) for which Q≈1 was easily obtained at normal pressure. The same value of Q can be obtained without perforations by reducing the pressure equal to ≈1/30th of the atmospheric pressure. For further increasing the Q, both options can be combined (perforations and low pressure), a Q≈5 was thus obtained with perforations and at 1/7th atmospheric pressure. Figures 4 and 5 show the switching time for actuation voltages 15V and 25V respectively, for different Q. It can thus be seen that at very low Q (high viscosity), the switching time is very large. Note from Figure 4 that very high Q also leads to a higher settling (release) time.

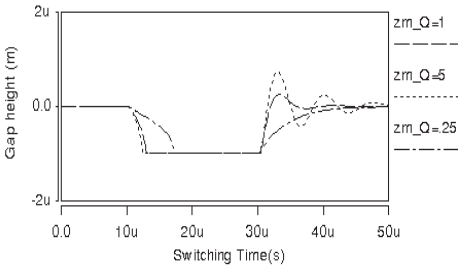

Figure 4: The switching and release time for V_a =15 V for different values of Q.

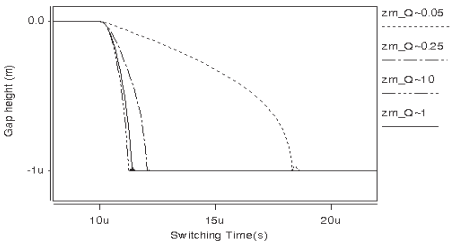

Figure 5: The switching time for actuation voltage 25 V for different Q.

At a higher Q the switching (pull down) time improves but increasing Q beyond 1 or 2 does not reduce the switching time much as compared to the reducing medium viscosity. So Q≈1-2 may be a fair choice for high speed switching. It can also be seen that at substantially higher Q≈10 and actuation voltage of 25V, the switching time is 1.25µs, which is very fast compared to the present technology [2, 3].

3.2 The residual stress consideration

One of the main concerns in the Fixed-Fixed beams is the residual stress. It can result in changes in the pull down voltage and in extreme cases render the structure useless. The residual stress usually arises form the process conditions and can be minimised by controlling the process parameters. It is possible to see the effect of residual stress on the switching time. When residual stress increases, it adds to the spring constant, thus the resonant frequency increases (ω_0=k/m) which reduces the switching time. Figure 6 shows the comparative study of resonant frequency with residual stress for our beam.

As seen, when the residual stress increases, the resonant frequency increases, which reduces the switching time. Thus care must be taken that the

residual stress does not exceed the limits because if the pull down voltage exceeds the desired actuation voltage then the beam cannot be switched.

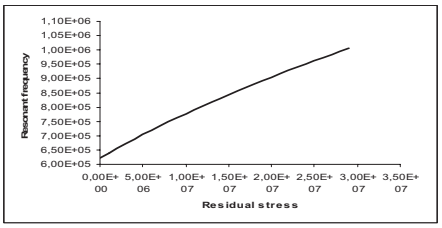

Figure 6: The resonant frequency vs. residual stress.

3.3 Different beam lengths

The effect of varying the beam length is investigated. For longer beams, the spring constant *k* decreases thus the resonant frequency and the actuation voltage are both reduced. This has a mixed effect on the switching time. Figure 7 shows the switching times for different beam length.

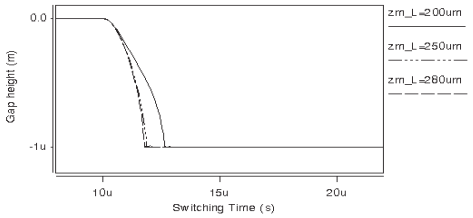

Figure 7: The switching time for actuation voltage 20 V for different length and Q≈1.

We choose an actuation voltage of 20V as the pull down voltage for the 200µm switch is more >15V. From Figure 7 it can be seen that from 200µm to 250µm there is a considerable improvement in the switching time but from 250µm to 280µm the switching time does not improve much. So it is not worth increasing the beam length further, to maintain the compactness.

3.4 The S-parameters

The simulation for the S- parameters is shown in Figure 8. The switch transmits the signal (ON state) while in upstate and the signal is capacitively grounded (OFF state) when the beam is in the downstate. It can be seen that we get an insertion loss less than 1dB in upstate position and have more than 15 dB isolation in the down state position for typical operating frequency range (>10 GHz) for a capacitive switch and more than 25 dB at higher frequency. The isolation can be improved by using high dielectric constant materials as shown below.

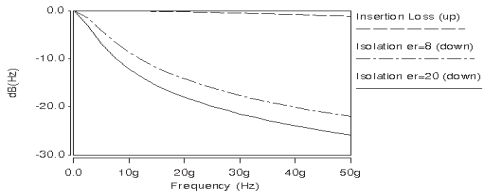

Figure 8: The isolation and the insertion loss in dB.

4. CONCLUSIONS

We have shown the design of an RF MEMS switch with a high switching speed at moderate actuation voltage. Switching speed increases with actuation voltage but we have a limitation on the maximum actuation voltage. Damping affects the switching speed and can be controlled by perforations on the beam and by regulating the medium and pressure. Detailed effect of *Q* and damping was shown in section 3.1. The switches will be fabricated in the SINTEF, MiNaLab, Oslo.

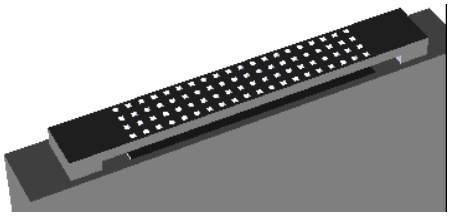

Figure 9: A 3-D view of the beam with perforation.

5. ACKNOWLEDGEMENT

Authors are grateful to Norwegian Research Council for sponsoring the work through SMiDA project (No 159559/130).

6. REFERENCES

[1] J.B. Mauldavin, Nonlinear Electro-Mechanical Modeling of MEMS Switches, IEEE MTT-S Digest, 2001.

[2] D.Peroulis, Electromechanical Considerations in Developing Low-Voltage RF MEMS Switches. IEEE Transactions on MTT, Vol.51, No. 1 January 2003.

[3] G.M. Rebeiz, RF MEMS Theory, Design and Technology, 1st ed. New York: Wiley, 2003, Ch 3,5.

[4] J. Bergqvist, A Silicon Condenser Microphone with a highly perforated backplate, In international conference on Solid-State Sensor and Actuators Digest, New York, 1991, pp 266-269.

Design and simulation of RF MEMS cantilever and bridge switches for high switching speed and low voltage operation and their comparison.

Shimul Chandra Saha, Tajeshwar Singh, Trond Sæther

Department of Electronics and Telecommunications, Norwegian University of Science and Technology (NTNU), N-7491 Trondheim, Norway.
shimul.saha@iet.ntnu.no

In proceedings of IEEE ISSCS 2005, pp 131-134, July 2005, Iasi, Romania

Design and Simulation of RF MEMS Cantilever and Bridge Switches for High Switching Speed and Low Voltage Operation and Their Comparison.

Shimul Chandra Saha, Tajeshwar Singh, Trond Sæther
Department of Electronics and Telecommunications, Norwegian University of Science and Technology (NTNU), N-7491 Trondheim, Norway.
shimul.saha@iet.ntnu.no

Abstract— **In this paper we present the design and simulations of RF MEMS cantilever and bridge switches with regard to their switching speed and pull-down voltage. The switches are required to fulfill the requirements of high speed and a moderate pull down voltage for the switching of Capacitive Micromachined Ultrasonic Transducer (CMUT) elements used for ultrasound imaging. The switch type can be either capacitive contact or DC contact, depending on the operating frequency requirement.**

I. Introduction

The objective of this paper is to present the design and comparison of a high speed RF MEMS cantilever series switch and a fixed-fixed beam shunt switch. MEMS are nowadays becoming increasingly popular in RF applications due to their attractive advantages such as high isolation and low insertion loss. Depending on the switch type (DC contact, or capacitive), the MEMS switches can show very good RF performance from DC to several tens of GHz. However this performance also comes with some trade-offs or disadvantages of the RF MEMS switches as compared to their solid-state counterparts. These include high pull-down voltage and slow switching speed. In this paper it is shown that by a careful design, a compact switch with a moderate applied voltage can be optimized for the switching speed (<6μs). The switch simulation is done for different beam materials and control parameters like actuation voltage, quality factor and so on. The outline of this paper is a discussion about the requirement of MEMS switches in CMUT applications, in section II, followed by the design & simulations in section III. The performance of cantilever and the fixed-fixed beams is compared in section IV and important trade-offs discussed. We conclude the paper in section V.

II. Background

CMUTs are an upcoming technology in the field of Medical Imaging which promises to offer advanced automation possibilities. It will also offer, unlike the conventional piezoelectric transducer probes, compatibility with the CMOS process and integration of the signal processing circuitry on the probe itself, thus drastically reducing the hard-wiring of the probe to the signal processing console. The possibility of signal processing near the transducers unveils new prospects of 'Smart probes' that are capable of handling large amount of data, required for example, for 3D ultrasound imaging. Another imaging application of the CMUTs is in the detection of plaque inside the coronary for an early heart disease diagnosis.

The active part of a CMUT is usually a metal coated Si_3N_4 [1] which forms the top membrane/electrode. A highly doped silicon substrate constitutes the bottom electrode. When a DC bias voltage is applied between the top and the bottom electrodes, the membrane is pulled towards the substrate due to electrostatic actuation. If an AC voltage is superimposed on the DC bias voltage, a harmonic motion is obtained; thus the membrane will generate AC detection currents. As in piezoelectric ultrasound probes, there are two separate regimes of operation namely, transmit, and receive. CMUT elements require to be switched ON and OFF at different times either to send the actuation signal, or to receive the reflected signal. Hence it is necessary to have a switching matrix to switch from the transmit mode to receive mode. As the actuation signal is low, it is necessary to have a low insertion-loss and very good isolation of the switching matrix, for which an RF MEMS switch is a lucrative option. However, as the vein radius is small, the time of flight of the signal to travel from the transducer to the vein wall and back to the transducer is very short. Thus it is necessary to design the switch with very short switching time. For our design we target for a switching time, (to switch from the up-state to down-state) <6μs which is 3-5 orders lower as compared to 15-30μs shown by the present designs, for example [3] and [4], operating at similar actuation voltages (15-20V).

III. Design & Simulations

We consider a very simple RF MEMS cantilever capacitive series switch and a fixed-fixed bridge shunt switch with electrostatic actuation for our design. The name 'bridge' shall be used interchangeably for the fixed-fixed beam. We consider the switches realized in *Al*, *Au* and, *Ni* and compare the performance of each of these metals as the beam material. As we will see later in this section that the switching performance, like pull-down voltage and the switching time depend on the beam material properties such as Young's modulus and material density. Selecting a metal membrane also means that the

0-7803-9029-6/05/$20.00 ©2005 IEEE

fabrication process is simple and compatible with CMOS technologies.

A. Cantilever

Preliminary calculations for the switching time & pull-down voltage were done with Matlab®.

The pull-down voltage V_p and switching time t_s of the bridge and cantilever are given by [2], [5]:

$$V_p = \sqrt{\frac{8 \cdot k \cdot g^3}{27 \cdot \varepsilon_0 \cdot W \cdot w}} \quad (1)$$

$$t_s = \frac{V_p}{\omega_0 \cdot V_s} \sqrt{\frac{27}{2}} \quad (2)$$

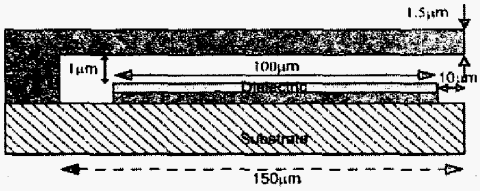

Figure 1. The cantilever switch.

Where k is the spring constant of the beam which depends on the beam dimensions and its material properties, g is the initial gap height, W and w are the length and the width respectively, of the electrode. V_p and V_s are the pull down voltage and the actuation voltage respectively for the device. The actuation voltage is selected slightly higher than the pull-down voltage as calculated in (1) in order to increase the switching speed, as can be seen in (2). The proposed cantilever switch is shown in Figure 1.

The dimensions of the cantilever beam are $150\mu m \times 40\mu m \times 1.5\mu m$; the bottom electrode is $100\mu m \times 40\mu m$, and initial gap $g = 1\mu m$. The dielectric (Si_3N_4) is 1000Å thick.

From the simulations in Matlab®, a pull-down voltage of 6V was obtained. Hence, with an actuation voltage of 16V, which is of the order of the present state-of-the-art (10-20V) [4], pull down time of t_s=6μs was obtained, which is around 4 orders lower as compared to the reported results [3][5].

Final device simulations were done in Coventorware®. Figure 12. shows the schematic used for simulations (3D view in Figure 11.). The beams were simulated with different values of Quality Factor 'Q' which depends on damping i.e., the gas and modal damping 'D' (D=a·M+b·K, where 'M' is the mass of the beam and 'K' is the beam spring constant, 'a' and 'b' depend on the damping medium and the beam structure). Q was varied from 0.3 to 3. Different values of the actuation voltage were simulated to optimize for the switching time. TABLE I. lists the switching times for *Al*, *Au*, and *Ni* cantilever beams with previously mentioned dimensions at different actuation voltages. Transient plot of the simulations is shown in Figure 2.

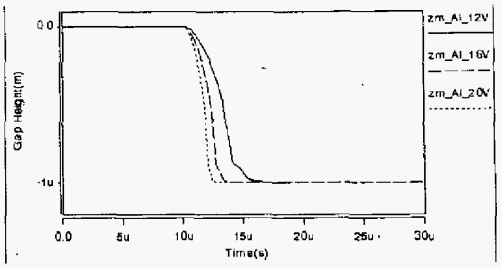

Figure 2. Switching time plots for *Al* caltilever beam with Q≈1. (10μs pulse delay) (zm means -motion in 'z' or vertical direction).

TABLE I. SWITCHING TIMES OF CANTILEVER BEAMS FOR VARIOUS ACTUATION VOLTAGES (Q≈1)

Material	Pull down voltage (V)	Actuation voltage(V)	Switching time (μs)
Aluminum	8.5	12	6.85
Aluminum	8.5	16	3.75
Aluminum	8.5	20	2.45
Gold	8.7	16	8.41
Gold	8.7	20	6.05
Nickel	14	20	7.27

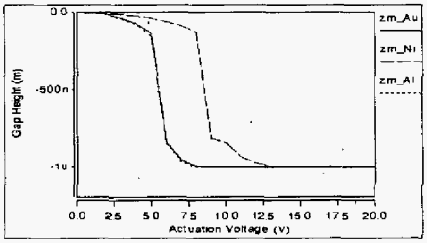

Figure 3. Pull-down voltage plots for *Au*, *Ni*, and *Al* cantilevers.

From Figure 3. it can be seen that the pull down voltage of *Au* and *Al* beams is almost the same. This is because as their young's modulus of the same order. Thus for the similar dimensions, beams made with either of these materials have the similar spring-constant, hence similar pull-down voltages.

The pull down voltage of the *Ni* beam is higher than its other two counterparts which is obvious since *Ni* has a higher young's modulus. Thus, for low voltage operation the *Ni* beam is not suitable. From TABLE I. it can be seen that as the actuation voltage is increased the switching time decreases.

From Figure 4. it can be seen that, although *Ni* beam has a higher pull-down voltage, its switching speed is not much different from the *Au* beam. This is because the density of *Ni* is

lower than *Au*, which means that the resonance frequency of the *Ni* beam is higher as compared to the *Au* beam of similar dimensions.

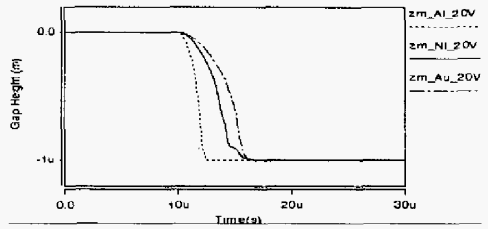

Figure 4. Switching time plots for *Al*, *Ni* and *Au* cantilever beams at voltage step of 20V with Q≈1. (10μs pulse delay).

The switching speed for *Al* is the best amongst all three as it has a moderate young's modulus and low density. The Quality factor '*Q*' also plays a very important role in the switching speed. This can be seen in Figure 5. wherein the dynamic damping is varied.

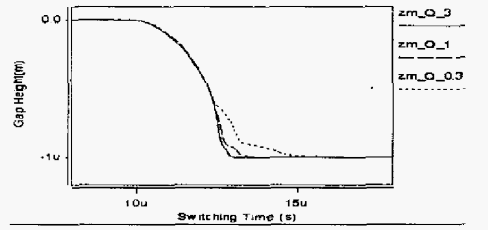

Figure 5. Swithing time plots for *Al* cantilever beam with Q≈0.3, 1, and 3 and voltage step of 16 V (10μs pulse delay).

B. Fixed-Fixed Beam (bridge)

The dimensions of the fixed-fixed beam (bridge) are $250\mu m \times 40\mu m \times 1.5\mu m$, the bottom electrode is $200\mu m \times 40\mu m$, and initial gap $g = 1\mu m$. The dielectric (Si_3N_4) is 1000Å thick.

The pull-down voltage and switching time was calculated similarly as in the cantilever's case, using (1) & (2). For the fixed-fixed beam a pull down voltage of 10.5V was obtained and with an actuation voltage of 16V the switching time $t_s \approx 3\mu s$ was obtained.

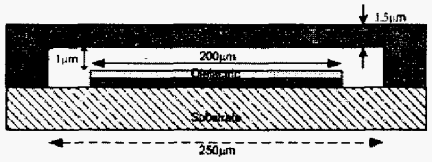

Figure 6. Fixed-fixed beam (bridge).

The pull down voltage and switching time for the fixed-fixed beam are listed in TABLE II.

TABLE II. SWITHING TIMES FOR ALUMINIUM & GOLD FIXED-FIXED BEAMS FOR VARIOUS ACT. VOLTAGES (Q≈1).

Material	Pull down voltage (V)	Actuation voltage(V)	Switching time (μs)
Aluminum	10.5	12	5.30
Aluminum	10.5	16	2.75
Aluminum	10.5	20	1.95
Gold	11	16	7.75

Figure 7. shows the switching time simulations for the fixed-fixed beam. Note that *Ni* was not considered in these simulations, as seen in the previous section *Ni* beams result in quite high actuation voltage so it will be not suitable for our application.

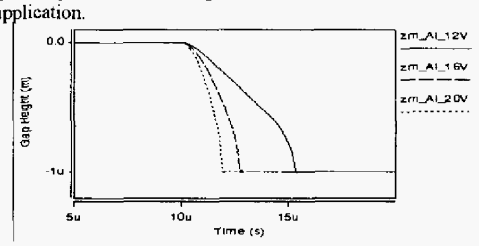

Figure 7. Switching time plots for *Al* fixed-fixed beam with Q≈1 (10μs pulse delay).

IV. COMPARISON

In this section we compare the performance the cantilever beam with the fixed-fixed beam. Note that the dimensions of the two beams are different as mentioned in the previous sections. This is done in order to have comparable performance parameters for both cases, such as switching time and pull-down voltage. The simulations were made by maintaining the same *Q*.

From Figure 8. it can be seen that the pull-down voltage of the fixed-fixed beam is higher than the pull-down voltage of the cantilever. However, for the same actuation voltage, the switching speed is better for the fixed-fixed beam. This is because of the higher stiffness of the fixed-fixed beam as compared to the cantilever.

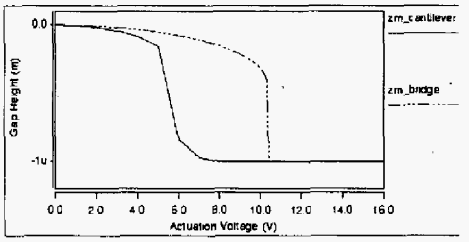

Figure 8. Pull-down voltage plots for the *Al* cantilever and Fixed-Fixed beams.

As seen from the plots in Figure 9. the cantilever beam needs more time to settle to the down position. In fact it will also take even longer time to settle to the up-position when released from the down-position. So, in order to have faster switching, a fixed-

fixed beam is ideal but this comes at a price of a higher pull-down voltage. This is another trade-off which needs to be considered in the switch design depending on the requirement.

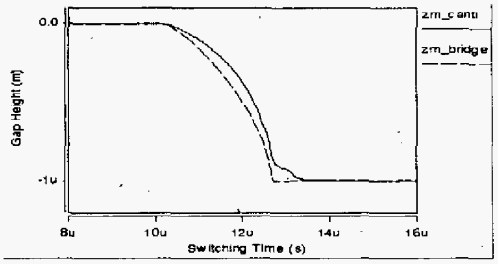

Figure 9. Switching time plots for *Al* cantilever and fixed-fixed beam with Q≈1 and a voltage step of 16V, (10μs pulse delay).

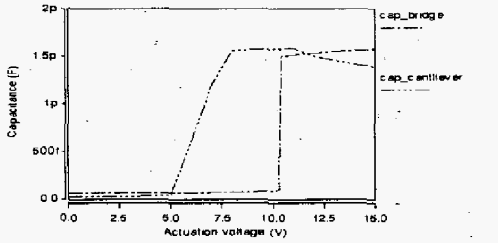

Figure 10. Capacitance ratio for Cantilever and bridge.

TABLE III. COMPARASON OF DIFFERENT PAPAMETERS FOR THE CANTILEVER AND THE FIXED-FIXED BEAM AT Q≈1.

Parameter	Cantilever	Bridge
Pull down voltage	8.5 V	10.5 V
Switching time	3.75 μs at 16 V	2.75 μs at 16 V
Capacitance Ratio	50	30

TABLE III. compares various parameters for the cantilever and the fixed-fixed beam (bridge). Although the bridge has larger electrode area (double) than the cantilever, the down-state capacitance of the beam is not much different as compared to the cantilever (Figure 10.). This is because the bridge when in the down-state does not touch the electrode all the places so it has less capacitance ratio. as compared to the cantilever. One way to increase the capacitance ratio for both bridge and cantilever is by using hi-dielectric materials and smaller dielectric thickness. But care must be taken such that the actuation voltage does not exceed the breakdown voltage due to a high electric field.

V. CONCLUSIONS

We have shown the design of RF MEMS capacitive cantilever and fixed-fixed beam (bridge) switches with high switching speeds at moderate actuation voltage. Switching speed increases with actuation voltage but we have a limitation on the maximum actuation voltage. In addition we have compared the actuation voltages, switching speed performances and capacitance ratio of the cantilever and fixed-fixed beams. Important trade-off between the speed and the actuation voltage with respect to the switch design is also presented. The Damping affects the switching speed of the MEMS switch and can be controlled by the beam structure (e.g., perforations) and by regulating the medium (lower pressure means lower damping and higher Q). Increasing Q will reduce the pull down time but it will also increase the release time, which poses another design trade-off. Q of around 1 is good choice for both switching and release times. Both switch types presented in this paper can be fabricated on the same wafer as the process parameters are same. The devices will be realized at the MiNa lab SINTEF, Oslo, Norway.

VI. ACKNOWLEDGEMENT

Authors are grateful to Norwegian Research Council for supporting the work financially through SMiDA project.

REFERENCES

[1] B. Bayram, " A new regime for operating capacitive micromachined ultrasonic transducers", IEEE Transactions on UFFC, Vol.50, No.9,09/03

[2] J.B. Muldavin, "Nonlinear electro-mechanical modeling of MEMS switches", IEEE MTT-S Digest, 2001

[3] D. Peroulis, "Electromechanical considerations in developing low-voltage RF MEMS switches", IEEE Transactions on MTT, Vol.51, No. 1 January 2003.

[4] N. Nishijima, " A Low-voltage high contacts force RF-MEMS switch, IEEE MTT-S Digest, 2004.

[5] G.M. Rebeiz, "RF MEMS Theory, Design and Technology", 1st ed. New York: Wiley, 2003, Ch 3,5.

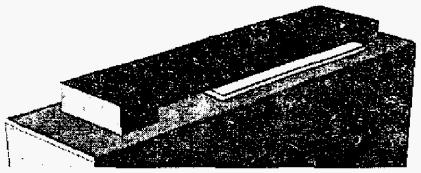

Figure 11. 3-dimentional view of the cantilever switch.

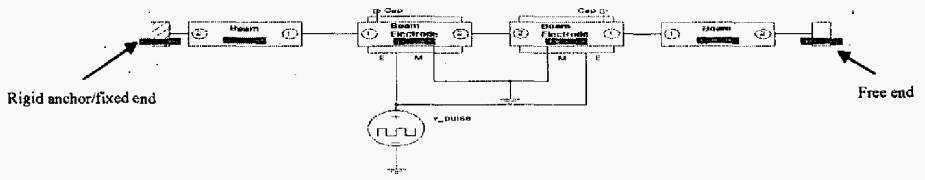

Figure 12. The schematic arrangement of Cantilever in Coventorware®.

MODELING AND SIMULATION OF HIGH CAPACITANCE RATIO RF MEMS SHUNT SWITCH

Shimul C. Saha[1], Ulrik Hanke[2], Geir U. Jensen[3], Anton M. Bøifot[4], Tor A. Fjeldly[1], Trond Sæther[1].

1: Department of Electronics and Telecommunications, Norwegian University of Science and technology, 7491 Trondheim, Norway.
2: SINTEF ICT, NO-7465 Trondheim, Norway
3: SINTEF ICT, Gaustadalleen 23, 0371 Oslo, Norway
4: MicroConsult, Hallsetreina 10, 7027 Trondheim, Norway.
E-mail: shimul.saha@iet.ntnu.no, ulrik.hanke@sintef.no, geir.jensen@sintef.no, antonmar@online.no torfj@unik.no, trond.saether@iet.ntnu.no

In proceedings of third IASTED international conference on Circuits, Signals and Systems CSS 2005, pp 186-193, October 2005, Marina Del Rey, CA, USA.

Is not included due to copyright

Modeling and Simulation of Low Pass Filter using RF MEMS Capacitance and Transmission line

Shimul Chandra Saha, Trond Sæther

Department of Electronics and Telecommunications, Norwegian University of Science and Technology (NTNU), 7491 Trondheim, Norway
E-mail: shimul.saha@iet.ntnu.no

Proceedings of IMAPS Nordic conference 2005, pp 155-159, September 2005, Tønsberg, Norway.

Modeling and Simulation of Low Pass Filter using RF MEMS Capacitance and Transmission line

Shimul Chandra Saha, Trond Sæther

Department of Electronics and Telecommunications, Norwegian University of Science and Technology (NTNU), 7491 Trondheim, Norway
E-mail: shimul.saha@iet.ntnu.no

Abstract

Radio Frequency Micro electromechanical systems (RF MEMS) technology offers an attractive capability for RF systems, particularly in support of switching and tuning functions. One such component is a micro electromechanical voltage tunable capacitor, which can enable wide tuning range and high quality (Q) factors. In this paper we present a design of 5.9 GHz 3rd and 5th order low pass filter using the theory of stepped impedance transmission line filter. In a traditional lumped element low pass filter the series element is an inductor and the shunt element is a capacitor. In the stepped impedance transmission line filter, the high impedance transmission line is used to replace the inductor; the capacitance is replaced by low impedance line. This topology does not give the flexibility of tuning the cut off frequency. So we replace the low impedance line or the shunt capacitance by RF MEMS capacitance which will provide the tuning capability.

In this paper we have shown the design of a low actuation voltage RF MEMS switch and modeling of the switch as variable capacitance. The capacitance can be varied as a function of the actuation voltage. The capacitance is used as a lumped component in a conventional low-pass LCR filter. The design uses a novel approach to implement both distributed transmission line and RF MEMS capacitance together to replace the lumped elements with having tuning capability of the cut-off frequency.

Key words: RF MEMS Capacitance, Low pass filter, Stepped impedance filter, Tuning.

Introduction

Filters are an essential part of any high frequency circuit. It plays an important role in signal processing like reducing intermodulation product, removing image frequency. It is also an essential part for channel preselect block.

Conventionally low pass filter are lumped element at low frequency. It is easier to produce, and the theory is straight forward to develop. So it can be produced at low cost. But it has some disadvantage like it does not have automatic frequency tuning capability without switching different elements. For high frequency usually lumped elements are bigger so they are not suitable for miniaturization. At higher frequency usually distributed element is used for filter application. But for distributed element filter it is difficult to tune the cut-off frequency.

In this paper we develop a filter which uses both the transmission line topology and RF MEMS capacitance [1]. The RF MEMS capacitance can be tuned by actuation voltage so the cut-off frequency can be changed accordingly. This will give both miniaturization and frequency tuning capability for the filter. The RF MEMS capacitance has high Q compared to the distributed elements. This is a plus point for filter stop band characteristic and they are attractive for tuning and switching action [2].

Theory of Stepped-impedance Filter

According to transmission line theory [3] the Z parameters of a transmission line of length ℓ and characteristic impedance of Z_0 can be represented as shown if figure 1.

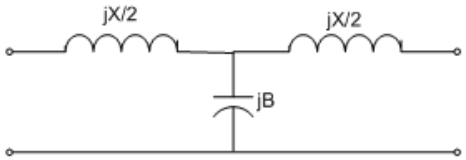

Figure 1: T equivalent circuit for a transmission line.

The element of the T section in the equivalent circuit for a transmission line is given by following equation [3].

$$\frac{X}{2} = Z_0 \tan(\frac{\beta\ell}{2})$$

$$B = \frac{1}{Z_0}\sin\beta\ell$$

If the length of the transmission line is short and the characteristic impedance is higher the equivalent circuit can be reduced to as shown in figure 2 and the parameter is given by

$$X_L = Z_0\beta\ell$$

B≈0

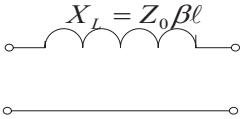

Figure 2: Equivalent circuit for small length of transmission line and high characteristic impedance

So a high characteristic impedance and short length of transmission line can be represented by series inductor. Although it is preferred to have very high impedance and short line length ($\beta\ell < \pi/4$) we choose medium impedance too avoid narrowing. For narrow line width it will be difficult to obtain the desired MEMS capacitance. So the line was chosen bit longer. In the lumped elements filter model, the shunt capacitor will be replaced by RF MEMS capacitance which will give the tuning capability.

Capacitance model of MEMS switch

A low voltage RF MEMS capacitive shunt switch is designed for the tuning capacitor. The side view and top view are shown in figure 3 and 4. The bridge can be modeled as a capacitance between the bottom electrode and the beam. The capacitance modeling and simulation is done in Coventorware®.

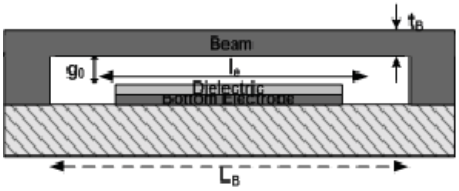

Figure 3: The side view of RF MEMS bridge

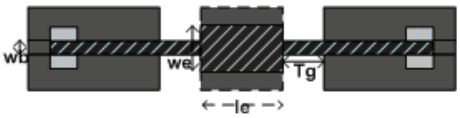

Figure 4: The top view of RF MEMS bridge

During upstate the capacitance is in the range of fF depending on the width of the beam. When a DC voltage is applied between beam and bottom electrode the gap will change and the capacitance also changes accordingly. So by changing the actuation voltage the capacitance can be changed which can tune the cut-off frequency of the filter. When the voltage is equal to or greater than the pull down voltage the beam collapses to the downstate position. The capacitance in the down state position is in the range of pF. This capacitance can be used as high value lump element capacitance. The dimension of the propose switch is, L_B=500 μm, g_0=1.5 μm, t_B=1.5μm and w_b=50μm/100μm. The electrode length l_e and the electrode width w_e are varied depending on the requirement of capacitance and transmission line parameter. A 0.1 μm Si_3N_4 is used as dielectric. The chosen beam material is Al but Au can be a good option. The transmission line is made of Gold. A comparative study for pull down voltage and the variation of capacitance with beam width 100μm and l_e=224μm and w_e=400μm is shown below in figure 5. As the electrode (beam) width become more, two beams can be used parallel for convenience.

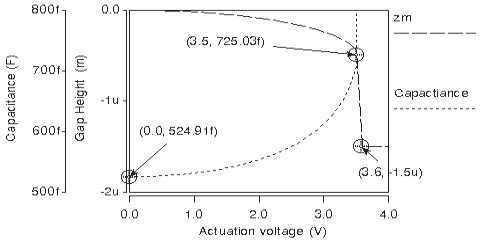

Figure 5: Pull down voltage and capacitance simulation in Coventor.

Form the figure above it can be seen that the pull down voltage is very low 3.6 volt. It may increase due to residual stress. The residual stress can be controlled by the process parameter. The upstate capacitance varies from 524 fF to 725 fF before the beam collapse to downstate. This is almost 40% more than that of the zero bias voltage. So we can have a large tuning range capacitance.

A third order filter design and simulation

A third order low pass filter design is shown in figure 6. The basic filter element is extracted from the maximally flat low pass butterworth filter prototype [3].

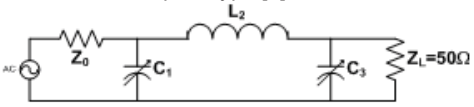

Figure 6: A third order low pass filter topology

The basic filter elements are given by g_1=1.00, g_2=2.00, g_3=1.00 and g_4=1.00 is the load impedance. Using the maximum transmission line impedance of 90Ω the length of the transmission line becomes 63° and two nominal capacitances value is 550 fF. For transmission line we used coplanar waveguide. This makes it easier to have the ground on the same plane. The MEMS beam will easily form the capacitance between center conductor and ground plane. The filter topology is shown with transmission line and MEMS capacitance in figure 7 below. The substrate parameters used for simulation are substrate thickness of 500 um, with relative permeability of 10 and transmission line thickness of 1 um. For 90Ω transmission line the dimension is 200μm/55μm/200μm (G/W/G) and the length is 3.5 mm at frequency 5.9 GHz. The 50Ω line dimension is 100μm /224μm/ 100μm. If the higher impedance is more than 100Ω then the signal line will be very narrow and it will be difficult to obtain the required variable upstate capacitance. The required beam dimension is equal to the MEMS switch model described earlier in the capacitance model of MEMS switch section.

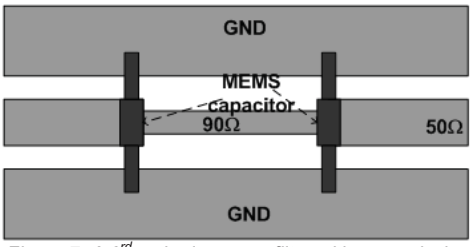

Figure 7: A 3rd order low pass filter with transmission line MEMS variable capacitor

The RF simulation is done in ADS® from Agilent with the parameter mentioned using the capacitance model from Coventor®. The simulation result for the designed low pass filter with a comparison of filter performance with lumped elements is shown in figure 8.

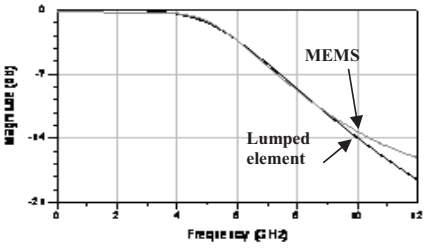

Figure 8: The MEMS filter and Lumped element filter performance.

The filter characteristic with variable capacitance is shown in figure 9. From the figure it can be seen that the cut-off frequency can be varied from 5.55 GHz to 6.4 GHz for actuation voltage from 3.5V (725 fF) to 0V (525 fF). So the filter gives a good flexibility of tuning cut-off frequency with bias voltage.

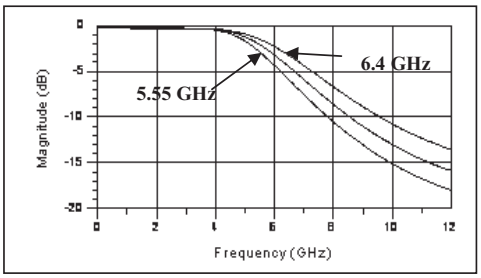

Figure 9: The cut-off frequency variation for the MEMS filter.

A fifth order filter design and simulation

A fifth order low pass filter design is shown in figure 10. The basic filter element is extracted from the maximally flat low pass butterwoth filter prototype [3].

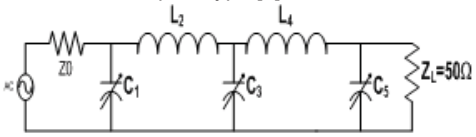

Figure 10: A third order low pass filter topology

The basic filter element is given by g_1=0.6180, g_2=1.6180, g_3=2.00, g_4=1.6180, g_5=0.6180. Using the maximum transmission line impedance of 90Ω the length of the both transmission line becomes 51.5° (3.14mm) and the nominal capacitance value is obtained C_1=C_5=365fF and C_3=1.06 pF. The C_3 is used as down state capacitance and C_1 and C_5 is used as upstate capacitance. For transmission line it was used the same topology as 3rd order. The filter topology with transmission line is shown in figure 11 below. The substrate parameters are same as 3rd order described earlier.

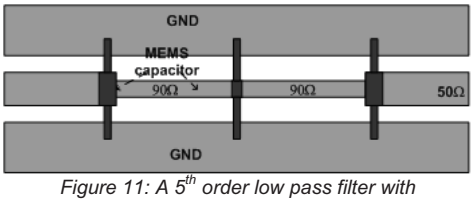

Figure 11: A 5th order low pass filter with transmission line MEMS variable capacitor

The frequency tuning behavior is shown in figure 12 below. The C_1 and C_5 are varied from 285fF to 395fF. The cutoff frequency varies from 5.77 GHz to 5.95 GHz. The tuning range is not so high. Because the dominant capacitor is C_3 and it can control the frequency more efficiently. The dimension of the electrode and beam width is given in the table 1 below keeping other parameters as the beam parameters mentioned earlier.

Table 1: The beam parameters with other parameters as mentioned earlier

Capacitance	W_b(μm)	w_e(μm)	l_e(μm)	state
C_3	25	28	55	Down
C_1/C_5	50	200	224	Up

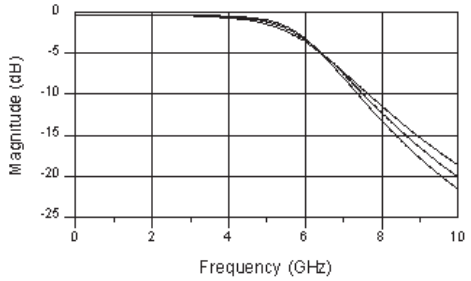

Figure 12: The cut-off frequency variation for the MEMS filter.

Fifth order filter design with high tuning range

From the above figure 12 it can be seen that the cut-of frequency does not vary much with tuning voltage. So in order to have high tuning range the 3rd element of the 5th order filter or C_3 have to be tuned. And we need to design the C_3 as an upstate capacitance. The transmission line width of the high impedance becomes very narrow. So we are going to choose a bit lower impedance 75Ω. For lower impedance the width will be higher and it will be easier to obtain the desired upstate capacitance. The transmission line will be bit longer compare to the higher impedance. The lumped element topology is same as figure 10 and the transmission line topology is shown in figure 13. Here four parallel beams are used as the beam width is too big. It can also be used several no of parallel beams. For 75Ω transmission line the dimension is 185μm/100μm/185μm (G/W/G) and the length is 3.8 mm (optimized) at frequency of 5.9 GHz.

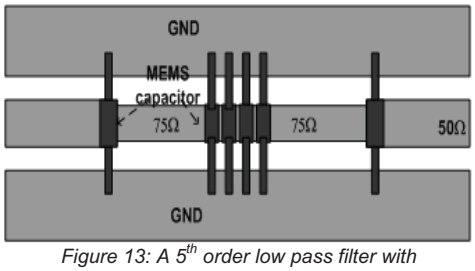

Figure 13: A 5th order low pass filter with transmission line MEMS variable capacitor

The dimensions of one of the beam are l_e=100 μm, w_e=360 μm and w_b=100 μm with other parameter as mentioned earlier. The capacitance is obtained from combination of 4 equal upstate capacitances. The upstate capacitance variation of one beam is shown in figure 14 with actuation voltage. The pull down voltage may be bit higher due to residual stress.

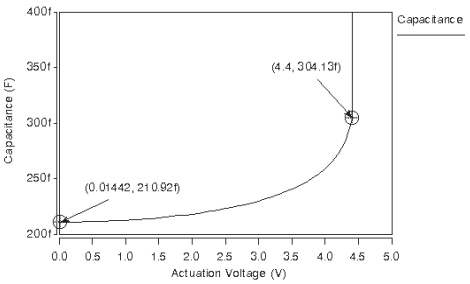

Figure 14: A capacitance simulation of one beam.

The frequency variation of the designed filter with capacitance is shown in figure 14. The C_1 and C_5 are kept constant and their dimensions are same as mentioned in previous section. From the figure it can be seen that the cut-off frequency varies form 5.55 GHz to 6.51 GHz at actuation voltage 4.4 V to 0 volt. So it gives more tuning range than 3rd order filter.

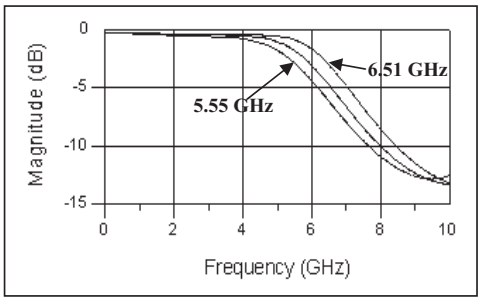

Figure 15: The cut-off frequency variation of the MEMS filter with C3 variation

For comparison the simulation is also done with one capacitance altogether. The comparison between 4 parallel beams and one beam capacitance is shown in figure 15. From the figure 15 it can be seen that when one beam is used the frequency is much sharper. So it is preferable. And it is necessary to consider the process point of view. So if it is possible to fabricate wider beam then it is preferable.

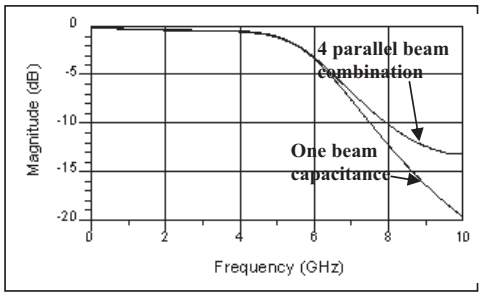

Figure 15: The magnitude response for one beam and 4 beam parallel

Conclusion

We have shown a design of tunable and miniature MEMS low pass filter. The use of transmission line at higher frequency is easier and favorable as the dimensions become smaller.

For a distributed filter the Q factor is usually lower than for lumped element. In this filter we use both distributed element and MEMS capacitance which has high Q. So we can have both advantages. The miniature MEMS filter also gives tuning capability. The tuning voltage is comparatively very small from 0 to 5V in most cases and always less than 10 V. Due to residual stress the pull down voltage can be increased to some extent. For higher upstate capacitance the initial gap height can be reduced, this will also reduce the pull down voltage. In the simulation we did not include the inductance from RF MEMS switch. Because below 20 GHz the inductances do not play much role so they can be ignored. The inductances are in the range of tens of pH. These can be made negligible having small gap between signal and ground line and also increasing the beam width. A 3-D view of MEMS capacitance is shown in figure 16.

Acknowledgment

Authors are grateful to Norwegian Research Council for sponsoring the work through Smart Microsystems for Diagnostic Imaging in Medicine (SMiDA) project (No 159559/130).

References

[1] A. Abbaspour-Tamijani, A high performance MEMS miniature tunable band-pass filter, IEEE MTT-S Digest, 2003

[2] R. L. Borwick, Variable MEMS capacitors implemented into RF filter systems, IEEE Transaction on MTT, Vol.51, No.1,01/03

[3] David M. Pozar, Microwave Engineering, Ch 8, Second Edition, John Willey & Sons, 1998.

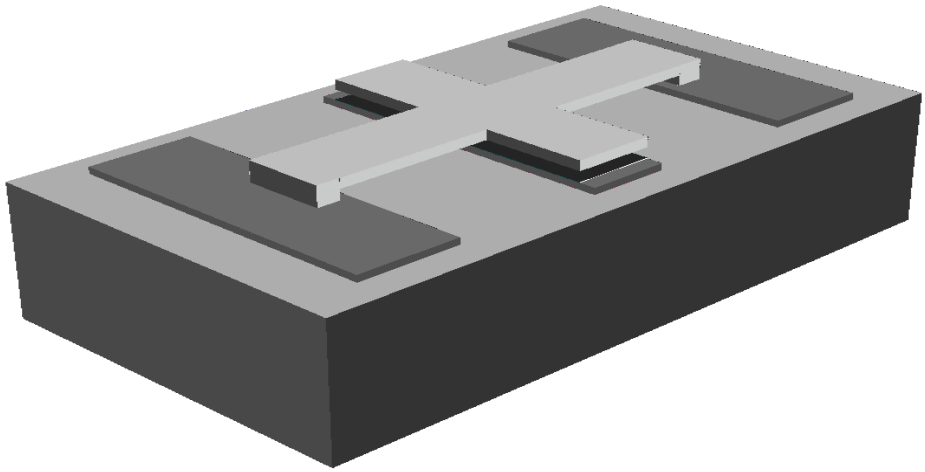

Figure 16: 3-D view of one of the proposed MEMS capacitance in CPW configuration.

Modeling, Design and Simulation of Tunable Band Pass Filter using RF MEMS Capacitance and Transmission line

Shimul Chandra Saha *[a], *Ulrik Hanke* [b], *Trond Sæther* [a]

[a] Department of Electronics and Telecommunications, Norwegian University of Science and Technology (NTNU), 7491 Trondheim, Norway
[b] SINTEF ICT, NO-7465 Trondheim, Norway

In Proceedings of Microelectronics: Design, Technology, and Packaging II, Vol. 6035, pp 60350-C1-C11 part of SPIE Symposium on Microelectronics, MEMS, and Nanotechnology, December 2005, Brisbane, Australia.

Is not included due to copyright

Modeling of Spring Constant and Pull-down Voltage of Non uniform RF MEMS Cantilever

Shimul Chandra Saha[1], *Ulrik Hanke*[2], *Geir Uri Jensen*[3], *Trond Sæther*[1]

[1]Department of Electronics and Telecommunications (IET), Norwegian University of Science and Technology (NTNU), 7491 Trondheim, Norway

[2]Institute of Microsystems Technology, Vestfold University College, 3103 Tønsberg, Norway

[3] SINTEF ICT, Gaustadalleen 23, 0371 Oslo, Norway

In proceedings of 2006 IEEE International Behavioral Modeling and Simulation Conference, pp 56-60, September 2006, San Jose, California, USA

Modeling of Spring Constant and Pull-down Voltage of Non uniform RF MEMS Cantilever

Shimul Chandra Saha
Department of Electronics and Telecommunications (IET), Norwegian University of Science and Technology (NTNU), 7491 Trondheim, Norway
shimul.saha@iet.ntnu.no

Ulrik Hanke
Institute for Microsystems Technology, Vestfold University College, 3103 Tønsberg Norway
Ulrik.Hanke@hive.no

Geir Uri Jensen
SINTEF ICT Gaustadalleen 23, 0371 Oslo Norway
Geir.Jensen@sintef.no

Trond Sæther
Department of electronics and Telecommunications (IET), Norwegian University of Science and Technology (NTNU), 7491 Trondheim, Norway
trond.saether@iet.ntnu.no

ABSTRACT

In this paper, we are going to present a model of spring constant and pull down voltage for non uniform RF MEMS cantilever. In order to reduce the pull down voltage, it is usual to use a beam, which is narrower close to anchor and wider at the end or electrode area for a cantilever. Compare to uniform beam, this beam will have lower spring constant which will reduce the pull down voltage. A comprehensive model for spring constant and pull down voltage of the non uniform cantilever is developed through basic force deflection mechanism of the suspended beam.

1. INTRODUCTION

Nowadays RF MEMS components are becoming popular, due to their very good performance at RF and microwave frequencies. RF MEMS switches have very low insertion loss at on state and very high isolation at off state. The operating principle of an electrostatic actuated RF MEMS switch is very simple. A beam (bridge or cantilever) is suspended from the anchor with an actuation electrode placed underneath. When a DC voltage is applied between the beam and actuation electrode the beam moves down due to an electrostatic force. The DC actuation voltage, at which the beam fully moves down, is called the pull down voltage.

Usually the actuation voltage for RF MEMS switches is higher than their solid-state counterparts. In order to reduce the pull down voltage for RF MEMS switches, techniques like folded spring, narrower beam close to the anchor than actuation electrode are used [1]. To calculate the required pull down voltage for a beam, it is necessary to have an accurate mechanical model for the spring constant of the beam. The spring constant will determine the pull down voltage. The pull down voltage (spring constant) also depends on the position and orientation of the actuation electrode. The model of the spring constant and the pull down voltage for a uniform beam is presented in the literature [1]. For non uniform beam, some work has been published recently [2, 3]. In the work presented in [2], the model assumes that the force is concentrated on the tip of the cantilever. Therefore the accuracy strongly depends on the size and position of the actuation electrode. In [3], a comparison of pull down voltage between uniform and non uniform beam is presented using numerical simulations. It shows that a non uniform beam may have a lower pull down voltage than a uniform beam. In this paper we develop an analytical model for the spring constant and pull down voltage for a non uniform cantilever taking into account that the force may be distributed along the beam. The model will be very useful for analysis of spring constant and pull down voltage of non uniform beam, using simple mathematical program. It will be much faster and simpler compared to the commercial tools using 3-D modeling. The model of the spring constant and its verification is described in section 2.The modeled pull down voltage is compared with CoventorWare simulation in section 3. The paper is concluded in section 4 followed by an appendix.

2. MODELING OF CANTILEVER

There are two basic types of RF MEMS switches, fixed-fixed bridge and cantilever. Usually the spring constant of fixed-fixed bridge is higher than cantilever, because the bridges are rigidly anchored at both sides. In circuit point of view, bridges are more useful in shunt configuration and cantilevers are more useful in series configuration. The cantilever can be used both as a DC and capacitive contact switch. For DC contact switch, a separate actuation electrode is required. For capacitive contact switch the same electrode may be used both for actuation and capacitive contact. In this section we are going to develop the model for the spring constant of a non

uniform cantilever with a wider section at the end of the beam.

The top view of a non uniform cantilever is shown in figure 1. The width of the beam close to the anchor is 'w' and the width of the beam above the actuation electrode is 'wy', where 'y' is a constant and it can be 1≥y≥1. For RF MEMS application y≥1 is desired, as it will reduce pull down voltage.

A side view of the non uniform cantilever is shown in figure 2. The width of the beam above the actuation area is higher than the rest of the beam. This will give higher actuation force, with lower spring constant compared to a uniform beam. The pull down voltage will be reduced.

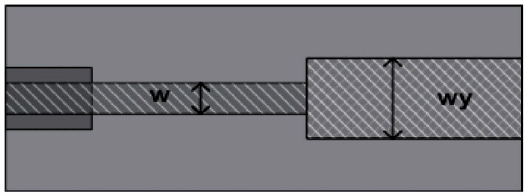

Figure 1: Top view of a non uniform cantilever

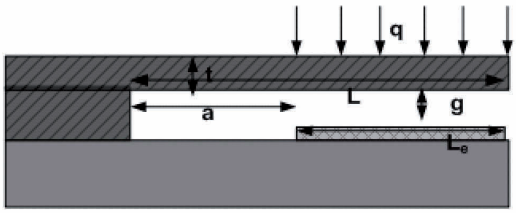

Figure 2: Side view of a non uniform cantilever

In order to develop the model, we need to use the beam diagram with actuation force, moment and reaction force acting on the beam at different positions. Figure A1 in the appendix shows such a model.

The derivation of the spring constant of the non uniform beam is presented in the appendix using the Euler-Bernoulli theory [4]. The equation of the deflection at any position of beam is given by,

$$v = \frac{q}{24EIy}(4Lx^3 - 6L^2x^2 - x^4) + C_3x + C_4 \quad (1)$$

With C_3 and C_4 given by,

$$C_3 = \frac{qaL(a-L)}{2EI}\left(1-\frac{1}{y}\right) + \frac{qa^3}{6EIy} \quad (2)$$

$$C_4 = \frac{qa^2L}{12EI}(3L-4a)\left(1-\frac{1}{y}\right) + \frac{qa^4}{12EI}\left(1+\frac{1}{2y}\right) - \frac{qa^4}{6EIy} \quad (3)$$

For a cantilever, the maximum deflection occurs at the end of the beam or at x=L. The deflection at the end is given by,

$$v_L = -\frac{qL^4}{8EIy} + C_3L + C_4 \quad (4)$$

After simplification the maximum deflection of the beam becomes,

$$v_L = \frac{-q(L-a)^2(L+a)^2}{8EIy} - \frac{q(L-a)a(a+3L)}{12EI} - \frac{qa^2L}{2EI}(L-a)^2\left(1-\frac{1}{y}\right) \quad (5)$$

The spring constant of the cantilever is given by,

$$k = -\frac{P}{v_L} = -\frac{q(L-a)}{v_L} \quad (6)$$

If we insert equation (5) into equation (6), the spring constant becomes,

$$k = \frac{24EIy}{3(L-a)(L+a)^2 + 2ya^2(a+3L) + 12aL(L-a)(y-1)} \quad (7)$$

When the beam is uniform, i.e. y=1, the expression for C_3 and C_4 becomes,

$$C_{3u} = \frac{qa^3}{6EI} \quad (8)$$

$$C_{4u} = -\frac{qa^4}{24EI} \quad (9)$$

The deflection of the cantilever at any point is given by,

$$v = -\frac{q}{24EI}\left[x^4 - 4Lx^3 + 6L^2x^2 - 4a^3x + a^4\right] \quad (10)$$

This matches with the expression of deflection in [4].

To test the more validity of this expression we can take some well known limits in equation (7). If we take the limits, a=L, a=0 and y=1 we obtain the following spring constants,

$$k \xrightarrow{a=0} \frac{8EIy}{L^3} = \frac{2Ewy}{3}\left(\frac{t}{L}\right)^3 \quad (11)$$

$$k \xrightarrow{a=L} \frac{3EI}{L^3} = \frac{Ew}{4}\left(\frac{t}{L}\right)^3 \quad (12)$$

$$k \xrightarrow{y=1} 2Ewt^3 \frac{L-a}{3L^4 - 4La^3 + a^4} \quad (13)$$

The expressions for spring constant (11)-(13) match with the expressions given in [1, Ch2].

Using equation (7) we have calculated the spring constant in MathCAD, for two different beam lengths of the cantilever versus width of the electrode. The two beam lengths are 150 μm and 200 μm respectively and the thickness of the beam is 2 μm. The width of the beam at the anchor is 100 μm. The length of the electrode is L_e=100 μm and the width of the electrode is varied from 100 μm to 300 μm (1≤y≤3). The material of the beam is chosen Aluminum. The variation of the spring constant versus the electrode width is shown in figure 3. From figure 3 it can be seen that, the spring constant increases to some extent with electrode width, from uniform beam i.e. w=100 μm, and it is more prominent for shorter beam. For a long beam the spring constant is much lower than for the short beam and its spring constant varies very little with electrode width. But as the actuation area increases, it will reduce pull down voltage significantly.

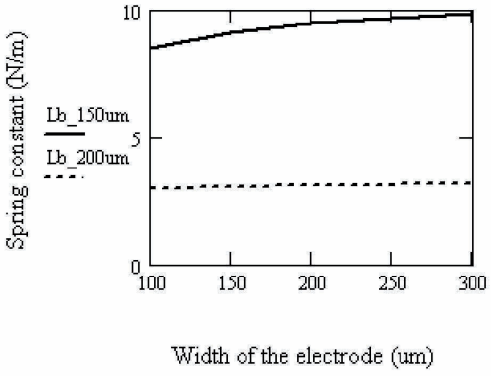

Figure 3: Variation of spring constant of cantilevers with electrode width

We have also compared the spring constant of beam with different lengths and same electrode width. For uniform beam, the electrode width and length are 100 μm and 100 μm respectively. For non uniform beam, the beam width is 100 μm. The electrode length is 100 μm and width is 200 μm. The thickness of the beam is 2 μm. The variation of spring constant and comparison between non uniform beam (NU) and uniform beam width (U) with beam length is shown in figure 4.

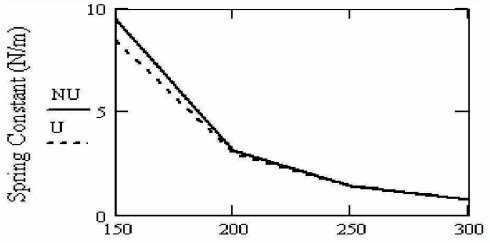

Figure 4: The variation of spring constant with beam length

3. COMPARISON OF MODEL WITH SIMULATION RESULT

The pull down voltage of a cantilever beam for electrostatic actuation is given by [1, 5].

$$V_p = \sqrt{\frac{8kg_0^3}{27\varepsilon_0 L_e wy}} \quad (14)$$

Here 'k' is the spring constant, 'g_0' is the initial gap height and 'wyL_e' is the actuation electrode area of the cantilever. We have implemented the analytical expressions in MathCAD to calculate the spring constant and pull down voltage for a cantilever. We also simulated the pull down voltage of the beam using CoventorWare, to compare the results. The simulation in CoventorWare is done, assuming no stress gradient and residual stress in the beam material. The dimensions of the cantilever are as follows. The length of the cantilever is 150 μm, length of the electrode is 100 μm, initial gap is 2 μm and thickness of the cantilever is 2 μm. The beam material is aluminum with young's modulus E=77 GPa. The results are shown in table 1. The simulation results of pull down voltage in CoventorWare are shown in figure 5. For convenience we have stopped the simulation, just before the beam collapses, to save simulation time. However we can extract the pull down voltage, at which the beam moves close to one third of the initial gap.

Table 1: Pull down voltage comparison of different electrode widths for a 150 μm long and 100 μm wide beam at anchor

Electrode width, wy (μm)	Spring constant (N/m)	Pull down voltage (V)	Pull down voltage in Coventor-Ware (V)	Error (%)
100	8.50	15.20	18.4	17
150	9.10	12.90	15.5	17
200	9.50	11.40	13.6	16
300	9.90	9.50	11.3	16

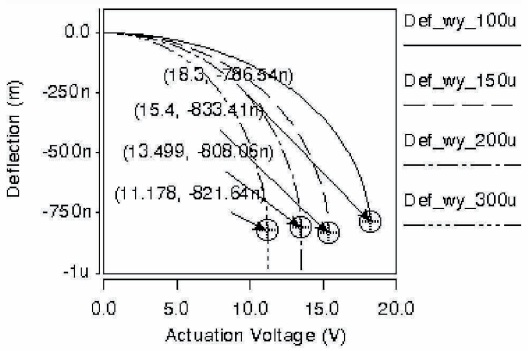

Figure 5: The pull down voltage simulation in Coventor-Ware for 150 μm long and 100 μm wide beam.

We have also made a comparison for a 200 μm long beam with 100 μm long electrode. The initial gap is 2 μm and thickness of the cantilever is 2 μm. The comparison is shown in table 2. The simulation results for pull down voltage in CoventorWare are also shown in figure 6.

Table 2: Pull down voltage comparison of different electrode widths for a 200 μm long and 100 μm wide beam

Electrode width, wy (μm)	Spring constant (N/m)	Pull down voltage (V)	Pull down voltage in Coventor-Ware (V)	Error (%)
100	3.01	9.05	10.5	14
150	3.08	7.48	8.7	14
200	3.12	6.52	7.5	13
300	3.16	5.40	6.2	13

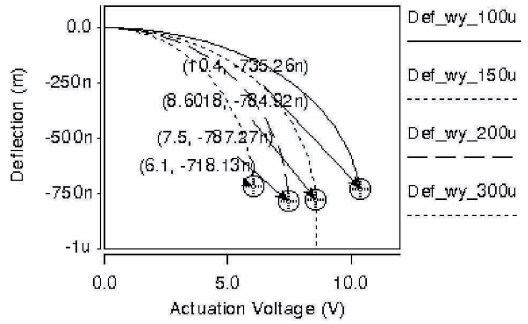

Figure 6: The pull down voltage simulation in Coventor-Ware for 200 μm long and 100 μm wide beam at anchor.

In the table 1 and table 2, we have seen that, the model has much lower error compare to the presented model in [2]. The error is almost constant for different electrode widths compare to a large variation of error for different electrode size and location presented in [2]. The model also matches for uniform beam formula presented in standard text book [1]. However, the pull down voltage is underestimated. In our analytical model, it is assumed that, the beam will collapse when the cantilever end moves 1/3rd of its initial gap. In CoventorWare the beam end needs to go beyond the 1/3rd of the initial gaps before it collapses, which may require higher pull down voltage. Another reason may be the non-linearity, which may further increase the pull down voltage in CoventorWare.

4. CONCLUSION

We have made a comprehensive analytical model for non uniform cantilever. The model matches quite closely with the CoventorWare simulation result. The ratio between the model and CoventorWare result is almost constant for different electrode widths. When the cantilever is longer (200 μm) the spring constant is very low and the electrode width has very low effect on spring constant. This will reduce the pull down voltage as the actuation force is higher. This model will be very useful for predicting pull down voltage of non uniform cantilever. This model can be implemented by any simple mathematical tools and calculation can be done within very short time.

ACKNOWLEDGEMENT

Authors are grateful to Norwegian Research Council for sponsoring the work through SMiDA project (No 159559/130) and IRRFT project (No 159259/I40).

APPENDIX

A force moment diagram of cantilever is shown in figure A1.

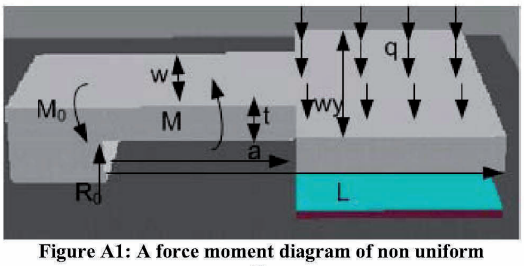

Figure A1: A force moment diagram of non uniform cantilever

In figure A1, 'L' is the length of the cantilever, 't' is the thickness of the cantilever, 'w' is the width of the cantilever close to the anchor and 'wy' is the width of the cantilever above the actuation electrode region. The distributed force acting on the cantilever electrode is 'q' per unit length. The distance from anchor to start of the actuation electrode is 'a'. The anchor is rigid so a moment

of inertia will be applied to keep the cantilever fixed at that position (no vertical movement and rotation). M_0 is the moment working at the anchor positions. R_0 is the reaction forces acting opposite to the actuation force to balance the vertical force [4].

The moment M_0 working at the anchor of the cantilever is given by [4],

$$M_0 = q(L-a)\left[a + \frac{L-a}{2}\right] = \frac{q}{2}(L^2 - a^2) \quad \text{(A1)}$$

The vertical force working on the anchor is given by,

$$R_0 = q(L-a) \quad \text{(A2)}$$

The equation of moment working on the beam shown in figure A1, at the region $0 \le x \le a$, is given by

$$M = q(L-a)x - \frac{q}{2}(L^2 - a^2)$$
$$EIv'' = q(L-a)x - \frac{q}{2}(L^2 - a^2) \quad \text{(A3)}$$

Here 'I' is the moment of inertia of the beam in this region and given by, $I=wt^3/12$.
By integrating equation (A3) in terms of x, and simplifying we get,

$$v' = \frac{q}{2EI}\left[(L-a)x^2 - (L^2 - a^2)x\right] + C_1 \quad \text{(A4)}$$

As the anchor is rigid no rotation can take place at the anchor. So at x=0, v'=0, which gives $C_1=0$ from equation (A4). So equation (A4) becomes,

$$v' = \frac{q}{2EI}\left[(L-a)x^2 - (L^2 - a^2)x\right] \quad \text{(A5)}$$

By integrating equation (A5) in terms of 'x' again, we get

$$v = \frac{q}{2EI}\left[(L-a)\frac{x^3}{3} - (L^2 - a^2)\frac{x^2}{2}\right] + C_2$$
$$= \frac{qx^2}{12EI}\left[2(L-a)x - 3(L^2 - a^2)\right] + C_2 \quad \text{(A6)}$$

As the anchor is rigid no vertical movement can occur at that region. At x=0, v=0, which gives $C_2=0$, so the equation of deflection in this region becomes,

$$v = \frac{qx^2}{12EI}\left[2(L-a)x - 3(L^2 - a^2)\right] \quad \text{(A7)}$$

For the region $a \le x \le L$, the equation of moment can be written as,

$$M = q(L-a)x - \frac{q}{2}(L^2 - a^2) - \frac{q}{2}(x-a)^2$$
$$\Rightarrow EIyv'' = qLx - \frac{qL^2}{2} - \frac{q}{2}x^2 \quad \text{(A8)}$$

Here 'Iy' is the moment of inertia of the beam above the electrode region, with the width 'wy' and thickness 't'. By integrating equation (A8) we get,

$$EIyv' = qL\frac{x^2}{2} - \frac{qL^2x}{2} - \frac{q}{6}x^3 + C_3'$$
$$v' = \frac{q}{6EIy}(3Lx^2 - 3L^2x - x^3) + C_3 \quad \text{(A9)}$$

Using the continuity of the slope of deflection at x=a, the constant C_3 is given by.

$$C_3 = \frac{qaL(a-L)}{2EI}\left(1 - \frac{1}{y}\right) + \frac{qa^3}{6EIy} \quad \text{(A10)}$$

By integrating the equation (A9) in term of x again we can get the equation for deflection,

$$v = \frac{q}{24EIy}(4Lx^3 - 6L^2x^2 - x^4) + C_3x + C_4 \quad \text{(A11)}$$

By using continuity of deflection at x=a we find

$$C_4 = \frac{qa^2L}{12EI}(3L - 4a)\left(1 - \frac{1}{y}\right) + \frac{qa^4}{12EI}\left(1 + \frac{1}{2y}\right) - \frac{qa^4}{6EIy} \quad \text{(A12)}$$

The maximum deflection of the cantilever occurs at x=L or at the end of beam. The deflection at x=L from the equation (A11) is given by (without replacing the value of C_3 and C_4 for simplification),

$$v_L = -\frac{qL^4}{8EIy} + C_3L + C_4 \quad \text{(A13)}$$

The spring constant of the cantilever is given by,

$$k = -\frac{P}{v_L} = -\frac{q(L-a)}{v_L} \quad \text{(A14)}$$

REFERENCES

[1] G.M. Rebeiz, *RF MEMS Theory, Design and Application,* New Jersey, *John* Wiley and Sons 2003.

[2] S. Afrang et al, *Design and Simulation of Simple and Varying Section Cantilever and Fixed-Fixed End Types MEMS Switches*, Proceeding of ICSE 2004. pp. 593-596.

[3] L. Lv et al, *Analysis and Simulation of RF MEMS for Wireless Communication*, Proceedings of ISCIT 2005, pp 1095-1098.

[4] J.M. Gere et al, *Mechanics of Materials*, Boston, 4th Edition, PSW publication, 1990.

[5] J.B. Mauldavin et al, *Nonlinear Electro-Mechanical Modeling of MEMS Switches*, IEEE MTT-S Digest, 2001.

Modeling of Spring Constant and Pull-down Voltage of Non-uniform RF MEMS Cantilever Incorporating Stress Gradient

Shimul Chandra Saha[1], Ulrik Hanke[2], Geir Uri Jensen[3], Trond Sæther[1]

[1]Department of Electronics and Telecommunications (IET), Norwegian University of Science and Technology (NTNU), 7491 Trondheim, Norway

[2]Institute of Microsystems Technology, Vestfold University College, 3103 Tønsberg, Norway

[3] SINTEF ICT, Gaustadalleen 23, 0371 Oslo, Norway

Has been submitted to Sensors and Transducers Journal.

Is not included due to copyright

MODELLING OF SPRING CONSTANT OF A NON-UNIFORM RF MEMS BRIDGE

S. C. Saha[a], U. Hanke[b], G. U. Jensen[c], T. Sæther[a]

[a] Department of Electronics and Telecommunications (IET), Norwegian University of Science and Technology (NTNU), 7491 Trondheim, Norway. E-mail: shimul.saha@iet.ntnu.no, trond.saether@iet.ntnu.no

[b] Institute of Microsystems Technology, Vestfold University College, 3103 Tønsberg, Norway. E-mail: Ulrik.Hanke@hive.no

[c] SINTEF ICT, Gaustadalleen 23, 0371 Oslo, Norway. E-mail: Geir.Jensen@sintef.no

Has been submitted to International Journal of Modelling and Simulation (ACTA press/IASTED)

Is not included due to copyright

Tuning of resist slope for RF MEMS with hardbaking parameters

Shimul Chandra Saha [1], Håkon Sagberg [2], Geir Uri Jensen [2], and Trond Sæther [1]

[1] Department of Electronics and Telecommunications, Norwegian University of Science and Technology (NTNU), NO-7491 Trondheim, Norway.
[2] Department of Microsystems and Nanotechnology, SINTEF ICT, PO Box 124 Blindern, NO-0314 Oslo, Norway

In proceedings of 19th international Microprocess and Nanotechnology Conference (MNC 2006), pp 314-315, October 2006, Kanagawa, Japan.

Is not included due to copyright

Tuning of resist slope with hard-baking parameters and release methods of extra hard photoresist for RF MEMS switches

Shimul Chandra Saha[1], Håkon Sagberg[2], Erik Poppe[2], Geir Uri Jensen[2], Tor A. Fjeldly[1] and Trond Sæther[1]*

[1]Department of Electronics and Telecommunications (IET), Norwegian University of Science and Technology (NTNU), NO-7491 Trondheim, Norway
[2]Department of Microsystems and Nanotechnology, SINTEF ICT, PO Box 124 Blindern, NO-0314 Oslo, Norway

Journal of Sensor and Actuators A: Phys. Vol. 142 (2), pp 452-461, 2008.

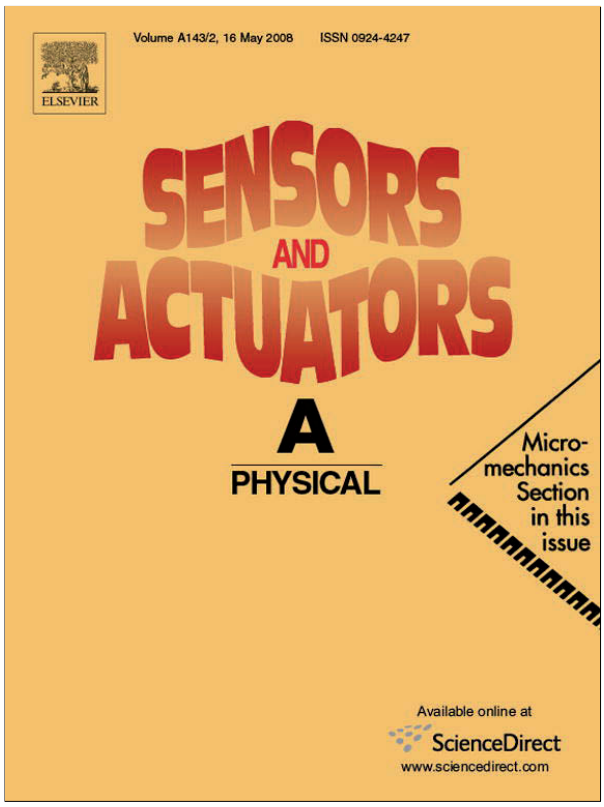

Available online at www.sciencedirect.com
ScienceDirect
Sensors and Actuators A 143 (2008) 452–461
SENSORS AND ACTUATORS A PHYSICAL
www.elsevier.com/locate/sna

Tuning of resist slope with hard-baking parameters and release methods of extra hard photoresist for RF MEMS switches

Shimul Chandra Saha [a,*], Håkon Sagberg [b], Erik Poppe [b], Geir Uri Jensen [b], Tor A. Fjeldly [a], Trond Sæther [a]

[a] *Department of Electronics and Telecommunications (IET), Norwegian University of Science and Technology (NTNU), NO-7491 Trondheim, Norway*
[b] *Department of Microsystems and Nanotechnology, SINTEF ICT, P.O. Box 124 Blindern, NO-0314 Oslo, Norway*

Received 6 July 2007; received in revised form 12 October 2007; accepted 21 October 2007
Available online 1 November 2007

Abstract

We have studied the properties of photoresist (resist) as a sacrificial material for fabricating suspended metal bridges and developed a process to release RF MEMS switches by dissolving thermal cross-linked extra hard photoresist. At the edges of the patterned photoresist, the contact angle with the substrate can be tuned using hard-baking parameters. From the experiment we have found that the resist angle reduces both with baking temperature and time. The baking temperature has a stronger effect on resist slope than the baking time has. It is also observed that at a certain baking temperature, and after a certain time, the resist angle does not reduce further. The RF MEMS switch with photoresist as the sacrificial layer can be released by plasma ashing to strip the initial resist skin, followed by dissolution of the bulk resist in Microposit 1165 solution with heating. The heating of the Microposit 1165 solution accelerates and improves the dissolving process. The Piranha solution is also very effective in dissolving hard resist for releasing RF MEMS switches.

Keywords: RF MEMS; Resist angle; Hard-baking parameters; Thermal cross-linking; Resist skin; Plasma stripping

1. Introduction

Radio frequency microelectromechanical systems (RF MEMS) devices are becoming increasingly popular owing to their very good performances at RF and microwave frequencies [1,2]. RF MEMS switches have very low insertion loss in on-state and very high isolation in off-state. Electrostatically actuated MEMS switches consume very little power. They are very linear and have very high third order intercept point compared with any other solid-state counterparts. Surface micromachining is the most common fabrication process for RF MEMS. We are developing a process to fabricate capacitive RF MEMS switches at SINTEF MiNaLab, Oslo, Norway.

In order to fabricate suspended bridges or cantilevers, photoresist can be used as a sacrificial layer [3], as shown in Fig. 1. There are several advantages in using resist as a sacrificial layer. First of all, it will reduce the number of required process steps. If we use another material as a sacrificial layer, it will require extra process steps like patterning and etching. Second, we can tune the resist angle for a climbing anchor pattern bridge at the edge, by optimizing the photolithography process parameters like hard-baking parameters (temperature and time), exposure gap (gap between the mask and the resist surface), etc. For sacrificial materials like oxide or metal, it would be much more difficult to obtain the desired sloping profile or tune its angle at the edge.

In order to have a simple fabrication process for the suspended bridge, a climbing anchor is preferred to a vertical anchor. If we want to fabricate a vertical anchor as shown in Fig. 2, we have to sputter the metal first for the anchor and then do the lithography to define the vertical anchor. Subsequently, we need to sputter again and define the bridge, which increases the number of required process steps. RF MEMS switches perform switching (on/off) by the mechanical movement (up/down) of the suspended bridge. Fig. 3 shows an actuated bridge in downstate. For reliable switch operation, the anchor should have sufficient

* Corresponding author. Tel.: +47 7359 2784; fax: +47 7359 1441.
E-mail address: shimul.saha@iet.ntnu.no (S.C. Saha).

0924-4247/$ – see front matter © 2007 Elsevier B.V. All rights reserved.
doi:10.1016/j.sna.2007.10.067

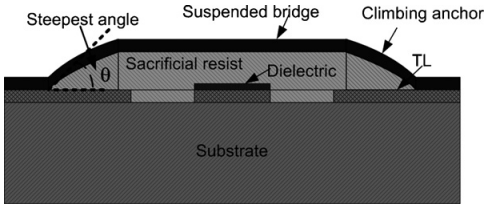

Fig. 1. A cross-section view of the sputtered bridge on sacrificial layer with climbing anchor.

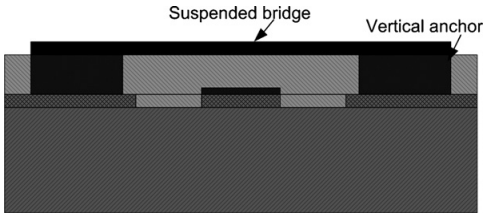

Fig. 2. A cross-section view of the suspended bridge with vertical anchor.

thickness compared with the rest of the bridge. To guarantee this, the resist angle should be fewer than 45° at the (steepest) position of the anchor. If we have a steeper angle, more than 45°, the metal thickness of the anchor may be significantly thinner than the rest of the bridge [4]. The improvement of the step coverage with decreasing sidewall angle is also supported by (Figs. 5, 7 and 8 presented by [5]). The thinner metal at anchor will reduce the reliability of the suspended bridge significantly. If the angle is very small, the planarity of the switch will be worse. To obtain a smaller angle, the resist needs to be hard-baked at a higher temperature for an extended period of time. The resist will be harder and it will be difficult to dissolve during the release process of the MEMS switch afterwards.

We deposited gold by dc sputtering to form the suspended bridge on the tuned resist. After lithography and patterning of the switch, the sacrificial resist need to be dissolved to release the suspended bridge. Acetone and Microposit 1165 provided by Shipley can be used for dissolving resist. We used both acetone and Microposit 1165 with heating but found some residue left and the samples were not fully cleaned. The residue looks like threads, which gives us the indication of thermal cross-linking. The residue can cause possible stiction during actuation of the switch.

Here we have shown that it is possible to obtain a desired angle by optimizing the combination of baking temperature and baking time. This is more efficient compared with work published on resist angle tuning by either baking temperature or baking time [4,6]. The exposure gap between the mask and the resist surface could also be optimized to tune the resist angle as mentioned in [7,8]. We have also developed a systematic process to release the RF MEMS switches by dissolving the hard resist. From the experiment we have found that we can use the plasma stripping to ash the initial strong resist skin. Afterwards we can use heated Microposit 1165 to dissolve the rest of the resist completely. This process looks very efficient and we can obtain very clean switches without any resist residue on the substrate. It was also found that the Piranha solution could be very effective in dissolving hard and cross-linked resist. The Piranha solution is a mixture of H_2O_2 and H_2SO_4 (1:2) and it was heated at 140 °C. To dissolve hard resist with the ordinary method of using a typical solvent would require hours or even a day of soaking in the solvent with ultrasound stirring. Even so in some cases it would not completely dissolve the resist. Our developed method is very successful and time-efficient. This work will be very helpful for fabrication of any kind of surface micromachining MEMS device for tuning the initial sacrificial layer angle and to release it at the final stage of the process.

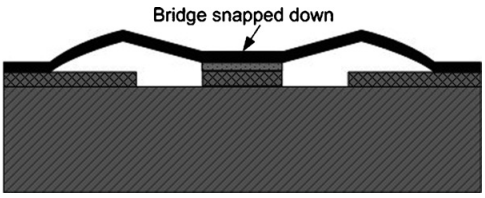

Fig. 3. An actuated MEMS switch in down state.

A review of the thermal reflow and thermal cross-linking of photoresist is presented in Section 2. The experimental methods, with reference to previous work, are presented in Section 3. The results and discussion are presented in Section 4, followed by the conclusion in Section 5.

2. Thermal reflow of photoresist, thermal cross-linking of photoresist and formation of hard skin

2.1. Thermal reflow of photoresist

When photoresist is hard-baked at a temperature higher than the glass transition temperature (T_g), the resist viscosity decreases and at a certain temperature the resist becomes fluid with a fixed surface tension. The system tries to achieve a state of minimal potential energy and therefore minimizes its surface. Since the smallest surface for a given volume is a sphere, a cubic pattern tends to form a hemispherical surface [9]. The thermal reflow of resist depends on various factors such as baking temperature, baking time, resist characteristics and resist volume, etc. According to [10], the shrink bias or shrinking of the critical dimension (ΔCD) as shown in Fig. 4, can be expressed as a functional relationship of the baking temperature, normalized volume $V(V_n)$, and the native property (K_r) of the resist, as shown in Eq. (1):

$$\Delta\mathrm{CD} = (T_b, V_n, K_r) \tag{1}$$

Here T_b is the baking temperature for a fixed time and V_n is the normalized value as square area–circular area [10].

The critical dimension shrinkage depending on temperature is given by

$$\Delta\mathrm{CD} = B \times \exp(A \times T_b) + C \tag{2}$$

where A, B, C are constants [10].

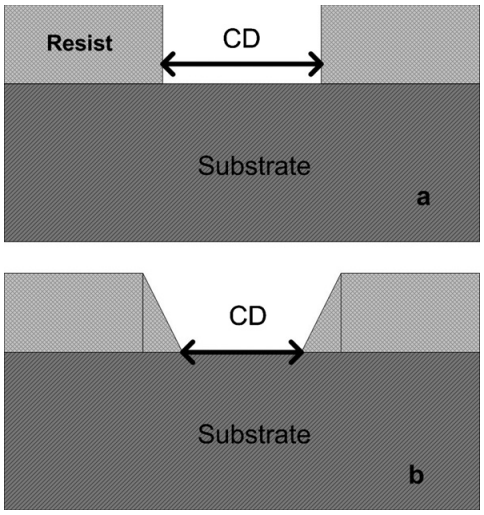

Fig. 4. The change in critical dimension (CD) before thermal reflow (a) and after thermal reflow (b).

The resist reflow also depends on the baking time. For a typical resist structure the thermal reflow length is given by [11]

$$L = \sqrt{\frac{\mu t}{\rho}} \tag{3}$$

where ρ is the resist density, t the baking time and μ is the fluid viscosity. The fluid viscosity $\mu(T)$ at specific temperature is given by

$$\mu(T) = \mu_0 \exp\left(\frac{E}{RT}\right) \tag{4}$$

where E is the activation energy, μ_0 the pre-exponential factor and R is the universal gas constant. A fitted viscosity function used for simulation is given by [11]

$$\mu = (4.84414 \times 10^{16}) \exp\left(-\frac{4848.2}{T}\right) \tag{5}$$

From Eqs. (2) and (3) it can be seen that the baking temperature has a more pronounced effect on the resist edge (angle) than the baking time. The resist extension or angle at the edge can be varied more effectively with temperature than with time. This is also supported by [12]. The HIPR resist containing Novolac resin, which we used for our experiment, has a glass transition temperature of $T_g = 90\,^{\circ}\mathrm{C}$.

2.2. Thermal cross-linking in positive tone resists

Moon et al. [13] presented results on three-component photoresist based on thermal cross-linking. From their experiment it was found that the vinyl ether groups react with hydroxyl groups of the binder polymer at high temperatures (from pre-baking) through electrophilic addition reaction to form cross-linked networks. These authors also suggest that thermal cross-linking does not occur at temperatures around or below 50 °C. But after pre-baking at 80 °C for 10 min, the dissolution rate of the resist is greatly decreased, and when the resist is baked at 120 °C the dissolution rate is very low, as presented by Moon et al. (Fig. 2; [13]). Post-exposure baking also increases the thermal cross-linking in the unexposed area. That means that the unexposed resist is hardened twice, which makes the resist difficult to dissolve. Miyagawa et al. [14] also presented work on thermal cross-linking of positive tone photoresist with *o*-naphthoquinone diazide (NQD). They mentioned that in the polymer matrix the thermal reaction of multifunctional NQD compound with copolymers with hydroxyl groups yielded sufficiently cross-linked structures at high temperatures around 140 °C for 10 min. It was also observed that heating made a great difference in solubility between exposed and unexposed areas. They also found that the gel fraction (the degree of cross-linking) increased with the post-exposure baking temperature (Fig. 8; [14]).

2.3. Formation of hard resist and skin on the surface

From Section 2.2 we can see that for high temperature and longer baking time a thermal cross-linking occurs for positive tone resist (in fact, this is also the case for negative resist [15,16]). The resist at the unexposed area becomes twice hardened by both pre-bake and post-bake. To release RF MEMS switches we have to dissolve mainly unexposed and baked resist. The increase in the resist hardness with thermal cross-linking is also supported by [17]. Kawai [17] has presented work on the thermal properties of photoresist. The resist used was a Novolak resin mixture and he found that the Knoop hardness of the resist increases with baking temperature (Fig. 1; [17]). The work also shows the indentation rate of AFM (atomic force microscope) tips with baking temperature, which shows a depth profile at mid-temperature range. The author suggests that the data for the depth profile region of hardness show that a hardened rigid resist layer is formed on the resist surface and that the inner layer still remains soft. This hard layer is called skin and is also mentioned in Ref. [18]. According to [18], the hard skin can form as a result of reactive ion etching (RIE) or ion implantation. This can also be caused by hard baking of the resist or if the resist is exposed to a high temperature process. In the processing of the switches, the resist experiences several high temperature cycles. One of them is high temperature hard baking, around 115–120 °C, to tune the resist angle, as mentioned in Section 1. During the metal sputtering for the suspended bridge, the sacrificial resist can also experience high temperature back sputtering.

For the positive tone resist, a short delay time between coating and DUV exposure can produce a 'lip' at the top surface of the relief image. A long delay time between coating and exposure causes a thin skin to form between resist and air interface [19].

3. Experiments

A two-mask process was used for our experiments. The aim of the experiments was to develop several process steps. One was to tune the resist angle at the anchor position for the climbing anchor/bridge. Another was to develop a successful release pro-

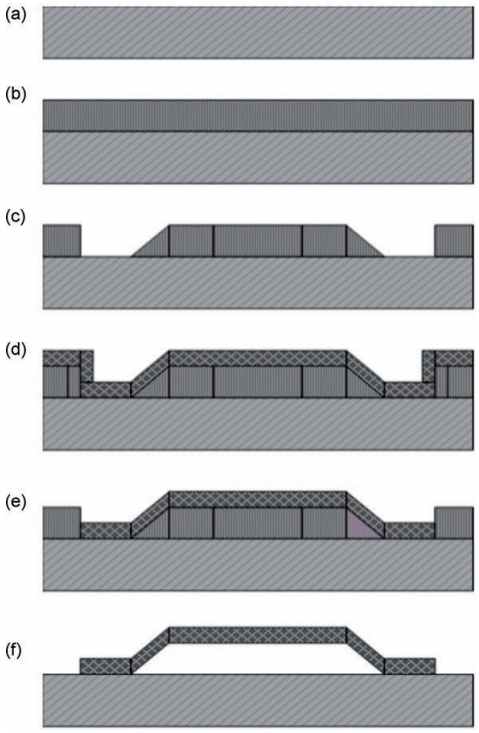

Fig. 5. A brief overview of the process flow for two masks process.

cess by dissolving the sacrificial resist and subsequently drying the switches.

A brief process overview is shown in Fig. 5. A p-type, one side polished, 350 μm thick (1 0 0) 4″ silicon wafer was used for the fabrication (a). A 2.5 μm thick resist was coated on the silicon substrate by spin coating (b). The resist was pre-baked at 100 °C for 90 s on a hotplate and then exposed to form the opening by means of the anchor mask. The resist was developed in the MF 312 (1:1) solution for 1 min (c). The wafers were then hard-baked at the desired baking parameters, and then gold was sputtered onto the sacrificial layer and substrate. The thickness was close to 1 μm (d). The gold was patterned by the switch mask and etched in a KI_4 solution to form the switch (e). Subsequently, the resist was dissolved by the process developed in this work, followed by drying and release in a CO_2 critical point dryer (f).

3.1. Resist angle tuning

Some work has been published on the dependence of resist angle on different parameters. The resist angle depends on the baking time [4], the baking temperature [6] and the exposure gap [7]. The work in [4] aims for a 45° angle. Refs. [6,7] seek to obtain a vertical profile. The goal in Ref. [4] is to obtain the desired angle by varying the baking time. The authors of [6] try to optimize the resist angle by tuning the baking temperature. Ref. [7] tries to optimize the desired resist angle by controlling the wavelength of the exposure light. This is rather complicated, because it will require a special filter for wavelength selection. This will increase the cost of the fabrication. We have performed an experiment to inspect the combined effects of baking time and temperature on resist angle.

Some results of the resist angle tuning have already been presented as a short abstract [20]. We used two types of resist for the resist tuning experiment, HIPR 6517 and diluted AZ 4562. We targeted a thickness of 2.5 μm for the sacrificial layer. For HIPR 6517, we got a thickness of 2.55 ± 0.01 μm at a spin speed of 2000 rpm. AZ 4562 is a thick resist and we diluted it with solvent in a 20:7 ratio. We obtained a thickness of 2.55 ± 0.03 μm at 3250 rpm spin speed. Here 0.01–0.03 μm was the deviation over the wafer. The solvent used was MICROPOSIT EC SOLVENT (2-methoxy-1-methylethyl acetate) from Rohm and Haas. After spinning, the resist was soft-baked at 100 °C for 90 s on a hotplate. Then we exposed the resist in automatic exposure tools through the anchor mask (opening for metal deposition to substrate). The exposure power was 35 mW/cm^2. We exposed the HIPR 6517 resist for 5 s with an exposure gap of 25 μm. The diluted AZ 4562 resist was exposed for 5 s with an exposure gap of 30 μm. We also varied the exposure gap for a few wafers to investigate its effect on the resist slope. After exposure, we developed all the wafers in MF 312 solution (1:1) for 1 min.

After development, the resist was hard-baked on a hotplate at temperatures ranging from 100 °C to 130 °C for duration of 90–180 s. A few wafers were also baked for a longer time (5 min) and at a higher temperature (150 °C). For some wafers the exposure gap was changed to 50 μm, instead of the standard gap. The detailed conditions and obtained resist angle are presented in Section 4.

After baking we cut the wafers through the anchor position or opening in the sacrificial resist layer. Then we mounted the wafers vertically on the sample holder. We inspected the edge profile of the patterned resist in a scanning electron microscope (SEM). We took SEM images at several positions on each wafer. Owing to charging it can be difficult to obtain a clear SEM image of polymer materials, so we used a very low vacuum (∼0.5 mbar) and low excitation voltage (3–5 kV) for the SEM inspection. Other surface profile measurement systems, such as a profilometer (needle), optical interferometry and atomic force microscopy (AFM), can also be used for this purpose. The profilometer uses a sharp needle and a small amount of force/weight to scan the surface. The resist is usually soft, which may cause the needle to penetrate beyond the surface into the bulk resist. As we were interested only in the steepest part with a very sharp image of the rising part, this system was not suitable for finding the exact angle. Optical interferometers usually give a very accurate result, but not for samples where the surface has steep slopes as in our example. In our sample the ratio of the vertical distance to the horizontal distance at the sloping part was close to unity, which made it difficult to get an accurate surface profile of this region. The AFM would have been a good option, but we did not have access to it in our lab.

The reliability of the sputtered bridge depends on the steepest angle of the resist. We measured the resist angle at the steepest part of the edge for different baking conditions. The

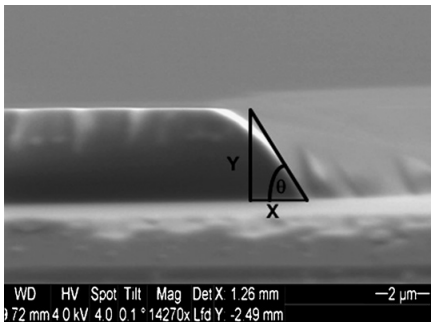

Fig. 6. A schematic view of angle measurement from SEM image.

resist angles were obtained by measuring the horizontal and vertical distance at the steepest part of the anchor, using the equation $\theta = \tan^{-1}$(Vertical distance (Y)/Horizontal distance (X)), as shown in Fig. 6.

3.2. Release methods of hard resist

Owing to availability and ready-to-use facilities, we used the HIPR 6517 resist as a sacrificial layer for our test device fabrication. This positive tone resist, HIPR 6517, is provided by Fujifilm. The chemical compounds of the resist are ethyl lactate (45–60%), ethyl-3-ethoxypropionate (20 to <25%), Novolac resin (15–25%), and naphthoquinone diazide ester derivative (3–10%).

Acetone can be used to dissolve ordinary resist. We kept the sample in acetone for several hours (overnight) and also heated the solvent for 1–2 h with magnetic stirring. After drying, we inspected the samples in an optical microscope and found that the resist was not completely dissolved and a lot of residue material remained on the substrate. The Shipley Microposit 1165 resist remover is specially used to dissolve hard resist. We also used this solvent to release our switches. We kept the sample in Microposit 1165 for some 4–5 h followed by an additional 1–2 h of heating with stirring, and found that still some resist residues remained on the sample. The residue looks like threads, which gave us the indication of thermal cross-linking. If the resist residue is left after release it could change the electrical characteristic of the switch and possibly also cause stiction.

In order to release RF MEMS switches, the solvents have to dissolve both the resist on the substrate around the bridge and also the resist underneath the suspended bridge. The sacrificial layers are usually few micrometers thick and in our case it was 2.55 μm. The bridge width may be several tens of micrometers and in our design the bridge width ranged from 20 μm to 100 μm. The solvent also has to dissolve the resist underneath the bridge from the side, as shown in Fig. 7, and this will take longer to clean the resist fully. Microposit 1165 is regarded as a better option to dissolve hard resist compare with acetone. So we used Microposit 1165 for our experiment. From discussion with the relevant people, it was found that heating could accelerate the dissolution of resist in the solution. It was also suggested [18] that a short plasma strip at the beginning could remove the skin. The rest of the bulk resist can be effectively dissolved by Microposit 1165 with heating. It was also learned that the Piranha solution could effectively dissolve hard resist. We conducted an experiment to dissolve hard resist with possible skin with all the different options available in our lab.

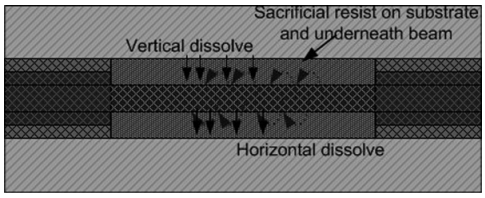

Fig. 7. A top view of the switch with possible way of access the resist by solvent.

Another suggestion [18] was that ashing of the top 10–20% of the total resist would be enough for subsequent release. So we targeted to ash the (around) 300 nm thick resist skin with plasma ashing. We did a brief plasma stripping trial to measure the ashing rate of the plasma tool in our lab. From this experiment we found that the plasma tool can ash 300 nm skin at 150 W in 45 min. We chose low power intentionally to avoid high temperature during stripping, which could buckle the patterned bridge by annealing.

We selected eight samples with the same process parameters (i.e. baking temperature, gold sputtering, etc.) for our experiment. The resist was pre-baked at 100 °C for 90 s and post-baked at 120 °C for 5 min on a hotplate. The samples were labelled RS (resist stripping) 1–8 for convenience of identification. A brief plan of the experiment is shown in Table 1. We ashed four samples, RS 1–4, in a plasma stripper. Four samples, RS 5–8, were kept without ashing. After that, we put all the samples RS 1–8 in Microposit 1165 for about 90 min at room temperature with magnetic stirring. Then we put the specific samples RS 1, 2, 5 and 6 in heated Microposit 1165 for 60 min with magnetic stirring. We heated the solution up to a temperature of around 60 °C. The rest of the samples we kept in Microposit 1165 for the same time at room temperature. Finally we put all the samples again in Microposit 1165 at room temperature with magnetic stirring

Table 1
The experimental setup to dissolve hard resist with plasma ashing and Piranha dip

Plasma strip (150 W, 45 min)				No plasma strip			
Heating Microposit 1165 (~60 °C)		No heating Microposit 1165		Heating Microposit 1165 (~60 °C)		No heating Microposit 1165	
Piranha dip, 60 s	No Piranha dip	Piranha dip, 60 s	No Piranha dip	Piranha dip, 30 s	No Piranha dip	Piranha dip, 30 s	No Piranha dip
RS 1, very clean	RS 2, very clean	RS 4, very clean	RS 3, almost clean	RS 5, Very clean	RS 6, thin skin left	RS 7, very clean	RS 8, not clean

Table 2
The resist angle of HIPR 6517 for different baking conditions

Baking temp. (°C)	Baking time (s)	Exposure gap (μm)	Resist angle (°)
No bake		25	65
100	90	25	59
100	120	25	57
100	180	25	55
115	90	25	49
115	120	25	45
115	180	25	43
115	300	25	41
130	90	25	34
130	180	25	35
150	90	25	28
100	90	50	45

for another 60 min. After this, we dipped the specific samples RS 1,4,5 and 7 in a Piranha solution. Two samples, RS 1 and 4 were kept in Piranha for 30 s and the remaining two samples, RS 5 and 8, were kept for 1 min. This was done intentionally to check if the Piranha attacked the gold switches. We did not find any evidence of such an attack in either of these samples. After the experiment, we dried all the samples and inspected them in an optical microscope. In order to avoid stiction during wet release, we used CO_2 critical point dryer to release our fabricated RF MEMS switches.

4. Results and discussion

4.1. Resist angle tuning

The variation of the resist angle with time and temperature can be seen from the SEM images shown in Fig. 8. For comparison the SEM images for HIPR 6517 have been scaled to the same magnification and compared in Fig. 8. From Fig. 8 it can be easily seen that the resist angles decreased with both baking temperature and baking time. The measured resist angles, for both HIPR 6517 and diluted AZ 4562, with different baking conditions, are shown in Tables 2 and 3. A variation of resist angle with baking temperature for a baking time of 90 s is shown in Fig. 9. Also the variation of resist angle with baking time at a baking temperature of 115 °C is shown in Fig. 10.

From Tables 2 and 3, it can be seen that the resist angle decreases with both baking temperature and time. The baking temperature has greater effect on resist angle than the baking time does. It is also seen from Fig. 9 that the angle decreases at a lower rate at higher temperatures. The baking time has very little effect at higher baking temperatures. Also, the resist angle decreases little after a certain period of baking. The effect of baking temperature and time has similar effect on both kinds of resist. The resist angles of diluted AZ 4562 decrease at a slower rate with baking time than HIPR 6517, as can be seen from Fig. 10.

Table 3
The resist angle of diluted AZ 4562 for different baking conditions

Baking temp. (°C)	Baking time (s)	Exposure gap (μm)	Resist angle (°)
No bake		30	64
100	90	30	59
100	120	30	59
100	180	30	56
115	90	30	47
115	120	30	46
115	180	30	43
130	90	30	37
115	90	50	40

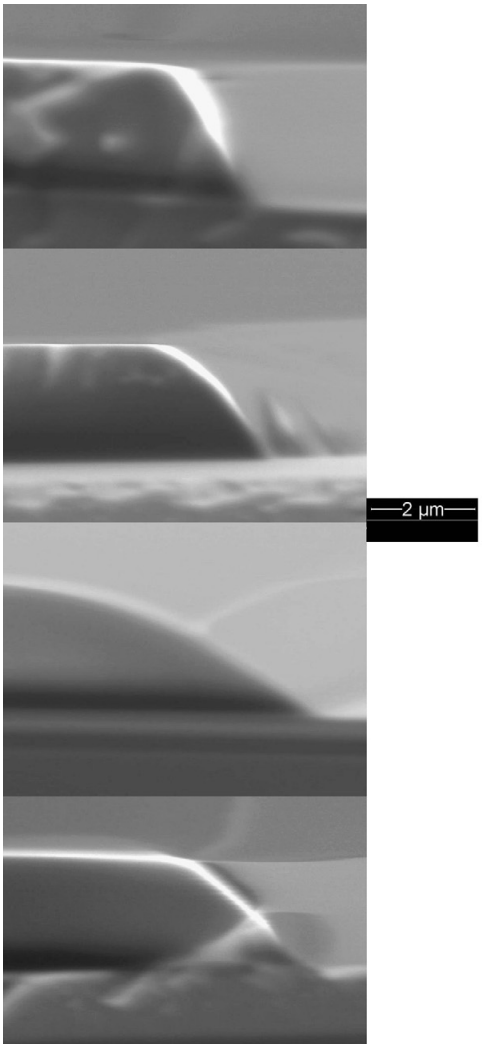

Fig. 8. The SEM images for HIPR resist at same scale. Baking temp 100 °C (top), 115 °C (second from top), 130 °C (third from top) all for 90 s baking time. Baking temp 115 °C for 120 s baking time (bottom).

Comparing our work with [4,6], it can be seen from Fig. 9 and the data from Puchner et al. (Fig. 5; [6]) that the variation of the angle with temperature is sharper in Ref. [6] (large resist pattern) than in our work. From Fig. 10 and the work presented by Grenier (page 42; [4]) it can be seen that the resist angle decreases at a

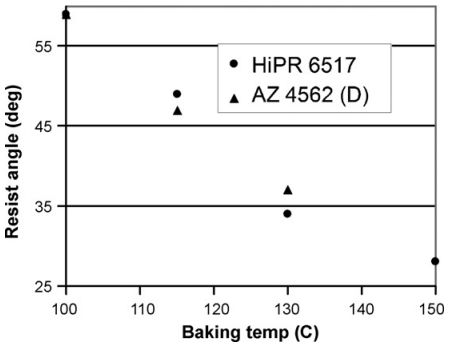

Fig. 9. Resist angle vs. baking temperature for 90 s baking time.

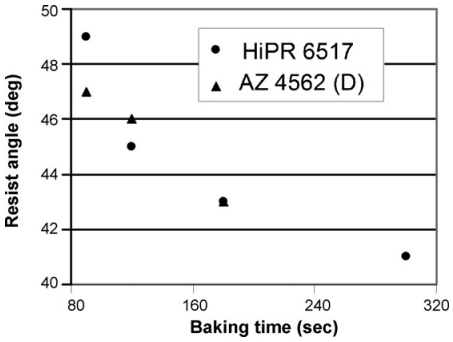

Fig. 10. Resist angle vs. baking time at 115 °C baking temperature.

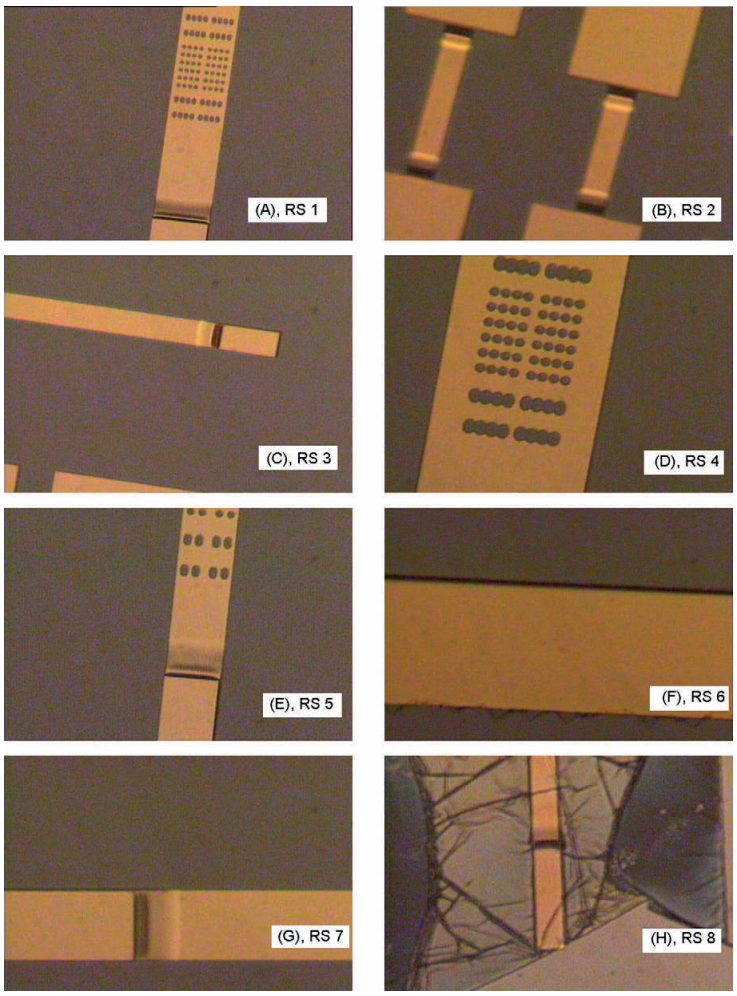

Fig. 11. The optical image of all the released samples together. The samples identification nos. RS 1–8 are marked on each image.

higher rate with increasing baking time [4] compared with our work. For both works the rate of reduction in angle decreases with time. In Ref. [4] the reduction in angle stops after a certain time but in our work it continues to decrease with time. An exact comparison is difficult because different hotplates were used. The initial angle was a little smaller in our experiment than the work presented in Refs. [4,6].

From the experiment it is seen that we can obtain an angle of around 45° by baking at 115 °C for 120 s. From Tables 2 and 3 it is also seen that the exposure gap has a strong effect on the resist angle, and the resist angle decreases with a higher exposure gap. From this experiment we have seen that we can combine the baking temperature with baking time in an optimum way to obtain a desired angle.

4.2. Release method of hard resist

The images of the dried samples are shown in Fig. 11. From Fig. 11B it can be seen that the hard resist can be dissolved completely by plasma stripping and hot Microposit 1165 solution. It is also seen from Fig. 11B and F that the ashing has great effect on the release. The sample in Fig. 11F, without ashing and with heating, still has some resist skin residue left, which can be seen on the bridge edge. It is also seen from Figs. 11F and H that heating has an effect on the dissolution of the resist. The amount of resist residues left on the sample without heating is much higher than with heating. From Fig. 11H it can be seen that the sample without ashing, heating and Piranha dip has still left a lot of resist skin and residue. From Fig. 11 A, D, E and G, it can be seen that Piranha is very effective in dissolving hard resist. It can dissolve the resist even without plasma ashing. One has to be careful, however, that the high temperature (around 140 °C) does not affect the device performance and that Piranha does not attack the metal membrane.

It is also possible to use only plasma stripping to release the RF MEMS switches. This is a dry process and usually simple to use. The vertical strip of 2.55 μm thick resist is very fast but it takes a long time to etch the resist underneath the bridge. The plasma cannot attack (access) the resist directly as the suspended gold bridge works as a mask. So the resist underneath the bridge (∼100 μm wide) has to be ashed from the side, through the initial gap of the bridge (2.55 μm), which will be quite time-consuming at low power. For some samples we used a high power around 400 watts for 1/2–2 h but the bridge and cantilever were buckled owing to the heating produced by plasma power. The anchor part got a high peak and the suspended part buckled down, which can be seen from the cantilever group shown in Fig. 12. The plasma stripping method can be made effective by introducing holes in the suspended part, allowing the plasma to access the resist quite easily and quickly.

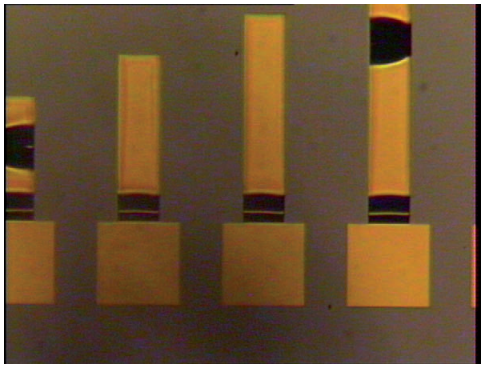

Fig. 12. The released cantilever by plsma strip at 400 watts for 45 min (It can be seen easily that at anchor the cantilever buckled up).

In order to test that there was no residue left underneath the bridge, some cantilevers were folded into an upside-down position and inspected in an optical microscope. For comparison a sample from ordinary release and one released by plasma stripping and heating (RS 2) were inspected. The comparison is shown in Fig. 13. From this figure it can be seen that RS 2 is completely clean while the sample with ordinary release has some residue left on the backside of the bridge and cantilever. Using these developed methods, we have fabricated the complete switch with transmission line and dielectric layer. The SEM images of the released switch have been shown in Fig. 14 (top view) and Fig. 15 (15° tilted).

In order to release the MEMS structure completely, without any residue and threads on the bridge and substrate, one can use plasma stripping first to remove the top layer of thin skin. Afterwards the sample can be put in Microposit 1165 with possible heating. It is also advantageous to use some kind of

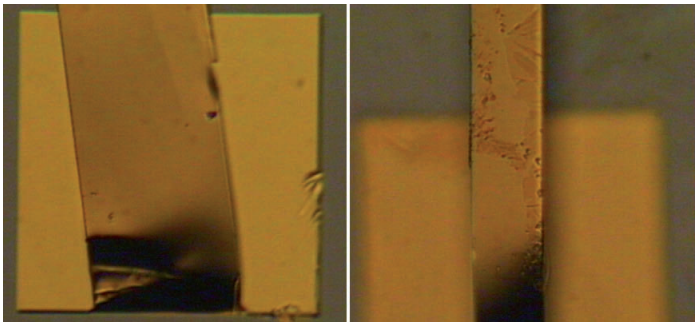

Fig. 13. The back side of the released cantilever folded backside upward, with our develop process, RS 2 (left) and with ordiany slovent release (right).

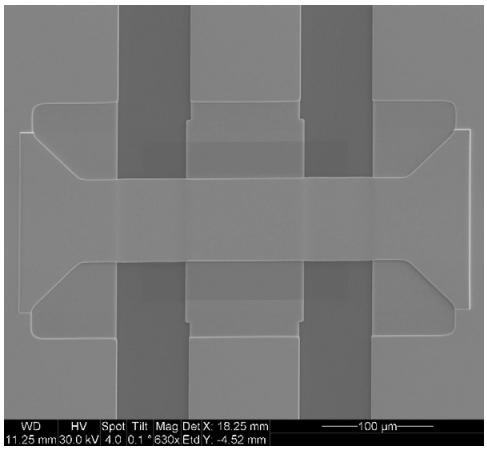

Fig. 14. The SEM image of a released RF MEMS switch (top view).

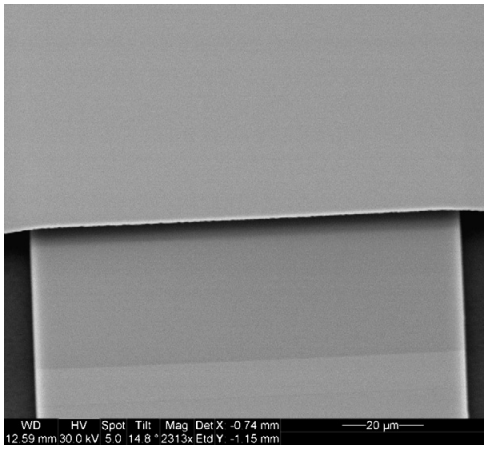

Fig. 15. The enlarged SEM image of the middle section of the switch bridge, above the electrode (tilted 15°).

stirring, which will improve the release quality and accelerate the process. This method is very effective and also less time-consuming. The total dissolution process may take 3–4 h. The ordinary solvent methods require hours and even days and also require ultrasound stirring for violent shaking, and sometimes this is still not enough to clean the sample completely. We have used this process on several occasions to release our samples and found it to be very effective without leaving any kind of residue on the substrate.

5. Conclusions

We have developed a method to tune the resist angle by different hard-baking parameters and optimized a process to release the RF MEMS switch without any resist residue left. The baking temperature and time can be combined in an optimum way to get a desired angle. The baking temperature has a prominent effect on the resist angle. From the release method experiment it is seen that plasma ashing followed by Microposit 1165 remover with possible heating can successfully dissolve the thermally cross-linked hard resist and release the RF MEMS switches. This work will be very helpful in tuning the resist angle and release of RF MEMS switches, which use resist as a sacrificial layer. The results of this experiment are applicable to any kind of surface micromachined MEMS device.

Acknowledgements

The authors are grateful to the Norwegian Research Council for sponsoring the work through the SMiDA project (no. 159559/130) and the IRRFT project (no. 159259/I40). The authors also thank MiNa Lab personnel for their support in the clean room.

References

[1] G.M. Rebeiz, J.B. Muldavin, RF MEMS switches and switch circuits, IEEE Microwave Magazine 2 (4) (2001) 59–71.
[2] H.J. De Los Santos, S. Rassoulian, J. Maciel, MEMS for future microwave system, in: Proceedings of 2005 IEEE MTT-S, Long beach, CA, USA, 2005, pp. 905–908.
[3] K. Walsh, J. Norville, T. Yu-Chong, Photoresist as a sacrificial layer by dissolution in acetone, in: Proceedings of 2001 IEEE Int'l MEMS conference, Interlaken, Switzerland, 2001, pp. 114–117.
[4] K. Grenier, (LAAS-CNRS), IMEC Training: MEMS in RF and MW Electronics, Belgium, April, 2005.
[5] T. Smy, R.N. Tait, K.L. Westra, M.J. Brett, Simulation of density and step coverage for via metallization, in: Proceedings of VMIC conference, Santa Clara, CA, USA, 1989, pp. 292–298.
[6] H. Puchner, R. Castagnetti, W. Pyke, Minimizing thick resist sidewall slope dependence on design geometry by optimizing bake condition, Microelectron. Eng. 53 (2000) 429–432.
[7] C.J. Hamel, A low cost robust method to vertical sidewalls for thick resist processing, in: Proceedings of 2004 IEEE/SEMI Int'l Electronics Manufacturing Technology Symposium, San Jose, CA, USA, 2004, pp. 247–250.
[8] W. Kang, E. Rabe, S. Kopetz, A. Neyer, Novel exposure methods based on reflection and refraction effects in the field of SU-8 lithography, J. Micromech. Microeng. 16 (2006) 821–831.
[9] S. Audran, B. Faure, B. Mortini, J. Regolini, G. Schlatter, G. Hadziioannou, Study of mechanism involved in photoresist microlens formation, Microelectron. Eng. 83 (2006) 1087–1090.
[10] J.-S. Kim, C.-W. Koh, G. Lee, J.-C. Jung, K.S. Shin, Novel routes towards sub-70nm contact windows by using new KrF photoresist, in: Proceedings of SPIE, vol. 4345, 2001, pp. 232–240.
[11] S.-K. Kim, Resist reflow process simulation study for contact hole pattern, J. Vac. Sci. Tech. B 24 (1) (2006) 200–204.
[12] T. Leveder, S. Landis, L. Davoust, N. Chaix, Optimization of demolding temperature for throughput improvement of nanoprint lithography, Microelectron. Eng. 84 (2007) 953–957.
[13] S.-Y. Moon, C.-M. Chung, T. Tamaoka, Three component photoresist based on thermal crosslinking and acidolytic cleavage, Polymer 41 (2000) 4013–4019.
[14] K. Miyagawa, K. Naruse, S. Ohinishi, K. Yamaguchi, K. Seko, N. Numa, N. Iwasawa, Study of thermal crosslinking reaction of *O*-naphthoquinone diazides and application to electrodeposition positive photoresist, Prog. Org. Coat. 42 (2001) 20–28.
[15] K.H. Chae, K.H. Sung, A polymeric photobase generator containing oxime-urethane groups: crosslinking reaction and application to negative photoresist, J. Polym. Sci. A: Polym. Chem. 42 (2004) 975–984.
[16] H.-H. Liu, W.-T. Chen, F.-T. Wu, Characterization of Negative tone photoresist based on acid catalyzed dehydration crosslinking of novolak having pendant carboxyl group, J. Polym. Res. 9 (2002) 251–256.

[17] A. Kawai, Measuring the thermal properties of photoresist thin film using atomic force microscopy, Thin Solid Films 273 (1996) 308–311.
[18] K. Shaw, online correspondence.
[19] S.A. MacDonld, Airborne chemical contamination of a chemically amplified resist, Proc. SPIE 1466 (1991) 2–12.
[20] S.C. Saha, H. Sagberg, E. Poppe, G.U. Jensen, T. Sæther, Tuning of resist slope for RF MEMS with hard baking parameters, in: Proceedings of MNC 2006, Kanagawa, Japan, 2006, pp. 314–315, Abstract.

Biographies

Shimul Chandra Saha received the BSc degree in Electrical and Electronics Engineering from Bangladesh University of Engineering and Technology (BUET), Dhaka, Bangladesh in 2001 and MSc degree in Hardware for Wireless Communications from Chalmers University of Technology (CTH), Gothenburg, Sweden in 2004. He is currently working toward his PhD degree in electrical engineering (focusing on RF MEMS switches and switch circuits) at the department of Electronics and Telecommunications (IET), Norwegian University of Science and Technology (NTNU), Trondheim, Norway. His current research work involves modeling, design and simulation of RF MEMS switches and MEMS filter at RF and microwave frequency. He also works on designing the mask and fabrication of the MEMS switches and circuits in clean room in collaboration with SINTEF Micro- and NanoLab (MiNa lab), Oslo, Norway. From September 2001 to August 2002, he worked as a lecturer in department of Electrical and Electronics Engineering (EEE), Chittagong University of Engineering and Technology (CUET), Chittagong, Bangladesh. From January to June 2003, he worked in a project on DDS for base station application at Ericsson AB, Molndal, Sweden. His research interest includes RF MEMS switch and switch circuits, RF and microwave circuits for wireless communications and micro-fabrication.

Håkon Sagberg received the siv.ing. (MSc) degree in physics from Norwegian Institute of Technology, Trondheim, in 1996, and his PhD from the University of Oslo in 2006. He has been affiliated with SINTEF since 1998, working as a research scientist at SINTEF Department of Microsystems and Nanotechnology since 2005. His main fields of research are optical MEMS and RF MEMS.

Erik Poppe received a MSc degree from the Department of Physics at the Norwegian Institute of Technology in 1994. He then worked as a Research Assistant in semiconductor laser fabrication at the Norwegian University of Science and Technology, before he started as a Research Scientist at SINTEF ICT, micromechanics and nanotechnology in 2001. The main field of work at SINTEF is process development for Si MEMS.

Geir U. Jensen received the MSc degree in physics and the PhD degree in electrical engineering from the Norwegian Institute of Technology, Trondheim, in 1984 and 1989, respectively. His PhD work was on Monte Carlo simulation of transport in III–V semiconductor devices. From 1989 to 1990, he was a Research Fellow at the University of Minnesota, Minneapolis, and from 1990 to 1991, he was a Research Scientist at the University of Virginia. Charlottesville. He was with SINTEF DELAB, Trondheim, from 1991 to 1993, and with Telenor R&D, Kjeller, Norway, from 1993 to 1995. His research during this period was in the area of design and fabrication of III–V semiconductor electronic and optoelectronic devices. Since 1995, he has been with SINTEF Electronics and Cybernetics, Oslo, Norway, where he works on silicon radiation detectors, micromachined sensors and RF MEMS.

Tor A. Fjeldly received the MSc degree in physics from the Norwegian Institute of Technology and the PhD degree from Brown University, Providence, RI. He was employed with Max-Planck-Institute for Solid State Physics, Stuttgart, Germany, and with the SINTEF research organization, Norway. Since 1983, he has been with the Norwegian University of Science and Technology (NTNU), where he is a Professor of Electrical Engineering. He is presently located at the University Graduate Center at Kjeller, Norway. Dr. Fjeldly has been a Visiting Professor at University of Virginia, Charlottesville, VA, at Rensselaer Polytechnic Institute, Troy, NY, and at University of Rovira i Virgili, Tarragona, Spain. His present research interests include nanoscale semiconductor devices and RF MEMS. He has written about 200 scientific papers, several book chapters, and has co-authored and co-edited several books. Dr. Fjeldly is a Fellow of IEEE and a member of the Norwegian Academy of Technical Sciences.

Trond Sæther was born in Ålesund, Norway, in 1958. He received the MSc and PhD degree in electrical engineering from the Norwegian University of Science and Technology, Trondheim, Norway, in 1981 and 1991, respectively. From 1981 to 1983, he was a Research Scientist at the microelectronics group at SINTEF in Trondheim. In 1983, he cofounded the fabless semiconductor company Nordic VLSI, where he worked as the Technical Director until July 1999. In July 1999, he joined the Circuits and Systems Group at the Norwegian University of Science and Technology as a full Professor. His research interests include RF CMOS, analog-to-digital converters and microelectromechanical systems.

Metallization scheme and release methods for fabrication of RF MEMS switches

Shimul Chandra Saha [a], *Håkon Sagberg* [b], *Erik Poppe* [b], *Geir Uri Jensen* [b], *and Trond Sæther* [a]

[a] Department of Electronics and Telecommunications, NTNU, NO-7491 Trondheim, Norway.
[b] SINTEF ICT, PO Box 124 Blindern, NO-0314 Oslo, Norway

In proceedings of 33rd Micro- and Nano- Engineering conference (MNE 2007), September 2007, pp 773-774, Copenhagen, Denmark.

Metallization scheme and release methods for fabrication of RF MEMS switches

Shimul Chandra Saha [a], Håkon Sagberg [b], Erik Poppe [b], Geir Uri Jensen [b], and Trond Sæther [a]

[a] Department of Electronics and Telecommunications, NTNU, NO-7491 Trondheim, Norway.
Ph: +47 735 92784, E-mail: shimul.saha@iet.ntnu.no
[b] SINTEF ICT, PO Box 124 Blindern, NO-0314 Oslo, Norway

Keywords: RF MEMS, sputtering, residual stress, stress gradient, resist skin, release method.

1. Introduction: Radio frequency micro electro mechanical systems (RF MEMS) devices are becoming increasingly popular due to their very good RF performance at high frequencies. RF MEMS switches have very low insertion loss in the on state and very high isolation in the off state. Electrostatically actuated MEMS switches consume very little power. They are very linear and have very high third order intercept point compared to any other solid state counterparts. A co-planar waveguide (CPW) MEMS shunt capacitive switch is shown in figure 1. The capacitance is formed between the suspended metal bridge and the bottom electrode, with a dielectric in between. When the bridge is in up state the capacitance is small (fF) and the switch is on. When the bridge is actuated as shown in Fig. 1 (right), the capacitance increases by two orders of magnitude the signal is shorted to ground, and the switch turns off. We are developing a process to fabricate surface micromachined capacitive RF MEMS switches in the SINTEF Micro and Nano Laboratories (MiNa), Oslo, Norway.

2. Design and Fabrication: Successful fabrication of suspended metal bridges requires three process steps: 1) Deposition and patterning of a sacrificial layer, 2) Deposition and patterning of the metal layer, and 3) Removal of the sacrificial layer. We have used a common positive photoresist (HiPR 6517) as a sacrificial layer. The photoresist is baked and the reflow creates a gradually increasing thickness at the edges. This is done in order to achieve a reliable bridge profile, rising with an angle of approximately 45° where it contacts the substrate [1]. We have used DC magnetron sputtering to deposit gold on the sacrificial layer to form the bridge. The reliability and performance of the switch depend on the mechanical properties of the bridge, and especially pull-down voltage and switching time are influenced by residual stress and stress gradients. The stress of the sputtered gold film depends on sputtering parameters such as pressure and power [2]. We have aimed for a low tensile stress, because compressive stress may cause buckling, and too much tensile stress will increase the pull-down voltage. The sputtering power must be low enough to avoid over-heating and burning the sacrificial resist. After patterning the gold bridge, the sacrificial resist needs to be dissolved to release the bridge. A thin layer of skin can be formed on the top surface of resist after the lithographic process and sputtering which makes it difficult to dissolve using a simple acetone soak. Some of the possible reasons for formation of the skin are, baking, and a delay between coating and exposure of resist [3].

3. Experiments and Results: Coating, patterning and baking of the sacrificial photoresist has been described in [1]. For all sputtering experiments described below we used standard lithography.

The sputtering pressure was varied from 10 mTorr to 20 mTorr to tune the film stress. We used a low sputtering power of 500 Watts for all experiments. The sputtering conditions and obtained results are shown in table 1. Example images of structures sputtered at 10 mTorr and 500 watts are shown in Figure 2. In order to measure the residual stress and stress gradient of the sputtered film, we used wafer curvature measurements and micro-machined test structures [4]. For wafer curvature method, we deposited gold directly on wafers and measured the wafers curvature before and after film deposition. In micro-machined test structures methods, cantilevers were used to measure the stress gradient, bridges were used to measure compressive stress, and guckel rings with CoventorWare simulations were used to measure the tensile stress. A lower tensile stress is obtained at higher pressure. A decrease in negative stress gradient was also found with increasing sputtering pressure.

To remove the sacrificial resist, acetone was quite ineffective, and we obtained better results with Shipley Microposit 1165 resist remover. An experiment plan as shown in table 2 was carried out to explore the different options for removal of resist skin. The samples were put in Microposit 1165 for about 90 min at normal temp, followed by 60 min with heating and another 60 min at normal temp, in all cases with magnetic stirring. Afterwards the samples were dried in a critical point dryer. Two released samples RS 2 and RS 8 are shown in figure 3. From the release test, it is found that the plasma ashing and heating has a great effect on the release process as shown in figure 3.

4. Conclusion: We can use 20 mTorr at 500 watts to deposit low stress planar gold. Plasma ashing, followed by Microposit 1165 with heating can be used for successful release of RF MEMS switch.

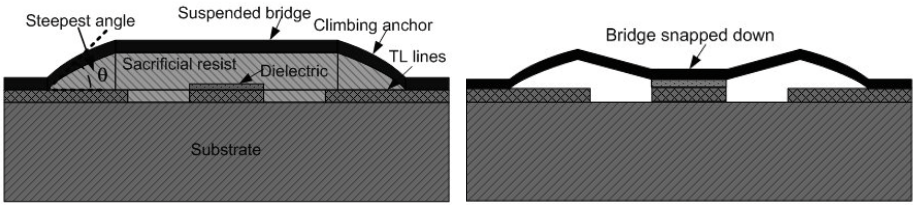

Figure 1: A side view of RE MEMS capacitive shunt bridge with sacrificial resist (left) and an actuated bridge (right).

Table 1: The sputtering parameters and measured residual stress and stress gradients

Wafer curvature methods		Micro-machined test structures method		
Sputtering pressure* (mTorr)	Residual stress tensile (MPa)	Sputtering pressure* (mTorr)	Stress gradient -(MPa/μm)	Residual stress, tensile (MPa)
10	42	10	35	70
16	31	15	5.2	55
24	31	20	4.8	45

*All the wafers are sputtered at 500 watts. The uncertainty of the stress value is 5-15 MPa.

Table 2: The experimental setup to dissolve hard resist with plasma ashing and piranha and obtained results

Plasma strip (150 watt, 45 min)				No plasma strip			
Heating Microposit 1165 (~60° C)		No heating Microposit 1165		Heating Microposit 1165 (~60° C)		No heating Microposit 1165	
Piranha dip, 60 s	No piranha dip	Piranha dip,60 s	No piranha dip	Piranha dip, 30 s	No piranha dip	Piranha dip, 30 s	No piranha dip
RS 1	RS 2	RS 4	RS 3	RS 5	RS 6	RS 7	RS 8
Very clean	Very clean	Very clean	Almost clean	Very clean	Thin skin left	Very clean	Not clean

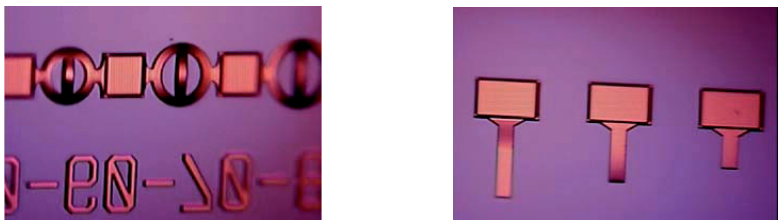

Figure 2: Optical images of buckled guckel ring and cantilever sputtered at 10 mTorr and 500 watt

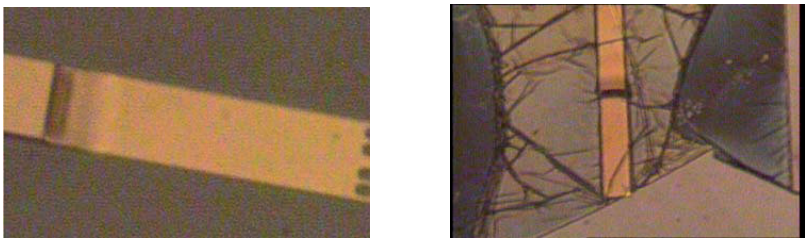

Figure 3: Released sample RS 2 (left) and Released sample RS 8(right)

Acknowledgments: Authors are grateful to Norwegian Research Council for sponsoring the work through the SMiDA project (No 159559/130) and the IRRFT project (No 159259/I40).

References:

[1] S. C. Saha, Tuning of resist slope for RF MEMS with hard baking parameters, Proceedings of MNC 2006.
[2] H Windischmann, Critical Reviews in Solid State and Materials Science, 17 (6): p 547-596 (1992).
[3] S.A. MacDonld, Proc. SPIE, vol 1466, p 2-12, (1991).
[4] C.-W. Baek, Sensors and Actuators A 117, p 17-27, (2005).

Tuneable Low-Pass Filter from C to X band with RF MEMS Capacitance and Transmission line

Shimul Chandra Saha[1], Ulrik Hanke[2], Håkon Sagberg[3], Tor A. Fjeldly[1] and Trond Sæther[1]*

[1]Department of Electronics and Telecommunications (IET), Norwegian University of Science and Technology (NTNU), NO-7491 Trondheim, Norway
[2]Institute for Microsystems Technology, Vestfold University College, 3103 Tønsberg, Norway
[3]Department of Microsystems and Nanotechnology, SINTEF ICT, PO Box 124, Blindern, NO-0314 Oslo, Norway

Has been submitted to Microelectronics Journal

Tuneable Low-Pass Filter from C to X band with RF MEMS Capacitance and Transmission line

Shimul Chandra Saha*[1], Ulrik Hanke[2], Håkon Sagberg[3], Tor A. Fjeldly[1]and Trond Sæther[1]

[1]Department of Electronics and Telecommunications (IET), Norwegian University of Science and Technology (NTNU), NO-7491 Trondheim, Norway

[2]Institute for Microsystems Technology, Vestfold University College, 3103 Tønsberg, Norway

[3]Department of Microsystems and Nanotechnology, SINTEF ICT, PO Box 124, Blindern, NO-0314 Oslo, Norway

*Contact Author, E-mail: shimul.saha@iet.ntnu.no, Phone: +47 7359 2784, Mobile: +47 905 36957, Fax: +47 7359 1441

Abstract: In this paper we have shown the design of an RF MEMS tuneable low-pass filter. The theory of traditional parallel plate capacitors and high capacitance ratio RF MEMS shunt capacitive switches is described. The variation of capacitance with actuation voltage for the high capacitance ratio switch is verified with simulation. The low-pass filter design uses both distributed transmission lines and RF MEMS capacitances to replace the lumped elements. The use of RF MEMS variable capacitances gives the flexibility of tuning the cut-off frequency of the low-pass filter. We have designed a low-pass filter at 7 GHz cut-off frequency using the theory of stepped impedance transmission lines and MEMS capacitances. A 3D electromagnetic simulation of the filter is performed and agrees quite well with ADS simulation. A prototype of the tuneable low-pass filter is realised by use of parallel plate capacitances for verification. The variable shunt capacitances are formed by combination of a

number of ordinary parallel plate RF MEMS capacitances. The cut-off frequency is tuned from C to X band by actuating different combinations of parallel capacitive bridges. The measurement results agree well with the simulation result.

Keywords: Low-pass filter, MEMS, Tuneable capacitance, Tuneable filter.

1. Introduction

Radio frequency micro electromechanical systems (RF MEMS) technology offers an attractive capability for RF systems, particularly in support of switching and tuning functions. One such component is a micro electromechanical voltage tuneable capacitor, which can enable a wide tuning range and high quality (Q) factor. In this paper we present a design of a tuneable low-pass filter at 7 GHz combining RF MEMS capacitors and high impedance transmission lines. The low-pass filter is designed by means of the theory of stepped impedance transmission line filters. The filter can be developed with surface micromachining without the need for any external inductors. This will give flexibility in integration and easy fabrication processing.

Compared with solid state varactors, MEMS tuneable capacitors have the advantage of lower loss and a potentially larger tuning range [1]. The interconnection loss and noise can also be reduced compared with the use of off-chip solid state RF components. Among all the MEMS capacitors developed to date, the parallel plate configuration is the most commonly used. The actuation mechanism is mostly electrostatic as it consumes very little power during actuation. A parallel plate tuneable capacitor can be fabricated with surface micromachining techniques. The theoretical tuning range of such a capacitor is, however, limited to 50%, as the beam will collapse to the downstate when the gap is less than 2/3 of the initial gap. High tuning range capacitors have been demonstrated recently. Among those, Zou et al. [1] developed a varactor with a tuning range of 69.8%. Two steps in the suspended beam are implemented. Another varactor reported by Dussopt et al. [2] has a tuning range of 90%. The switch fabrication is

somewhat complicated with several staircase profiles. Still, these capacitance ratios are not very high. Improved capacitance ratio (CR) RF MEMS capacitors have been reported by Nieminen et al. [3] CR=2.25 and Rijks et al. [4] CR=17.

In standard filter design at low frequency, the MEMS varactor is used as a lumped element with off-chip inductors. At high frequency, some low-pass filter designs were reported with integrated transmission lines and MEMS switches (see Cai et al. [5] and Fanget al. [6]). In [5] the tuning of the filter is obtained by changing the transmission line length using MEMS switches. In [6] planar spiral inductor and shunt capacitor are used but without any tuning capability. Also, low-pass and band-pass filters integrating capacitive MEMS switches and short inductive transmission lines have been realised above 10 GHz [7, 8, 9]. In [7], the tuning was in steps instead of being continuous and the tuning of the cut-off frequency was obtained by switching between different combination of inductance and capacitance. In [8, 9] the cut-off frequency was tuned by changing the inductance using MEMS switching. In this paper we have shown a design of a low pass filter with a high impedance transmission line and RF MEMS capacitors, where the tuning is obtained by capacitance tuning. Also it is shown that a continuous tuning of the frequency can be obtained instead of a stepwise tuning.

We show a design of high capacitance ratio RF MEMS shunt switches in a co-planar wave guide (CPW) configuration. The methodology for the shunt switch is similar to the one presented in [1, 3]. Instead of $g_2=3g_1$ as mentioned in [3], we proposed a design with $g_2>3g_1$ (sec 3, Fig 2). This design will have better control in tuning the capacitance than the design mentioned [3], as it has less chance of collapsing to the downstate. The

MEMS capacitive shunt switch is used in a stepped impedance low-pass filter instead of a low impedance transmission line. The series inductor in the low-pass filter is implemented using a short section of a high impedance transmission line [7]. A preliminary theory of low-pass filters using transmission lines and MEMS capacitances is presented in [10, 11]. This filter is much more elegant and compact than filters based on traditional $\lambda/8$ long stub and transmission line filters [12]. The designed filter has a large tuning range, over 60% of its nominal cut-off frequency. Although step impedance filters don't have a very sharp roll-off, they can be used for certain applications where compact size and a wide tuning range are required and less roll-off can be accepted. The low pass filter, for example can be used in harmonic suppression above the fundamental frequency in frequency synthesizer. The high tuning range will be very useful in the systems with multiple frequency band operation.

In this paper, the theory of parallel plate and the high capacitance ratio RF MEMS shunt switches are described in Section 2. The design of a high capacitance ratio MEMS switch and simulation of the pull-down voltage and the variation of the capacitance with actuation voltage are performed with Coventorware® in Section 3. A third-order 3 dB ripple chebyshev low-pass filter is described in Section 4. The filter is designed and optimised with Advanced Design System (ADS®) from Agilent. A comparison between ADS and Electromagnetic Design System (EMDS) is also presented in the Section 4. A prototype of the filter is fabricated by our own facility at SINTEF MiNaLab in Oslo, Norway. In the first prototype, instead of a high capacitance ratio switch, 3 ordinary parallel plate bridges were used as tuneable capacitances. The tuning of the capacitance was obtained by actuating different combinations of bridges. The fabrication of the filter

is presented in Section 5. The measurement of the filter is presented in Section 6. A comparison of the measurement result with re-simulation of the filter, taking into account the effects of process constraints, is discussed in Section 7.

2. Theory of capacitive switch

In this section we discuss the simple parallel plate switch and the high capacitance ratio switch. Both switches are used in shunt configuration by means of a CPW transmission line.

2.1 Theory of traditional parallel plate capacitive switch

A MEMS capacitive switch consists of a suspended top plate and a fixed bottom electrode plate with an overlap area $A_e=L_e\times W_e$, shown in Figs. 1 and 2. L_e and W_e are the length and the width of the electrode, respectively. A DC bias voltage, V_{DC}, is applied between the bridge and the two separate actuation electrodes on the two sides of the centre conductor as shown in Fig. 1. All electrodes are covered with a dielectric with thickness t_d and relative permittivity ε_r. The initial gap is g_0 at the centre of middle electrode when no DC voltage is applied. When a DC voltage is applied between the bridge and the actuation electrodes, the initial gap reduces according to the actuation voltage [13]. If the fringing field effect is neglected, the value of the capacitance between the suspended bridge and centre conductor for a deflection x of the bridge can be determined by

$$C(x) = \varepsilon_0 . \frac{A_e}{(g_0 - x) + \frac{t_d}{\varepsilon_r}} \quad (1)$$

When V_{DC} is applied between actuation electrodes and bridge, an attractive electrostatic force F_e is generated with the value

$$F_e = \frac{1}{2} \frac{C_a(x) {V_{DC}}^2}{(g_{a0} - x + \frac{t_d}{\varepsilon_r})} \quad (2)$$

Here $C_a(x)$ is the total capacitance between the bridge and the two actuation electrodes, x is the distance the top plate has moved from its initial position, V_{DC} is the actuation voltage and g_{ao} is the initial gap between actuation electrodes and suspended bridge. This electrostatic force tries to pull the top plate down. The beam has a mechanical spring constant (stiffness) which tries to pull the beam back to the upstate position. For small deflections the electrostatic and elastic force are equal in magnitude. When the beam is deflected one-third of the initial gap, the electrostatic force becomes stronger than the mechanical restoring force. At this point the beam collapses fully to the down state and this voltage is called the pull-down voltage. Before pull-down or when $x<g_o/3$ the capacitance increases to maximum 150% of the original value. So the maximum tuning range of the electrostatic actuated parallel plate capacitor is 50%.

2.2 Theory of high tuning range capacitive switch

The side view of the proposed high tuning range switch is shown in Fig. 2 (a) according to the topology mentioned in [3]. Instead of $g_2=3g_1$ as in [3], we proposed $g_2>3g_1$. It consists of separate actuation electrodes beside the centre conductor of the CPW

transmission line. In this case, the centre conductor is higher than the actuation electrodes. When g_1 is less than or equal to $g_2/3$, the capacitance ratio can be very high as the downstate capacitance will depend only on the thickness and the dielectric constant of the dielectric. The theoretical capacitance ratio for a given deflection can be derived as

$$\frac{C(x)}{C_0} = \frac{g_1 + \frac{t_d}{\varepsilon_r}}{(g_1 - x) + \frac{t_d}{\varepsilon_r}} \tag{3}$$

C_0 is the initial capacitance when x=0. When $x=g_1$, the beam touches the centre electrode and the maximum capacitance ratio becomes

$$\frac{C_d}{C_0} = g_1 \frac{\varepsilon_r}{t_d} + 1 \tag{4}$$

Here C_d is the downstate capacitance when $x=g_1$.

From equation 4 we can see that the capacitance ratio can be very high by choosing appropriate initial gap and maintaining a very small gap between dielectric and top plate. The proposed design has several advantages over the switch mentioned in the references [1] and [2]. It can have a very high capacitance tuning range. Owing to the dielectric the switch will not short-circuit when the beam is fully pulled down. As the switch has a $g_1 < g_2/3$, it is less prone to collapse to the downstate. The switch mentioned in [4] has extra bumps to avoid a full collapse of the beam. Finally, it has potential for a simpler fabrication process than the switches mentioned in [1, 2, 4], as the top beam is planar and no step is required. The proposed switch has the potential of higher capacitance ratio than the work mentioned [3]. The additional process steps required for

the proposed switch are the electroplating or sputtering of the centre conductor to make it higher and planarization of the sacrificial layer. Relevant works on planarization [14, 15] can be very useful for fabrication of such kind of switches.

3. Design and simulation of the high capacitance ratio RF MEMS shunt switch in CPW configuration

The proposed high capacitance ratio switch in side and top view is shown in Figs. 2a , 2b respectively. The switch is designed on a CPW 50 Ω transmission line. The proposed fabrication of the switch is done using a standard high resistivity silicon substrate with 280 μm thickness. The relative dielectric constant of the substrate is 11.9 and the resistivity is 8000 Ω-cm. For a 50 Ω CPW transmission line, the dimensions are 110 μm/204 μm /110 μm (G/W_c/G) (see Fig. 2). The dimensions could also be decreased by reducing the CPW gap (G) and the actuation electrodes. This will increase the required actuation voltage, which may be a disadvantage. A reduced g_1 will result in a higher upstate capacitance, which is required for a filter operating at a few GHz.

The dimensions of the proposed beam are as follows, as shown in Table 1. The beam width at the actuation electrode area W_e, is 200 μm. The beam width at the two ends W_b, is 100 μm. This will reduce the beam stiffness, which will reduce the actuation voltage for tuning the capacitance. The gap height at the centre g_1 is 0.5 μm, and the gap height at actuation electrode area g_2 is 2 μm, which gives a very wide tuning range of the capacitance ratio even before full contact with the centre electrode. The length of the actuation electrodes is 100 μm for each, with a gap of 5 μm on each side of the

electrode for isolation. The total beam length is 750 μm. This long bridge is chosen to reduce the actuation voltage. The thickness of the beam is 2 μm and the proposed material for the beam is gold. The thickness and length of the beam can be subject to a trade-off to optimise actuation voltage. Gold is the most frequently-used metal for RF MEMS switches, owing to its ductility and low Young's modulus. The thickness of the transmission line ground and actuation electrodes is 1 μm. The thickness of the centre conductor is 2.3 μm with 0.2 μm Si_3N_4 dielectric on top. The thickness of the dielectric can be reduced, in case it is necessary to have higher capacitance at downstate.

The simulation of the switch with respect to displacement and capacitance change with actuation voltage is done in Coventorware®. The displacement from the top position of the beam at centre and capacitance variation with actuation voltage are shown in Fig. 3. From this it can be seen that the top plate deflects fully to the centre conductor at 12.8 volts. In the Coventorware architect simulation the residual stress is not included. The tensile stress will increase the actuation voltage for the same deflection. The simulation of capacitance vs actuation voltage including residual stress can be performed using CoventorWare analyser. The capacitance in the upstate with zero actuation voltage is around 690 fF. The upstate capacitance value is high, because of the large overlap area. Before the beam is in contact with the centre electrode, the capacitance reaches 2.8 pF at 11.8 volts, which gives a capacitance ratio of 4. When the beam is in contact with the centre electrode at 20.5 volt actuation voltage, the capacitance is 15 pF which gives a capacitance ratio of more than 20. Fringing fields are not included in the Coventorware simulation. The real capacitance in upstate can be higher than the parallel plate

capacitance to some extent owing to fringing fields [15, p.91]. As the upstate capacitance is very high for our design the percentage of fringing capacitance will be small. To include the fringing filed effect, a CoventorWare Analyzer MemElectro simulation is performed with a very fine mesh. The capacitance at upstate is found to be 702 pF. The fringing capacitance is only ~ 2% higher than the Architect result. The fringing field can also increase the downstate capacitance to some extent. In downstate however, the capacitance will be reduced owing to roughness.

4. Theory, design and simulation of the proposed filter

In this section the theory and design of the stepped impedance low-pass filter are described.

4.1 Theory of the stepped-impedance filter

It is well known [12] that if the length of the transmission line is short ($\beta l < \pi/4$) and the characteristic impedance is high the transmission line can be represented by the equivalent circuit shown in Fig. 4 where the reactance is given by

$$X_L = Z_0 \beta \ell \tag{5}$$

Here the characteristic impedance of the line is Z_0, the length is l and the propagation constant is β.

So a series inductor can be represented by a short length of high characteristic impedance transmission line. In the lumped elements filter model, the shunt capacitor will be replaced by an RF MEMS capacitor which will give the cut-off frequency tuning capability.

4.2 A third-order low pass filter topology design and simulation in ADS and comparison with EMDS (Electromagnetic Design System)

A third-order low pass filter topology is shown in Fig. 5. The basic filter elements are extracted from the Chebyshev equal ripple low pass filter prototype [10, 11, 12]. The normalized filter elements for a 3 dB ripple Chebyshev are given by g_1=3.3487, g_2=0.7117, g_3=3.3487, and g_4=1.00 is the load impedance [12]. A ripple of 3 dB is used to give a sharper roll-off above the cut-off frequency. We have chosen a nominal cut-off frequency at 7.0 GHz. With a maximum transmission line impedance of 80Ω the length of the transmission line becomes 25. 5° and the nominal capacitance value becomes 1.52 pF when the cut-off frequency is 7 GHz. After optimization of the filter cut-off frequency in ADS the nominal shunt capacitor value becomes 1.1 pF and the length of the 80 Ω line becomes 1467 μm (30.7˚) for the desired responses. The substrate parameters used for simulation are mentioned in Section 3. For an 80Ω CPW transmission line, the dimensions are 160μm/53μm/160μm (G/W/G). A higher value, such as 100 Ω or more, can be chosen for the impedance of the series inductance. This will make the transmission line very narrow. One has to keep in mind the process parameters, because if the transmission line is thin, it will introduce extra insertion loss in the pass band also.

We have simulated the designed filter in ADS using the transmission line and the capacitance values obtained from CoventorWare. For verification we have simulated the filter with high capacitance ratio bridges in 3D electromagnetic simulation from Electromagnetic Design System (EMDS). A top view of the proposed filter is shown in

Fig. 6. The dimensions of the bridge are presented in Sections 3. The width of the centre conductor for the 50 Ω transmission lines is 204 μm with a gap of 110 μm. The thickness of the centre electrode dielectric is (Si_3N_4) 200 nm. A relative permittivity of 7 is used for the nitride to calculate the capacitance. The shunt capacitance is varied from 0.69 pF (when the bridges are at the initial position) to 2.81 pF (when the bridges are at 0.4 μm down from the initial position). Here it is assumed that the bridges remain parallel to the bottom electrode when they deflect from the initial position. The simulation result and comparison between ADS and EMDS are shown in Fig. 7.

In the figure. BD means deflection of the bridge from its original position. The red line is the simulation result in EMDS and the black line is the simulation in ADS. From Fig. 7 it can be seen that the cut-off frequency is tuned from 9 GHz to 4.7 GHz when the bridges deflects from the initial position to 0.4 μm. The tuning of the filter is 4.3 GHz which is 60% of the nominal cut off frequency 7 GHz. Also the simulation in ADS closely matches the 3D electromagnetic simulation in EMDS. The insertion loss is slightly high in the pass band as a 3 dB ripple Chebyshev filter element is used in the design. It is also observed that for higher capacitance value the insertion loss increases. As the capacitances are in shunt, for a higher capacitance values the shunt impedance will be lower and will increase the loss in pass band. For clarity the return losses are not included in the Fig. 7. In the pass band a higher return loss is present. There are few reasons for this. A 3 dB ripple chevyshev filter approach is used for the design. Also only capacitance tuning is used for the variation of cut-off frequency. In order to improve the return loss in pass band, a 0.1 dB or 0.5 dB ripple chevyshev or flat butterworth filter approach can be used. Capacitive tuning with an inductive inverter

can be used to reduce the return loss for the entire tuning range [16, 17]. Simultaneous tuning of both capacitance and inductance with stub can also be used to reduce return loss and insertion loss for the entire operating frequency range of the filter [18].

5. Fabrication of the filter

A top view of the fabricated filter is shown in Fig. 8. The fabrication was done at SINTEF MiNa lab in Oslo. Since the fabrication of RF MEMS is new to this facility, a simplified version of the filter was preferred, using traditional parallel plate capacitors. This will increase the probability of successful fabrication. Instead of high capacitance ratio switches, a combination of 3 parallel bridges is used for each capacitance as shown in Fig. 8. Each shunt capacitance is a combination of two 12 μm wide (on the two sides) and one 15 μm wide (middle) shunt bridge. The variation of the capacitance can be obtained by actuating individual bridges, or combining one or more bridges. The width of the centre conductor for the 50 Ω transmission lines is 140 μm with a gap of 80 μm. This is different from the dimensions mentioned in Section 3. Because of the non-uniform beam approach, a wider centre conductor is required to obtain the required capacitance. The thickness of the centre electrode and the actuation electrode dielectric is (Si_3N_4) 220 nm. The estimated total roughness of the dielectric and gold is to be 15 nm. Aluminium is planned for use as a transmission line.

A four-mask process was used to fabricate the proposed filter. The cross-section view of the process flow of the capacitive bridges is shown in Fig. 9. A 280 μm thick silicon wafer with 4-8 kΩ-cm (specified by supplier) resistivity was used for the fabrication. A 500 nm thick oxide was grown on the silicon wafer to obtain lower loss (A). Then a 500

nm thick Al was deposited by sputtering and patterned by wet etching (B). A 220 nm thick Si_3N_4 was deposited as dielectric by plasma-enhanced chemical vapour deposition (PECVD) and patterned by dry etch (C). HiPR 6517 photoresist was used as a sacrificial layer. The resist thickness was 2.55 μm and patterned by standard lithography and special baking methods (D) as described in detail in [19]. Then 1.1 μm thick gold was sputtered and patterned by wet etch (E). The gold sputtering was done with very low power and a sputtering pressure of 20 mTorr to obtain a low tensile stress [20]. When the gold was sputtered, the transmission line was also sputtered with 1.1 μm additional gold on aluminum. Low tensile stress ensures low-pull down voltage and gives better reliability. Finally the switches and filters were released with our developed methods and dried in a critical point dryer [19].

6. Fabricated low-pass filter and measured results

A SEM image of the fabricated low pass filter is shown in Fig. 10. An enlarged image at the capacitance region is also shown in Fig. 11. As shown in Fig. 8 the actuation electrodes are separated from the RF signal electrode, and each bridge has its own set of actuation electrodes. In Fig. 11 the centre narrow line is the 80 Ohm transmission line, which is equivalent to a series inductor. The capacitors are at both ends of the 80 Ohm transmission line, shunting a 50 Ohm transmission line. In the figure, the three parallel bridges of shunt capacitors can be seen. The extended 50 Ohm transmission lines are used for measurement purpose with a CPW probe.

The fabricated filters were measured in a vector network analyser. The filter characteristic was measured up to 30 GHz. Standard Line-Reflect-Reflect-Match (LRRM) methods were used for calibration of the network analyser. The measured filter S parameters are shown in Fig. 12. We have measured the filter characteristics with one bridge down (15 μm wide centre bridge), green line, and 2 bridges down (15 μm and 12 μm wide bridges), purple line. Due to lack of actuation facility, we could not actuate all three parallel bridges together.

7. The re-simulation in the light of fabrication constraint and comparison

After fabrication the filters were inspected in an optical interferometer to measure the actual width and height of the bridge. The actual initial heights of the bridges were 2.25 μm and the width was reduced on average 1 μm from each side owing to over-etching. Gold is usually smooth and it was found that the average roughness of the gold was 7 nm. The Si_3N_4 average roughness was 9 nm. But the main contribution to the roughness was from aluminum. This is because of the high temp (300 ° C) Si_3N_4 deposition. From an atomic force microscope (AFM) measurement, it was found that the height of the aluminum bumps was about 80 nm. As the nitride was deposited on aluminum, the total roughness for the downstate capacitance was 96 nm. Considering the over etch and roughness, the downstate capacitance becomes 0.38 pF for the 15 μm bridge (13 um real width). The filter was re-simulated with the above parameters. The simulation was

compared with measurement results of the fabricated filter as shown in Fig. 13. The measured results agree better with the simulated results, given the effect of over-etching and roughness. There is a slightly higher cut-off frequency in the measured filter. This can happen because of non-planarity of the bridge at downstate, which will further reduce the downstate capacitance.

By using same roughness as mentioned earlier, the estimated downstate capacitance becomes 0.30 pF for the 12 μm bridge (10 μm real width). The total capacitance at downstate becomes 0.68 pF when two bridges are down. The simulated and measured results for this state were compared and are shown in Fig. 13. From this figure it can be seen that the measured filter again has a higher cut-off frequency for the reason discussed above. Also, the narrower bridge will have relatively more over-etching and less planarity.

8. Conclusion

We have presented a tuneable low-pass filter design with transmission line and MEMS capacitance. A high capacitance ratio shunt switch is proposed, which can be used for continuous tuning of the cut-off frequency. A simulation of the filter with high capacitance ratio switch is performed in EMDS and compared with ADS. The results agree with each other very closely. A simpler parallel plate capacitance was investigated for the first prototype fabrication and comparison of the filter performances. The tuning

of the cut-off frequency is obtained by actuation of several parallel bridges. The measured results agree well with the simulated result considering the fabrication effects. The filter roll-off is not very sharp, but can be improved with the use of high impedance transmission line and a higher order of the filter. But this may have some drawbacks. As only the capacitance is used for tuning and the inductance is fixed, higher order filters will have reduced tuning range. Also it will be complicated to tune all the capacitor simultaneously. High impedance transmission line will increase the insertion loss significantly as the center line will be very narrow. The filter is very compact and has very good control of the tuning frequency.

Acknowledgement

The authors are grateful to the Norwegian Research Council for sponsoring the work through the SMiDA project (No 159559/130) and the IRRFT project (No 159259/I40). The authors also thank MiNa Lab personnel for their support in the clean room.

Reference:

[1] J Zou., C. Liu, J. Schutt-Aine, , J. Chen and , S. Kang, 'Development of a wide tuning range MEMS Tunable capacitor for Wireless Communication Systems',. International Electron Devices Meet. Tech. Digest 2000, 403-406.

[2] L. Dussopt and G. Rebeiz, High-Q Millimeter-Wave MEMS varactors: 'Extended Tuning range and Discrete position Designs', 2002 IEEE MTT-S Digest, 1205-1208.

[3] H. Nieminen, V. Ermolov and T. Ryhånen: 'Microelectromechanical Capacitor with wide tuning range', IEE Electronics letters, Vol. 37, (24), (2001)1451-1452.

[4] T. S.M. Rijks, J. T. M. V. Beek, P. G. Steeneken , M. J. Ulenaers, J. D. Coster and R. Puers: 'RF MEMS tunable capacitor with large tuning ratio', 17th IEEE International Conference on. (MEMS) Micro Electro Mechanical Systems, 2004 777-780.

[5] M. Cai, X. Guo, Y. Li, L. Liu, Z. Lai: 'Design and modeling of reconfigurable MEMS low pass filter, Solid-State and Integrated Circuit Technology', 2006. ICSICT '06. 8th International Conference on, 563-565 .

[6] J. Fang, , Z.W. Liu, , Z.M. Chen, L.T. Liu,; Z.J Li,.: 'Realization of an Integrated Planar LC Low-Pass Filter with Modified Surface Micromachining Technology', IEEE conference on Electron devices and Solid-State circuits, 19-21 Dec. 2005, 729-732.

[7] D. Peroulis, S. Pacheco, K. Sarabandi and L. P.B. Katehi: 'Tunable Lumped Components with Applications to Reconfigurable MEMS Filters', Microwave Symposium Digest, 2001 IEEE MTT-S, Volume 1, May 2001, vol.1 341 - 344

[8] S. Lee, J. Kim, Y. Kim and Y. Kwon, 'Millimeter-Wave MEMS tunable low pass filter with reconfigurable series inductor and capacitive shunt switches', IEEE Microwave and Wireless Components letters, vol 15, (10), (2005), 691-693.

[9] J. Park, S. Lee, J. Kim, H. Kim, Y. Kim and Y. Kwon: 'Reconfigurable millimeter-wave filters using CPW-based periodic structures with novel multiple-contact MEMS switches', IEEE Journal of Microelectromechanical Systems, Vol. 14, (3), (2005), 456-463.

[10] S. C. Saha and T.Sæther: 'Modeling and Simulation of Low Pass Filter using RF MEMS Capacitance and Transmission line', Proceeding IMAPS Nordic 2005 pp 155-159.

[11] S. C. Saha, U. Hanke, T. Sæther: 'Modeling, Design and Simulation of Tunable Band Pass Filter using RF MEMS Capacitance and Transmission line', SPIE International Symposium, Microelectronics, MEMS and Nanotechnology, Proc. of SPIE Vol. 6035, Microelectronics: Design, Technology and Packaging II, 11-14 December, Brisbane, Australia, 2005.

[12] D. M. Pozar, 'Microwave Engineering', Ch 8, Second Edition, John Willey & Sons, 1998.

[13] G. M. Rebeiz: 'RF MEMS Theory, Design and Technology', Ch 2 and 3, 2nd Edition, John Willey & Sons, 2003.

[14] M. Ohnmacht, V. Seidemann, S. Buttgenbach, Microcoils and microrelays- an optimal multilayer fabrication process, Sensor and Actuators, vol 83, (2000), 124-129,

[15] L. Wang, A. Cui, J.-S. Hong, E. P. McErlean, R. B. Greed, D. C. Voyce, Fabrication of high power RF MEMS switches, Journal of Microelectronic Engineering, Article in Press, doi 10.1016/j.mee.2006.01.067.

[16] K. Entesari, G. M. Rebeiz, A differential 4-bit 6.5-10 GHz RF MEMS tunable filter, IEEE Transaction of Microwave Theory and Techniques, vol 53, (3) part 2, (2005) 1103-1110.

[17] G. L. Matthaei, E. Young, and E. M. T. Jones, Microwave Filters, Impedance-Matching Networks, and Coupling Structures. Norwood, MA: Artech House, 1980.

[18] B. Pillans, A. Malczewski, R. Allison, J. Brank, 6-15 GHz RF MEMS tunable filters, 2005 IEEE MTT-S, pp 919-922.

[19] S. C. Saha, H. Sagberg, E. Poppe, G. U. Jensen, T. A Fjeldly, and T. Sæther, Tuning of resist slope with hardbaking parameters and release methods of extra hard photoresist for RF MEMS switches, Journal of Sensor and Actuators A: Phys. vol. 142 (2) (2008) 452-461,.

[20] S. C. Saha, H. Sagberg, E. Poppe, G. U. Jensen, and T. Sæther 'Metallization scheme and release methods for fabrication of RF MEMS switches', Proceedings of 33rd Micro- and Nano- Engineering conference (MNE 2007), September 2007, Copenhagen, Denmark.

List of Table and figures:

Table:

Figures:

Fig. 13: Comparison of the filter performances between re-simulated (blue line) and measured results (black line).

Table 1:

Dimensional parameters	***Value (μm)***
W_e	200
W_b	100
L_e	204
L_b	750
W_e	204
L_a	100
G	110
g_1	0.5
g_2	2
t_b	2
t_d	0.2

Fig. 1

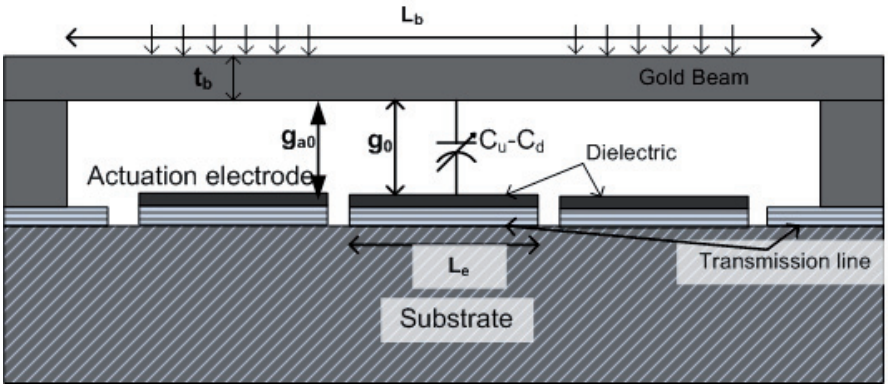

Fig. 2a

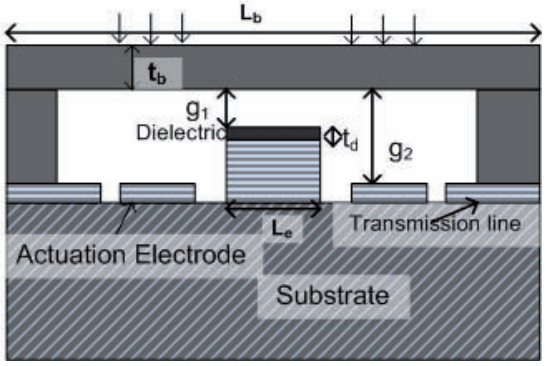

Fig. 2b

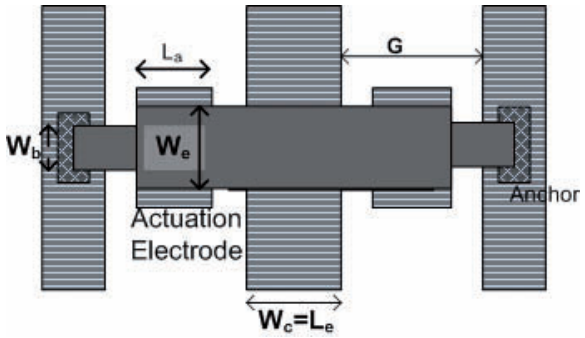

Fig. 3a

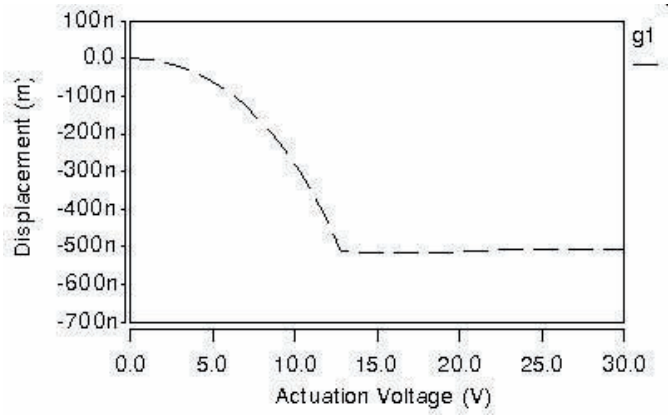

Fig. 3b

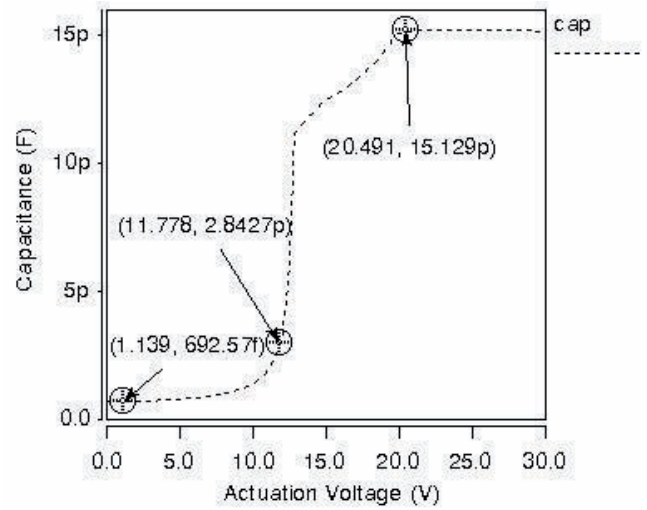

Fig. 4

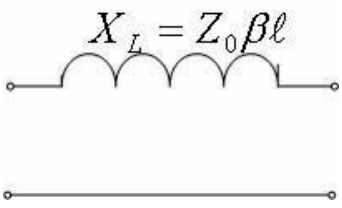

Fig. 5

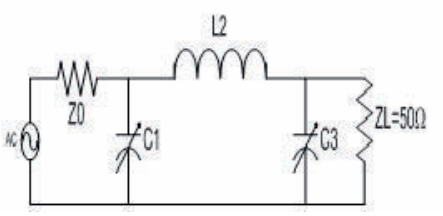
L2
Z0
C1
C3
ZL=50Ω
AC

Fig. 6

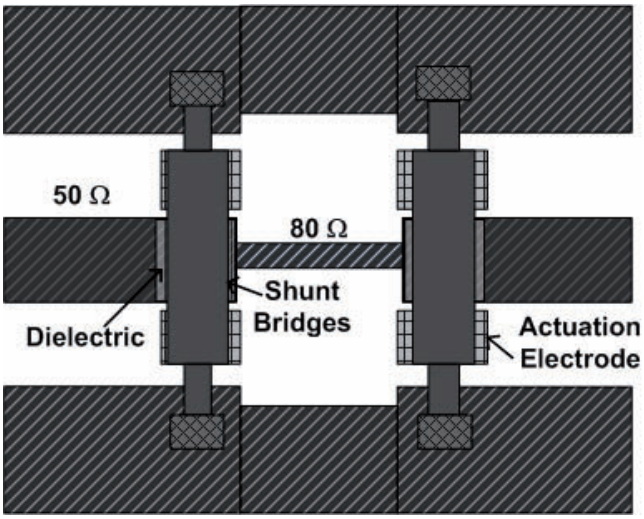
50 Ω
80 Ω
Shunt
Bridges
Dielectric
Actuation
Electrode

Fig. 7

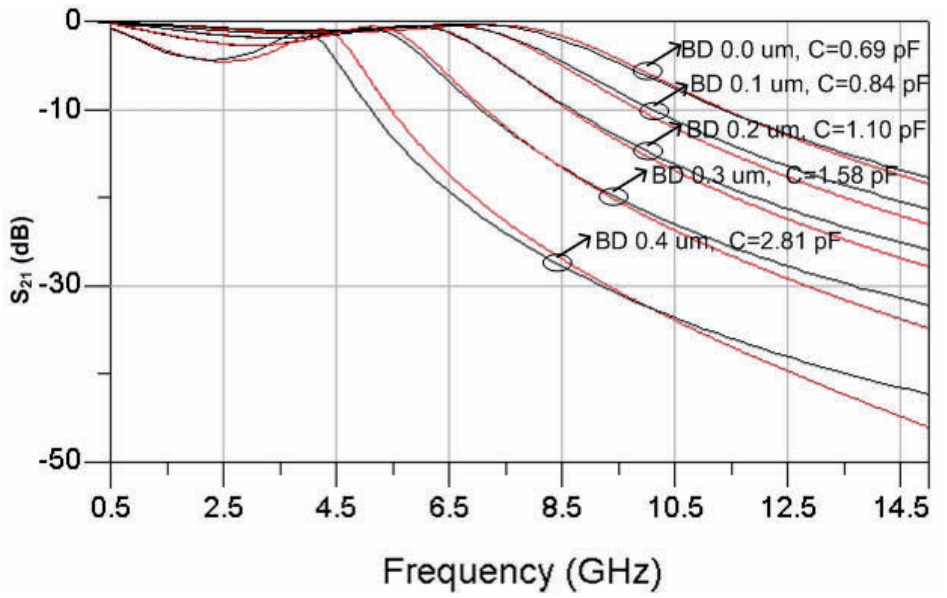
0
-10
-30
-50
S_{21} (dB)
0.5
2.5
4.5
6.5
8.5
10.5
12.5
14.5
Frequency (GHz)
BD 0.0 um, C=0.69 pF
BD 0.1 um, C=0.84 pF
BD 0.2 um, C=1.10 pF
BD 0.3 um, C=1.58 pF
BD 0.4 um, C=2.81 pF

Fig. 8

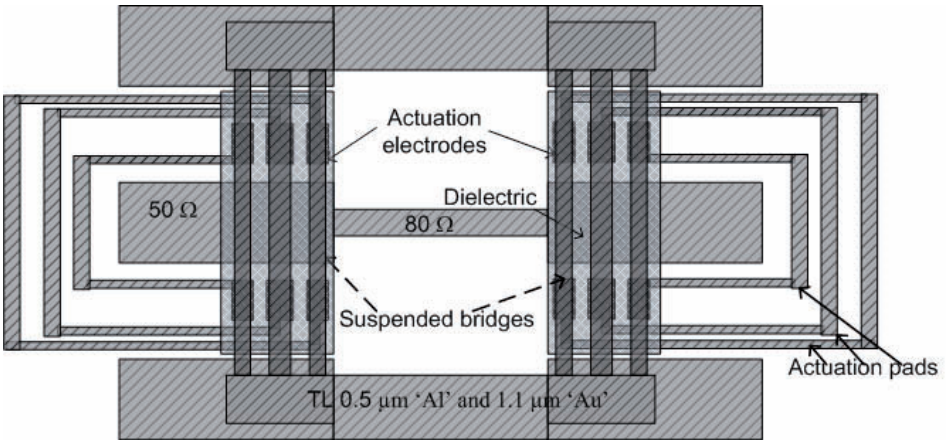
Actuation electrodes
Dielectric
80 Ω
50 Ω
Suspended bridges
Actuation pads
TL 0.5 µm 'Al' and 1.1 µm 'Au'

Fig. 9

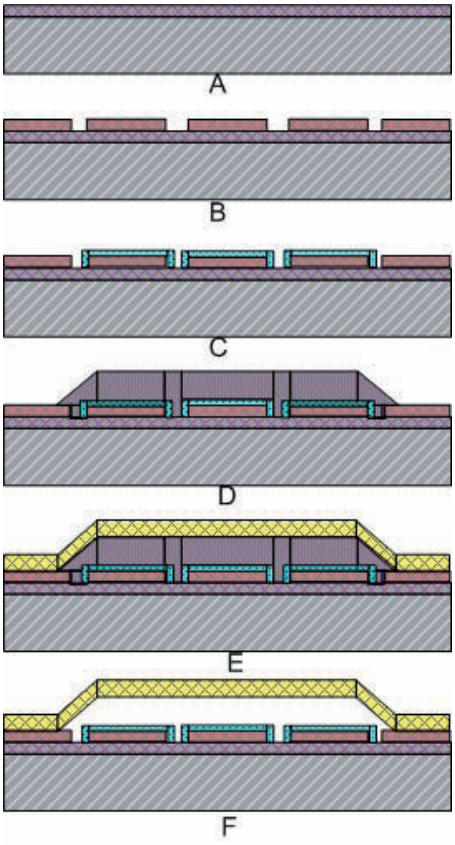

Fig. 10


LOW_PASS_300UM_GRA
WD
9.26 mm
HV
20.0 kV
Spot
5.0
Tilt
3.3 °
Mag
113x
Det
Etd
X: 5.86 mm
Y: 3.72 mm
500 µm

Fig. 11

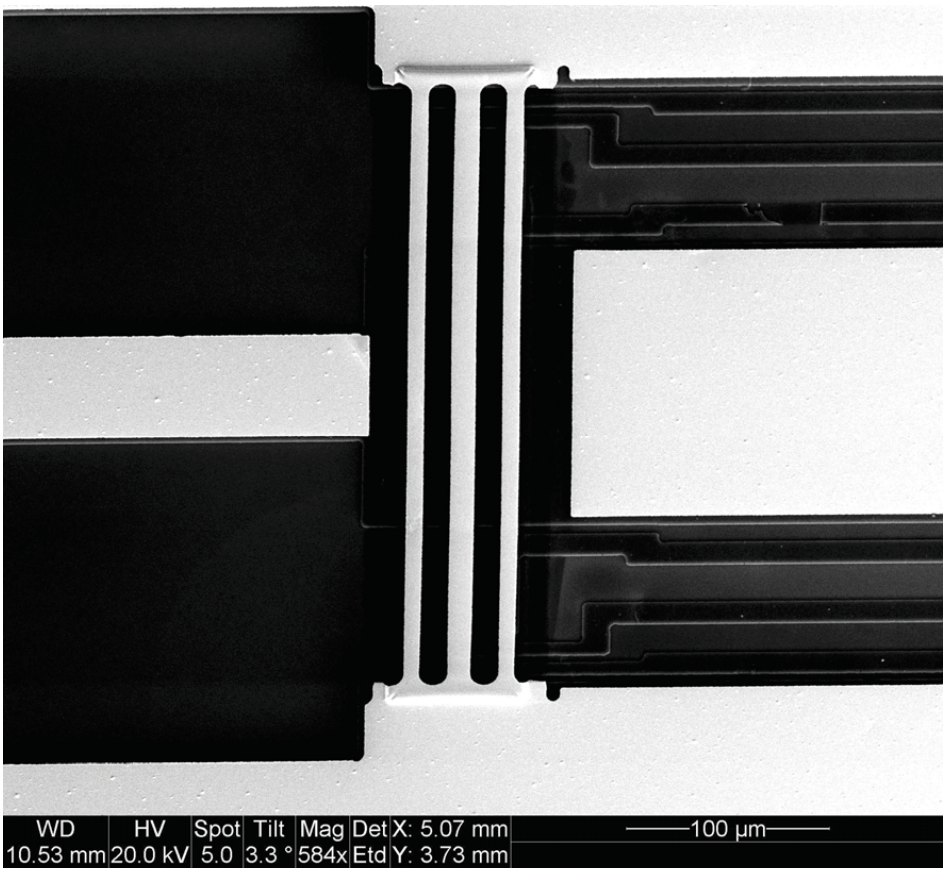
WD
10.53 mm
HV
20.0 kV
Spot
5.0
Tilt
3.3 °
Mag
584x
Det
Etd
X: 5.07 mm
Y: 3.73 mm
100 µm

Fig. 12

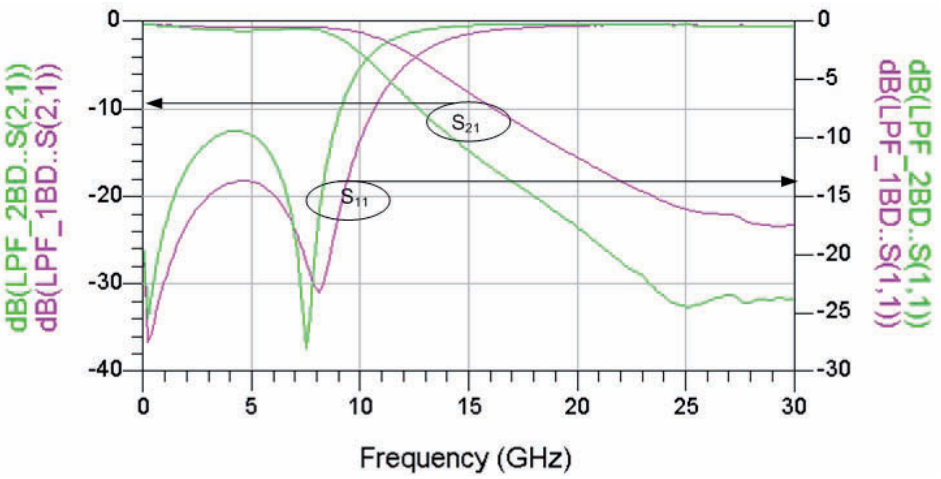
dB(LPF_2BD..S(2,1))
dB(LPF_1BD..S(2,1))
dB(LPF_2BD..S(1,1))
dB(LPF_1BD..S(1,1))
S21
S11
Frequency (GHz)

Fig. 13

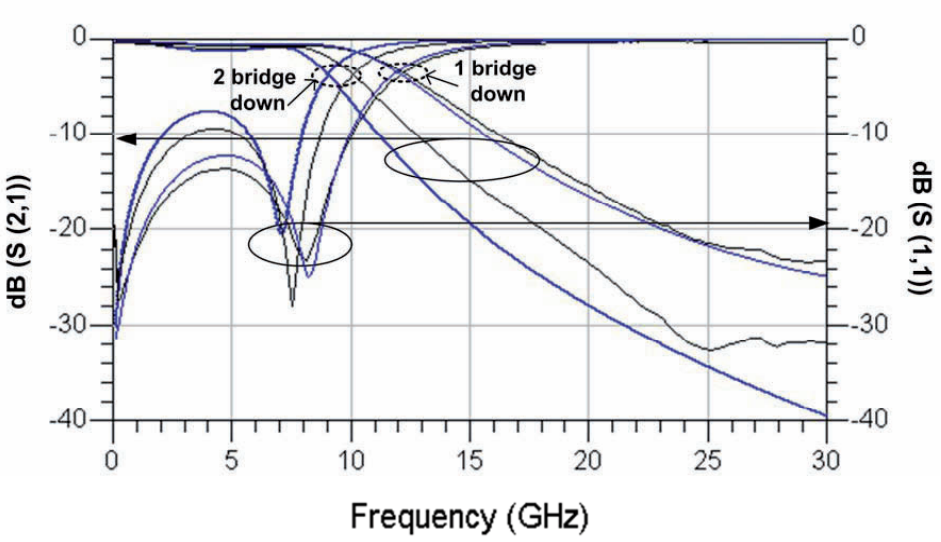
2 bridge down
1 bridge down
dB (S (2,1))
dB (S (1,1))
Frequency (GHz)

Tunable Band-Pass Filter at C band with RF MEMS Capacitance and Transmission line

Shimul Chandra Saha[1], Ulrik Hanke[2], Håkon Sagberg[3], Tor A. Fjeldly[1] and Trond Sæther[1]

[1] Department of Electronics and Telecommunications (IET), Norwegian University of Science and Technology (NTNU), NO-7491 Trondheim, Norway (e-mail: shimul.saha@iet.ntnu.no; torfj@unik.no, trond.saether@iet.ntnu.no)
[2] Institute for Microsystems Technology, Vestfold University College, 3103 Tønsberg, Norway (e-mail: Ulrik.Hanke@hive.no)
[3] Department of Microsystems and Nanotechnology, SINTEF ICT, PO Box 124, Blindern, NO-0314 Oslo, Norway (e-mail: Hakon.Sagberg@sintef.no) .

Has been submitted to Journal of European Microwave Association (EuMA)

Is not included due to copyright

The measurement of S parameters of the RF MEMS switches fabricated in SINTEF MiNa Lab

A MEMO on the measurement results of the fabricated CPW RF MEMS switches.

The measurement of S parameters of the RF MEMS switches fabricated in SINTEF MiNa Lab

1. Introduction:

The S parameter of the RF MEMS capacitive shunt bridge, at upstate and downstate is measured. Switches were fabricated with transmission line and dielectric in SINTEF MiNa lab in Oslo. The released switches looked completely clean and fully suspended when inspected in a optical interferometer from WYKO. A vector network analyzer from Agilent, with a coplanar waveguide (CPW) probe was used for the S parameter measurements. The SINTEF ICT department at Trondheim has developed a bipolar actuation source, which was used for reliability tests. A DC actuation is also used to measure the S parameters at upstate and downstate. The S parameters in upstate are close to the expected results from the simulation. In downstate the isolation is lower than the expected value, due to a reduced capacitance. It is found that if the actuation pulse width is reduced, the number of operating cycles increase and vice versa. The bridge sticks to the downstate after a certain number of cycles. The first version of the switch (bridge thickness ~ 1.1 μm) successfully operated up to ~300.000 cycles. The reason of stiction can be either charging at the electrodes (most probably) or mechanical failure of the suspended beam. A second version with thicker gold (bridge thickness ~ 1.2 μm) operated successfully more than 1.000.000 cycles.

2. The dimensions of the switches:

Several versions of the switch were designed and processed. The switch with title MAIN is fabricated as a reference design. An optical image of the fabricated and released RF MEMS switch (SHORT) is shown in Figure 1. The silicon is slightly over-etched (2.6 μm) during etching of tungsten transmission line (SF_6+C_4F_4). A SEM image of the switch (MAIN) is shown in Figure 2. Some other designs, with increased length and width are also included to test different parameters, like pulldown voltage, S parameters, etc. The switches were fabricated on 50 ohm CPW transmission line in shunt configuration. The center conductor width is 100 μm and the gap between the center conductor and ground is 62 μm as shown in Figures 1 and 2. The thickness of the dielectric is 210 nm. The initial gap of the switch is ~2.25 μm. A slight reduction has occurred (coated thickness was 2.50 μm) due to baking and other high temp processes. The tungsten transmission line thickness is ~500 nm with an additional layer of gold of 1.1 μm. The gold covers the entire tungsten transmission line except the dielectric area and the region below the suspended beam. The gold bridge thickness is 1.1 μm. The dimensions and measured pull-down voltage of the shunt bridges are shown in Table 1 below.

Table 1: The dimensions and pull-down voltage of different version of the shunt switch fabricated at SINTEF MiNa lab (first round).

Title	Length of the suspended bridge (µm)	Width of the suspended bridge (µm)	Thickness of the gold bridge (µm)	Pull-down voltage (V)
MAIN (1, 2)	300	80	1.1	17
MAIN (with CPW ground shorted)	300	80	1.1	18.8
SHORT	250	80	1.1	17.6
LONG	500	80	1.1	15.4
V LONG	500	80	1.1	15.5
WIDE BRIDGE	300	120	1.1	18.8
WIDE V LONG	500	120	1.1	14.9

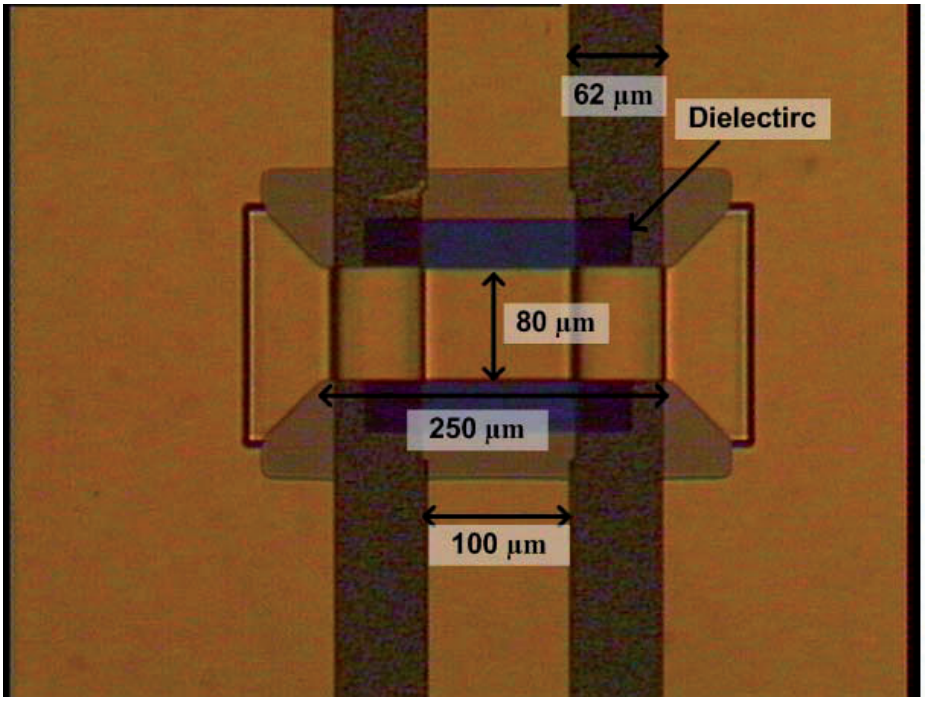

Figure 1: An optical image of the capacitive shunt switch fabricated in SINTEF MiNa lab Oslo.

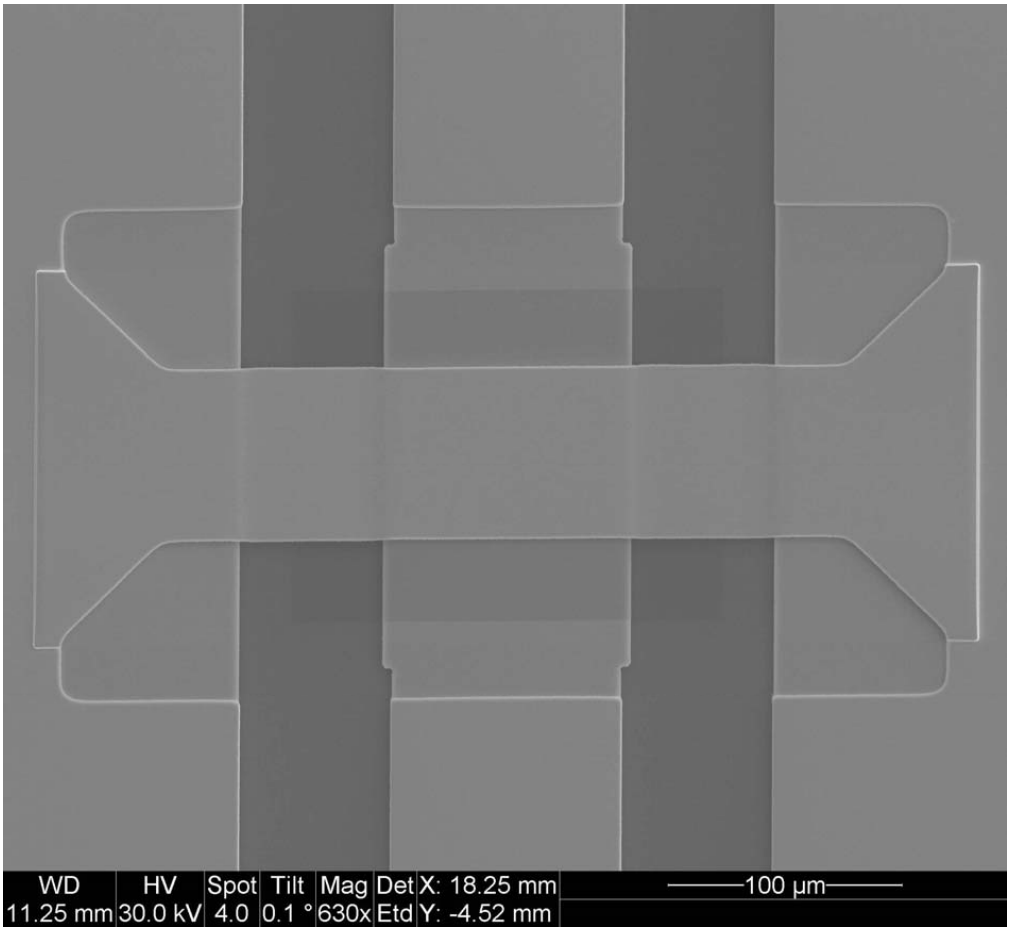

Figure 2: A SEM image of the RF MEMS switch (MAIN) fabricated at SINTEF MiNa Lab.

3. Measurement results:

The S parameters of the switches fabricated in 1st round are measured with a vector network analyzer HP 8510 from Agilent. The standard calibration method LRRM (line-reflect-reflect-match) is used for calibration. The measured S parameters of some of the switches are shown in Figures 3-6.

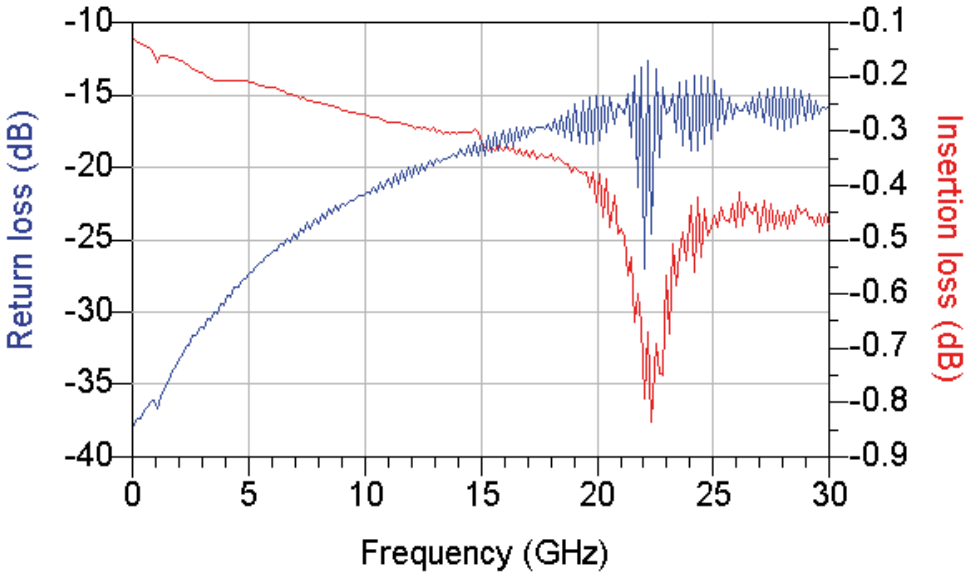

Figure 3: The insertion loss and return loss of the switch MAIN (1) in upstate

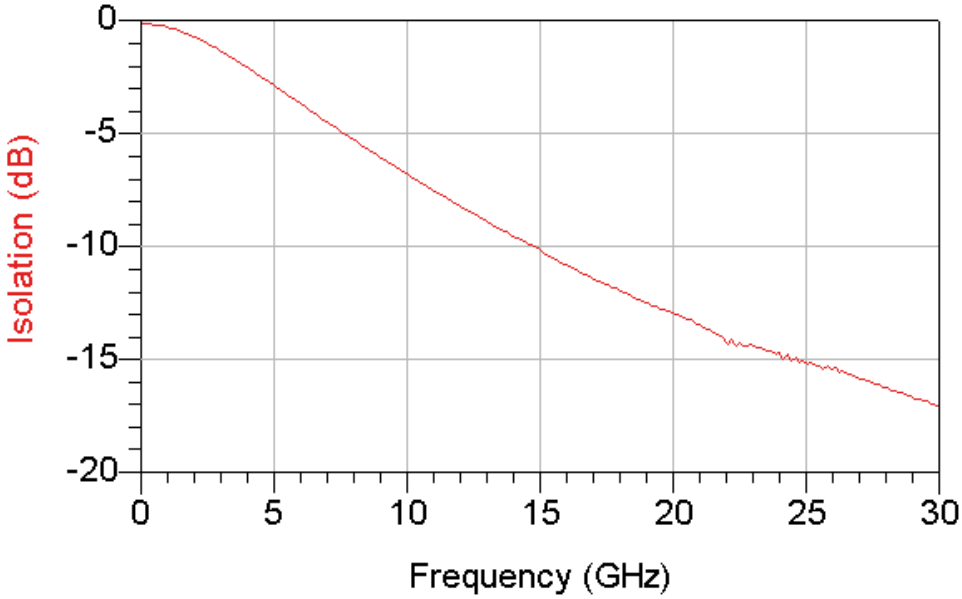

Figure 4: The isolation of the switch MAIN (1) in downstate

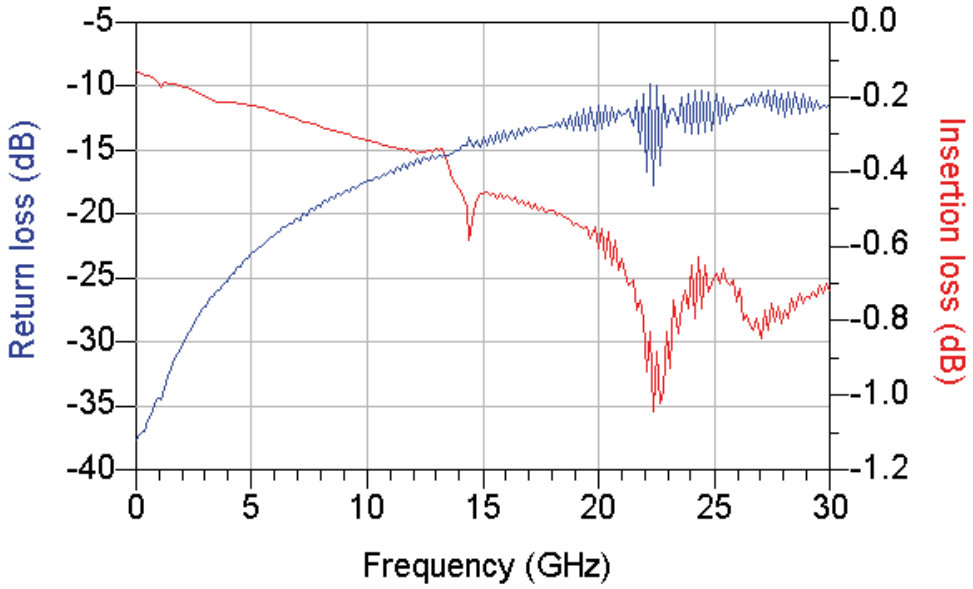

Figure 5: The insertion loss and return loss of the switch WIDE BRIDGE in upstate

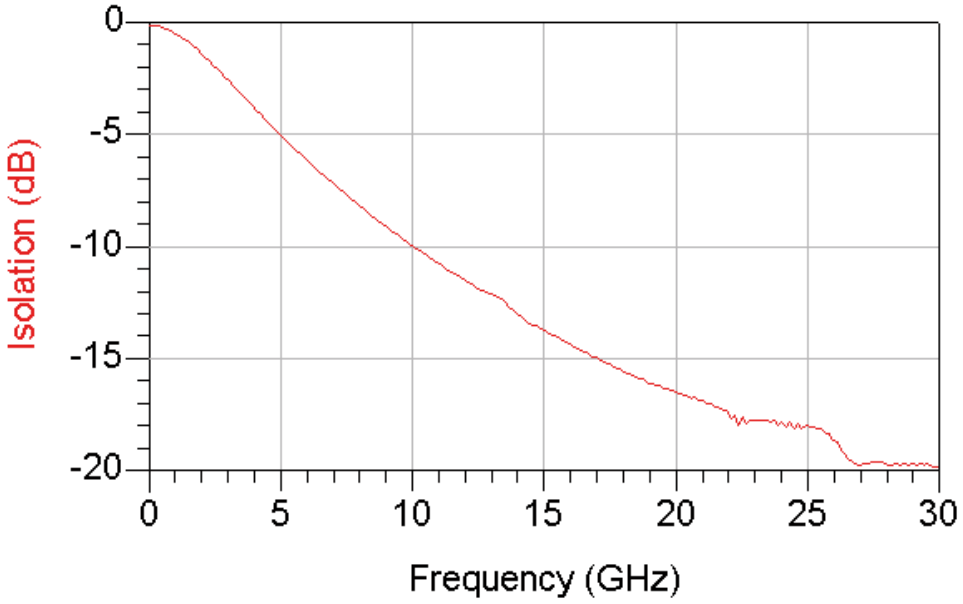

Figure 6: The isolation of the switch WIDE BRIDGE in downstate

For comparison the dimensions and the simulated results of the proposed switch at paper 3 is mentioned. The nominal switch length is L_b=600 μm. The initial gap height of the beam is g_0=3.75

μm. The dielectric material is silicon nitride with a relative permittivity of 8 and a thickness of 1000 Å. Gold is chosen as the membrane material with a thickness of t_b=1 μm. The width of the beam is W_b = 50 μm. The simulated S parameters are shown in Figures 7 and 8.

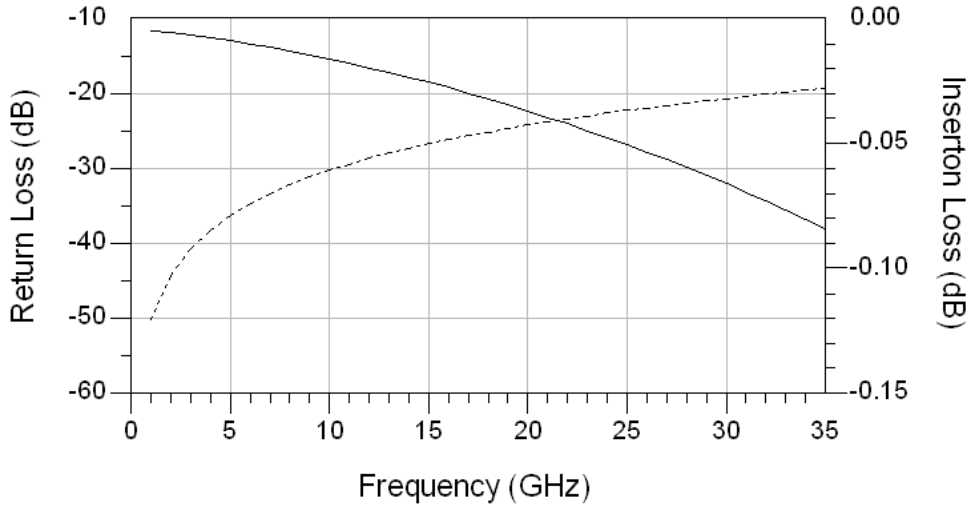

Figure 7: The simulated insertion loss (solid) and return loss (dotted) in upstate (paper 3).

.

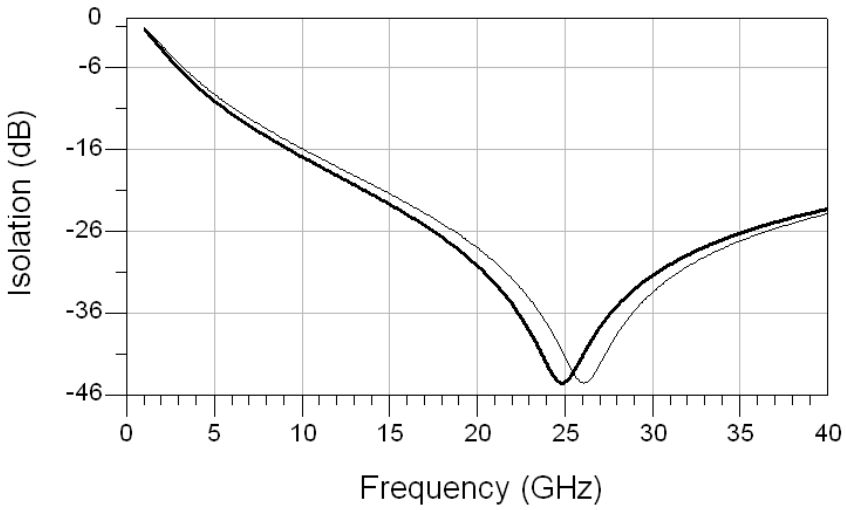

Figure 8: The simulated isolation in downstate with 50 Å roughness (thick line) and 100 Å roughness (thin line) (paper 3).

4. Result analysis:

The measured insertion loss at upstate for the MAIN switch (version 1) is less than 0.5 dB up to 30 GHz. The return loss is -16 dB at 30 GHz. The insertion loss and return loss are slightly higher than the simulated result in the paper 3. This is due to a higher upstate capacitance than the simulated value. There are two main reasons for higher upstate capacitance: a) the width of the bridge is 80 µm instead of 50 µm in the simulation and b) the initial gap is 2.25 µm instead of 3.75 µm used in simulation. Using return loss and back calculation the upstate capacitance value was found to be 50 fF. The insertion loss of the switch will be reduced to some extent if we deduct the loss of transmission line from the measured result. The isolation is much lower than the simulated value. At 10 GHz the isolation is -7 dB (fig 4) compared to -15 dB (fig 8) simulated value. The downstate capacitance is reduced significantly although the width of the beam is made larger. There are some reasons for the reduced capacitance; a) The dielectric thickness is 220 nm instead of 100 nm used in simulation, b) The roughness of the TL, dielectric and gold may reduce the downstate capacitance (~ 8-10 nm), c) The bridge may not be completely flat in downstate, which can be the dominant reason in our case and d) due to over etching, the beam width is reduced slightly. From back calculations using the formula mentioned [4], the downstate capacitance becomes 1.43 pF. In the simulations the isolation increased up to the resonant frequency at 25 GHz (fig 8) and then decreased again at higher frequencies. In the measured result we do not see this effect since the resonant frequency is higher than 30 GHz. This is due to reduced capacitance and reduced inductance. The inductance value will de reduced due to wider and shorter beam. From the measurement a capacitive ratio of 28 was obtained for our switch. From the stress test a stress value of ~40 MPa was found in the sputtered gold. The measured pull-down voltage is lower than the expected value. This may happen, due to the thinner bridge at the rising and falling edges at the middle of the bridge, as can be seen in figures 1 and 2. A wider bridge (WIDE BRIDGE) with a width of 120 µm is also measured. The measured result is shown in figure 5 and 6. As expected the insertion loss and return loss both increased due to higher upstate capacitance. The isolation is increased to some extent due to a higher downstate capacitance. The isolation is -10 dB at 10 GHz. Still this is lower than the expected isolation.

5. Reliability test:

The bipolar actuation source used for the RF MEMS switch reliability test is shown in Figure 9. Initially the pulse amplitude is slightly higher than pull down voltage. Then the voltage amplitude is reduced to the hold down voltage. As mentioned in the introduction the switches stick after 300.000 cycles with bipolar actuation. The actuation frequency is 250 Hz. The active actuation part, when the peak amplitude of the voltage is equal to or greater than pull down voltage is 100 µs. Then a reduced voltage was applied to keep the bridge down (called hold down voltage). After that the actuation

voltage is brought back to zero to release the beam in upstate. In order to improve the reliability and find the cause of stiction, a second round of fabrication is performed. The fabrication parameters are same for the first round except a thicker (1.2 μm instead of 1.1 μm) sputtered gold bridge. The reliability test shows that the switch can operate more than 1.000.000 cycles before stiction. The pull down voltage for the MAIN switch was 30 volt. Charge stiction is very common in the capacitive switching and this can be responsible for our switch also. A better test setup with nitrogen environment is planned for later reliability test. Also an additional layer of gold at anchor is planned for fabrication of later version of the switch. This may increase the reliability keeping pull down voltage at reasonable limit.

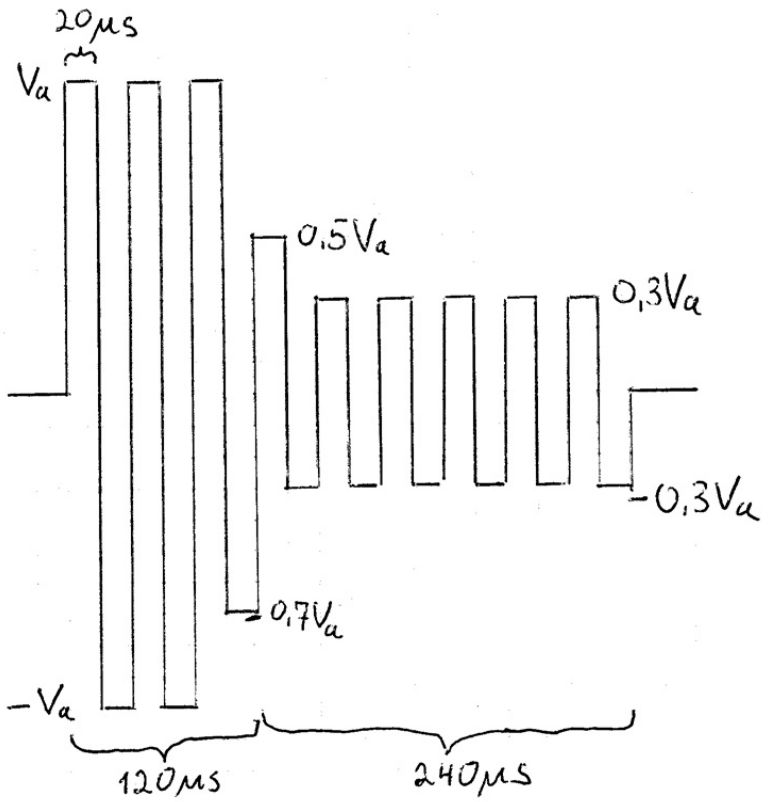

Figure 9: The bipolar actuation signals used for the RF MEMS reliability test

6. Conclusions

The work provides some key achievement. These are the first ever RF MEMS switches to be produced in Norway. The switches have a reasonable low pull-down voltage compared with the present state-of-the-art switches reported elsewhere. The switches employ rather simple beam structures. The capacitance ratio of the switches is also very promising compare to recent work published in elsewhere, considering Si_3N_4 used as a dielectric. The number of successful operating cycles before stiction exceeds more than 1.000.000 cycles. The operating cycles may increase when we do the test in the nitrogen environment. The reliability of the switch is very promising compare to the present state of art switches. The work will provide strong motivation and encouragement for future work on RF MEMS in Norway and international community. Based on the MEMO and the second version of the switch, an article is prepared and accepted in MEMSWAVE 2008, Greece and added as Paper no 15.

A capacitive shunt RF MEMS switch for coplanar waveguide transmission lines

Bengt Holter[1], Karsten Husby[1], Håkon Sagberg[2], Geir U. Jensen[2], Ulrik Hanke[3], and Shimul Chandra Saha[4] , Trond Sæther[4]

[1]SINTEF ICT, Communication Systems, O. S. Bragstads plass 2C, 7465 Trondheim, Norway, +47 73593000
[2]SINTEF ICT, Microsystems and Nanotechnology, Gaustadalleen 23, 0373 Oslo, Norway, +47 22067300
[3]Vestfold University College, Microsystem Technology, 3103 Tønsberg, Norway, +47 33031000
[4]Norwegian University of Science and Technology, 7491 Trondheim, Norway, +47 73595000

In press, MEMSWAVE 2008, 30th June -3rd July 2008, Crete, Greece.

A capacitive shunt RF MEMS switch for coplanar waveguide transmission lines

Bengt Holter[1], Karsten Husby[1], Håkon Sagberg[2], Geir U. Jensen[2],
Ulrik Hanke[3], Shimul Chandra Saha[4], and Trond Sæther[4]

[1]SINTEF ICT, Communication Systems, O. S. Bragstads plass 2C, 7465 Trondheim, Norway, +47 73593000
[2]SINTEF ICT, Microsystems and Nanotechnology, Gaustadalleen 23, 0373 Oslo, Norway, +47 22067300
[3]Vestfold University College, Microsystem Technology, 3103 Tønsberg, Norway, +47 33031000
[4]Norwegian University of Science and Technology, 7491 Trondheim, Norway, +47 73595000

***Abstract* — In this paper, performance results are presented for the first RF MEMS switch ever to be produced in Norway. It is a shunt capacitive switch integrated in a coplanar waveguide configuration. The switch uses a bipolar (square wave) bias voltage for both actuation and hold-down, and is designed to operate in the frequency range 10-32GHz. The fabrication process has been developed and performed at the Micro and Nano Laboratory at SINTEF, which has the only independent complete silicon processing line in Norway. In the targeted frequency range (10-32GHz), the measured insertion loss is between -0.17 and -0.4dB, the return loss between -23 and -12dB, and the isolation is between 7.5 and 20dB. The achieved capacitance ratio of the switch is 25. Some stiction problems have been observed for either a too high pull-in voltage or a too high hold-down voltage.**

I. Introduction

RF MEMS (Radio Frequency Micro-ElectroMechanical Systems) technology is currently regarded as a key enabling technology for future development of wireless communication systems due to superior performance and flexibility compared to existing technologies. In particular, RF MEMS components may be applied in future cognitive radio systems to enable reconfigurable RF front-ends such as flexible filtering, adaptive matching networks, and more efficient antenna designs. For the last four years, SINTEF has conducted research within a project entitled *Integrated reconfigurable radio front-end technologies (IRRFT)*, to gain experience in using RF MEMS components and devices in reconfigurable RF front-ends. One of the main objectives was to develop knowledge and experience to design and process an in-house RF MEMS switch, where the focus was on optimizing the probability of processing success rather than achieving ambitious electrical specifications. In this paper, the fabrication process and some selected performance results of the developed switch are presented. It is the first RF MEMS switch ever to be produced in Norway, and it has been fabricated at the Micro and Nano Laboratory at SINTEF.

The switch is a coplanar waveguide (CPW) capacitive shunt switch, where the suspended MEMS bridge is actuated by applying a bipolar square wave bias voltage between the bridge and the center conductor of the CPW transmission line (t-line). A scanning electron microscope (SEM) image of the fabricated switch is depicted in Fig. 1 (top view). When the bias voltage is applied, an electrostatic force causes the bridge to bend down onto a thin dielectric layer that covers the t-line beneath the bridge. In this down-state position, the bridge connects the t-line to ground (through a capacitance), realizing an RF short for microwave frequencies. When the bias voltage is removed, the electrostatic force is relaxed, causing the bridge to return to its original up-state position. In the literature, detailed analysis on modeling and design of CPW shunt switches are given in [1]-[3].

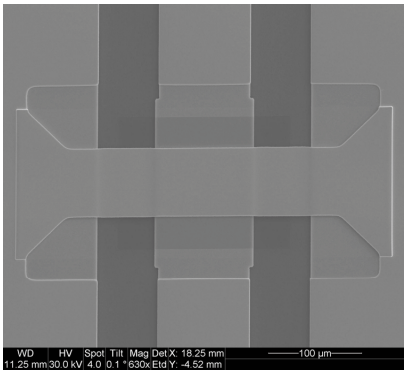

Fig. 1. The SINTEF RF MEMS switch

II. Fabrication process

The switches are fabricated on high-resistivity (4-8 kΩcm) Si with 500nm of thermal silicon dioxide. The switch bridge measures (80×300)µm, and is made of sputtered gold (Au) on top of a 2.5µm thick sacrificial photoresist layer. The 1.2µm thick Au bridge has a relatively low tensile stress (30-60 MPa), and 'climbs' the sloping sidewalls of the patterned photoresist. Below the bridge, the bottom electrode is made of sputtered tungsten (W) covered by a 200nm thick plasma-enhanced chemical vapour deposited (PECVD) silicon nitride layer (Si_3N_4).

Only four photomask levels were used, defining (1) The W for electrode and CPW bottom layer (2) The Si_3N_4 layer covering the bottom electrode (3) The patch of sacrificial photoresist that creates the bridge-to-dielectric gap, and (4) The Au bridge and CPW upper layer. An

additional layer of metal (Au) is often included for strengthening the bridge anchors and improving the t-line RF properties. Such a layer would probably have had a noticeable influence on the pull-in voltage, at least, but the SINTEF switch operates remarkably well without that layer. For implementation of circuits based on these switches, an additional step/mask for polysilicon bias lines is used.

A. Bottom electrode

The bottom electrode consists of a 100µm wide and 500nm thick stripe of sputter-deposited W with a 12-15nm Ti adhesion layer. Patterning is done by reactive ion etching (RIE). A refractory metal, W withstands the subsequent high-temperature processing without forming hillocks as, for instance, aluminium would do. A smooth electrode surface is essential for a high down-state capacitance. Unlike e.g., Al, W has no hillock formation.

Since the W electrode also serves as a section of the t-line, a sufficiently thick electrode is needed for transmission quality. However, two other effects call for a thin electrode layer: First, the subsequent deposition steps (nitride deposition, sacrificial resist and Au sputter) are (at least partly) conformal, so the edges of the electrode will create steps in the Au bridge, as illustrated in Fig. 2, which also shows the shape of the resulting bridge before and after release. Second, sputtered W has a large internal compressive stress (~1GPa); thus a thick W layer would produce wafer curvature and also adhesion problems (peeling). As such, the selected thickness of 500nm for the bottom electrode is a compromise.

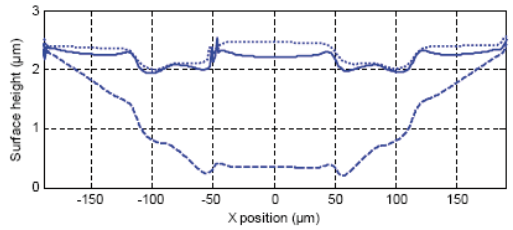

Fig. 2 Surface profile of the bridge in three states: *Pre-release* (dotted curve), *post-release* (solid curve), and *actuated* (dashed curve). The heights are relative to the top of the W-NiCr-Au stack. Pre-release data were obtained with optical profilometry on surfaces partially covered with photoresist, and the profile has been scaled and offset to obtain a good fit to the post-release data.

B. Dielectric layer

A 200nm thick layer of Si_3N_4 serves as the dielectric layer in the capacitive switch. The Si_3N_4 is deposited using PECVD at 300°C, and a (180×140)µm patch is patterned by RIE. The relative permittivity of the Si_3N_4 is around 8, but the surface roughness of the Si_3N_4 as well as that of the underside of the Au bridge results in a lower 'effective' permittivity.

C. Sacrifical photoresist

While achieving vertical photoresist sidewalls is the goal of many high-resolution photoprocesses, the switch requires a process resulting in roughly 45° sloping sidewalls so that the Au slope/wall remains thick enough for good mechanical as well as electrical properties. The correct sloping sidewalls were achieved with a combination of proximity exposure and careful fine-tuning of hard baking parameters (temperature and time). We used a standard DNQ-novolac positive photoresist (HIPR 6517), which is spin coated at 2000rpm and exposed at a gap of 25µm. The optimum hotplate hardbake conditions were found to be 115°C for 300s [4]. The temperature during subsequent processing steps must be kept well below the hard baking temperature, in order to prevent excessive baking of the photoresist.

D. Bridge

A 1.2µm Au layer, with an adhesion layer of 10nm NiCr, is deposited using low-power sputtering at relatively high pressure (20mTorr). The NiCr/Au is deposited partly on W (CPW lines), and partly on photoresist (bridges). A low sputtering power ensures that the sacrificial photoresist is not much affected, and the sputtering pressure was tuned to achieve a low tensile stress in the Au film. The resulting biaxial stress of the suspended Au bridge was characterized to lie in the range 30-60MPa using test structures such as Guckel rings.

The Au film was patterned using standard photolithography and a potassium iodide (KI) solution. The sacrificial photoresist was removed using O_2 plasma and Shipley 1165 microposit remover, and then the NiCr layer underneath the Au in the bridge was etched. Finally, the switches were dried with supercritical CO_2 drying to avoid stiction. Images of the device are shown in Fig. 3.

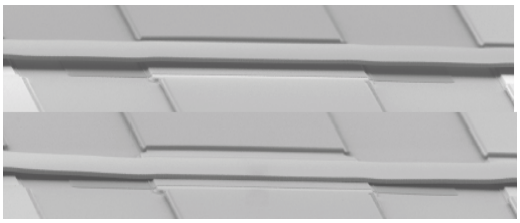

Fig. 3 SEM images of the fabricated switch in its idle (top) and actuated (bottom) states.

E. Mechanical properties and switch operation

A bias voltage applied between the bottom electrode and the bridge will cause the latter to move towards the former. The spring constant is often calculated under the assumptions of a fixed-fixed bridge and that there are no steps in the bridge. These assumptions do not apply in our case. When released, the bridge contracts and the parts close to the anchors deform slightly. This creates a sag or curvature of the released bridge, as seen in Fig. 2. Also, the bridge steps on each side of the bottom electrode result in local curvature changes and a softening of the bridge. A several µm thick additional top metal layer would reduce the first sag, but some electrode induced sag will always be present. However, the SINTEF switch exhibits an overall good performance. The measured pull-in voltage is 30V, and the down-state and up-state capacitance are 1.2pF and 49fF, respectively.

III. RF PERFORMANCE

The SINTEF RF MEMS switch has been characterized by observing static S-parameters during steady state operation, and by observing settling dynamics during transient operation. The measurements have been performed directly on wafer by the use of a probe station according to the measurement set up displayed in Fig. 4.

The use of a bipolar bias voltage was selected in order to reduce the possibility of dielectric charging commonly observed in capacitive switches [3]. According to [3], the dielectric will not charge if the bipolar signal has a period that is shorter than the charging time of the dielectric. Since the electrostatic force of the bias signal is proportional to the square of the voltage, it will represent a constant attractive force to the bridge even if the polarity changes. This force will however go to zero in the transition between the two bipolar levels, but as long as this transition phase is fast enough (20-100ns [3]), the bridge will not have time to react to the change. Based on these facts and the results reported in [Sec. 7.2, 3], a square wave bipolar bias voltage has been selected for both the actuation and hold-down cycle of the switch presented in this paper.

In our case, the bias/control voltage is generated by a high voltage arbitrary bipolar pulse generator, which is isolated from the sensitive measurement equipment by tees and attenuators. Due to the flexibility of this generator, it is possible to address mechanical switch dynamics and to identify a bias voltage for fast and careful excitation. The selected bias tee in Fig. 4 represents a capacitive loading of the pulse generator. However, the generator still managed to deliver up to ±60V pulses at a slew rate of 600V/µs. In Fig. 5, a magnified view of the probe tip ready for touch down on the RF MEMS switch is shown.

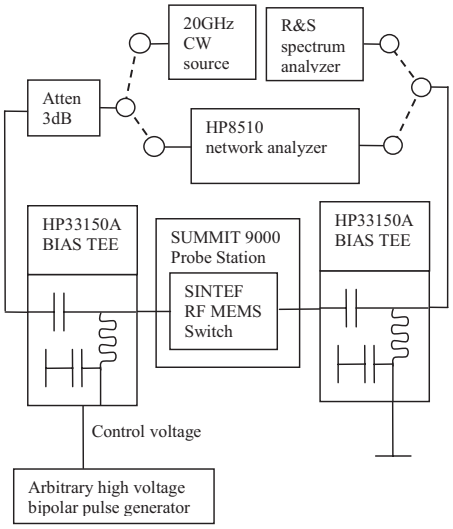

Fig. 4 Measurement set up for either S-parameters with network analyzer or for dynamic transient response with a high speed synchronized spectrum analyzer.

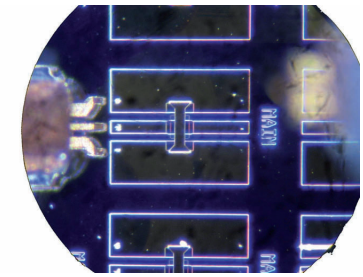

Fig. 5 The probe tip (GSG 200) ready for touch down on the SINTEF RF MEMS switch denoted MAIN

A. S-parameters

For the S-parameter measurements, the bias voltage was selected to be a rectangular bipolar signal at 10kHz slightly above the pull-in voltage, hence using a hold-in voltage that is identical to the pull-in voltage. The switch was released after 10s by setting the bias voltage to zero. Under these conditions, none of the tested samples returned to their initial up state position. However, as shown in Section IIIB, the switches did release when the bias voltage was quickly and gracefully reduced after pull-in to a lower hold-in voltage.

The measured S-parameters of the SINTEF switch are presented in Fig. 6 and Fig. 7. In Fig. 6, insertion and reflection loss are presented for the open switch (up-state) whereas in Fig. 7, similar results are presented for the closed switch (down-state). All the measured results are compared to a modelled result based on the lumped RLC model shown in Fig. 8.

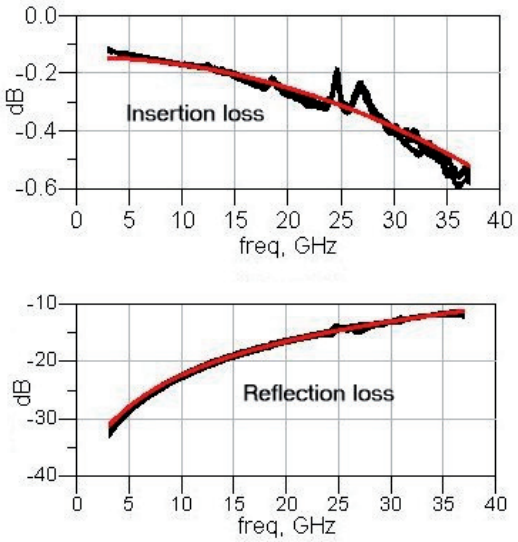

Fig. 6 Insertion and reflection loss for the open switch (black) together with the modeled result (red) for the T-model with C=49fF, R=0.82Ω and L=15pH.

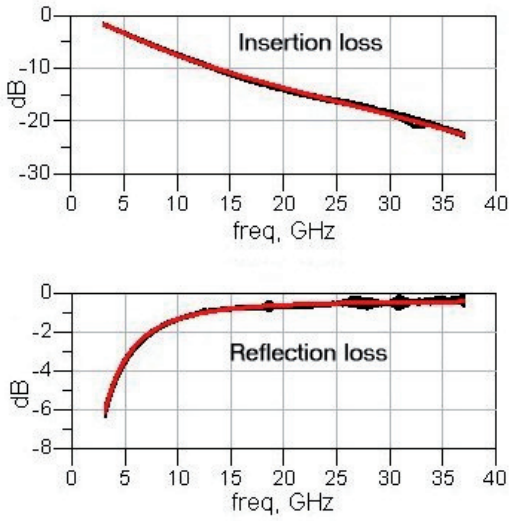

Fig. 7 Insertion and reflection loss for the closed switch (black) together with the modeled result (red) for the T-model with C=1.24pF, R=1.0Ω and L=6.5pH.

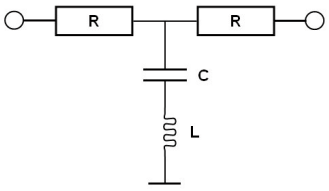

Fig. 8 Lumped T-model of a capacitive shunt switch

The impedance of the switch as a single port device with the output port left open is $Z = Z_0[(1+\Gamma e^{j\phi})/(1-\Gamma e^{j\phi})]$, where Z_0 is the characteristic impedance of the t-line, and Γ is the magnitude of the reflection coefficient. The highest Q-factor is found at the phase angle $\phi = \pm\frac{\pi}{2}$, where the total reflection coefficient is pure imaginary. From the measured S-parameters, the down-state Q-factor of the switch has been estimated to about 20-30 according to the equation $Q = \left|\frac{\mathrm{im}(Z)}{\mathrm{re}(Z)}\right| \approx \frac{1}{1-\Gamma}$.

B. Settling dynamics

The bias voltage level affects the settling time of the switch, so fast operation is possible if the bias voltage is increased. However, it has been observed that fast operation also introduces a mechanical bounce in the switch. Due to this, the settling speed was aimed to about 100µs. In Fig. 9, the RF attenuation through the switch is depicted as measured by a Rohde & Schwarz spectrum analyzer. The switch is operated with the bipolar bias voltage and a 30V pull-in voltage, which is gracefully reduced to a hold-in voltage of approximately 12V. After 360µs, the bias voltage goes from -12V to zero and the bridge starts to return to its original up-state position.

The switches have been turned on and off at a rate of 250Hz to provoke for any failure. After some time, a stiction tendency was observed. The delayed rise up movement is possibly caused by a stiction mechanism not yet identified. Charge buildup, mechanical failure and viscous tension from contamination are some candidate explanations for this behavior.

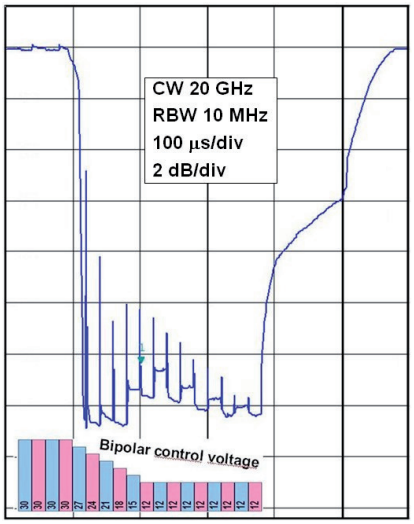

Fig. 9 Dynamic on/off response of the RF MEMS switch at 20GHz after one million cycles with a spectrum analyzer in zero span mode.

CONCLUSION

This paper has presented Norway's first RF MEMS switch, a capacitive shunt switch produced at SINTEF. Between 10-32GHz, the measured insertion loss is between -0.17 and -0.4dB, the return loss is between -23 and -12dB, and the isolation is between 7.5 and 20dB. The achieved capacitance ratio of the switch is 25.

ACKNOWLEDGEMENT

This work has been funded by the Norwegian Research Council through the IRRFT (159259/I40) and SMIDA (159559/130) projects. The authors would like to thank Prof. Gabriel Rebeiz of the University of California at San Diego for his valuable comments to the process development of the switch.

REFERENCES

[1] J. B. Muldavin and G. M. Rebeiz, "High isolation CPW MEMS shunt switches - Part 1: Modeling," IEEE Transactions on Microwave Theory and Techniques, vol. 48, no. 6, pp. 1045-1052, June 2000.

[2] J. B. Muldavin and G. M. Rebeiz, "High isolation CPW MEMS shunt switches - Part 2: Design," IEEE Transactions on Microwave Theory and Techniques, vol. 48, no. 6, pp. 1053-1056, June 2000.

[3] G. M. Rebeiz, RF MEMS: Theory, Design, and Technology, John Wiley & Sons, 2003.

[4] S. C. Saha, H. Sagberg, E. Poppe, G. U. Jensen, T. A. Fjeldly, and T. Sæther, "Tuning of resist slope with hard-baking parameters and release methods of extra hard photoresist for RF MEMS switches," *Journal of Sensor and Actuators A*: Phys., vol. 142 (2), pp. 452-461, 2008.